RHODES UNIVERSITY
Grahamstown • 6140 • South Africa

Petrological, mineralogical and geochemical studies of Zhongchang and Yantiangou ultramafic intrusions from the Panxi region, Sichuan Province, S-W China. Metallogenic and Exploration implications.

A thesis submitted in partial fulfilment of the requirements of Master of Science

at

Rhodes University

by

Tsholofelo S Malatji

December 2013

Department of Geology, Rhodes University

South Africa

ABSTRACT

The Emeishan Large Igneous Province is one of the largest igneous provinces in the world. It is marked by basaltic extrusives that vary in Ti amount, classified as high Ti and low Ti. Several mafic to ultramafic intrusions occur in the province as well as granitic intrusions. The mafic-ultramafic intrusions are associated with mineralization; large layered utlramafic intrusions bearing Fe-Ti-V mineralization, while small dyke like or sill like intrusions contain Cu-Ni-PGE mineralization.

The Zhongchang and Yantiangou mafic- ultramafic intrusions are small such intrusions bearing Ni-Cu-PGE mineralization. The deposits show a lot of similarities in source magma, evolution and mineralization. Parental magma for both deposits show alkaline tendencies, and a high Mg # indicative of primitive magma that underwent little crustal contamination. Mantle range Cu/Pd ratios show parental magma fertile in chalcophile elements and both deposits proceed to show depleted mantle normalized values as a result of sulphide saturation and subsequent mineralization.

Mineralization in Zhongchang is hosted at the contact between peridotite and pyroxenite, interstitial to olivine and clinopyroxene. Alteration minerals include epidote and chlorite. High Cu/Pd ratios suggest earlier sulphide saturation and removal of a PGE sulphide, and a second sulphide saturation phase resulted in Ni-Cu mineralization.

Mineralization in Yantiangou is hosted in biotite effectively following fractionation of olivine and clinopyroxene after which sulphide saturation occurred, precipitating sulphide minerals in biotite. Pyrite and millerite occur as a result of late stage hydrothermal alteration. Cu/Pd ratios are high indicating prior sulphide saturation occurred where PGE partitioned into sulphides.

Ni/MgO ratios observed for both deposits indicate a state of sulphide under saturation where PGE partitioned into tellurides and bismurthinides and Ni into olivine.

Average tenors for mineralized units are; Zhongchang at 5%Ni, 9% Cu, 4300ppb Pt and 2000ppb Pd, and Yantiangou having relatively lower tenors at 3.2%Ni, 6.5% Cu, 3000ppb Pt and 1300 ppb Pd.

If the wind will not serve, take to the oars. –Latin Proverb

DECLARATION

This thesis is the result of my own independent work/investigation, except where proper acknowledgement is given to the work of others.

Signed…………………………………………………………...... (candidate)

Tsholofelo S Malatji

Date ………………………

December 2013

Department of Geology

Rhodes University

Grahamstown

South Africa

ACKNOWLEDGEMENT

I wish to humbly thank the Baring Family for their kind and generous scholarship, without them this would have been but a dream. My sincere gratitude is extended to the trustees and administrators of the fund.

I would like to thank the course coordinator and my supervisor Prof Yong Yao for his guidance. My greatest appreciation goes to my co-supervisor Dr Marian Munteanu of the Romania Geological Institute for providing guidance throughout the writing of this thesis and invaluable insight into the area of study. This too would have been impossible without his guidance.

A heartfelt thank you goes to Mrs Ashley Goddard, put simply- you are a star for being there throughout the course of my study like a guardian angel. You made it all doable.

To all the people who contributed to this research, Dr Gelu Costin and those who helped with reviews, you are greatly appreciated.

To my classmates and colleagues; Godfrey Bitesigirwe; Luckmore Salimo; Thomas Branson; Ali Assane; Matt Terracin, and Demand Gwatinetsa we had a great time together. Here's to the class of 2013!!!.

The use of Jeol JXA 8230 Superprobe, instrument sponsored by NRF/NEP grant 40113 (UID 74464) is kindly acknowledged.

DEDICATION

To my parents, who remain the pillars of my existence.

To my siblings, whose love is a constant

To my husband whose love and support have been unwavering

To my children, to the future

And above all,

Praises be to God the almighty, the omnipotent, the beginning and the end.

Philippians 4:13

“I can do all things through Christ which strengtheneth me”.

TABLE OF CONTENTS

LIST OF FIGURES

LIST OF TABLES

LIST OF COMMON SYMBOLS AND ABBREVIATIONS

ELIP- Emeishan Large Igneous Province
Panxi- Panzhihua-Xichang Province
Permian- 290-250Ma
HT- High titatium
LT- Low titanium
D- Partition coefficient
Mss- Monosulfide solid solution
Iss- Intermediate solid solution
fO_2- Oxygen fugacity
fS_2- Sulfur fugacity
T- Temperature
°C- Degrees celsius
µm -Micrometre (1 µm = 0. 001mm)
< -Less than
> -Greater than
~- Approximately
%- Percent
wt % -Weight percent
ppm -Parts per million
ppb- Parts per billion
PGE- Platinum group element
PGM- Platinum group metal
Ni -Nickel
Cu- Copper
Co- Cobalt
Cpy- Chalcopyrite
Mil- Millerite
Pn- Pentlandite
Pyr- Pyrite
Po- Pyrrhotite
Qtz- Quartz
Epdt- Epidote
Chl- Chlorite
Plg- Plagioclase
Hbl- Hornblende
Carb -Carbonate
Mgt- Magnetite
Spry- Sperrylite
Ilm- Ilmenite
Olv- Olivine
Chr- Chrome spinel
Ab- Albite
An- Anorthite
Olg- Oligoclase
En- Enstatite

Wo- Wollastonite
Fs- Ferosillite

CHAPTER 1 INTRODUCTION

1.1 NI-CU-PGE DEPOSITS

Magmatic Ni-Cu-PGE deposits are commonly associated with mafic to ultramafic rocks. The deposits account for ~40% and > 99% of the global resources of Ni and PGE, and ~3% Cu (Song et al., 2011). Magmatic sulphide deposits account for over 60% of the worlds nickel supply and > 99% PGE (Song et al., 2011). A small quantity of Ni and Cu is recovered as a by product of PGE deposits while rest of the worlds production comes from lateritic deposits formed by weathering of olivine bearing ultramafic rocks (Eckstrand and Hulbert, 2007; Barnes and Lightfoot, 2005).

The world's most important Ni- Cu-PGE deposits (Fig 1) are are; Noril'sk (Russia), Sudbury (Ontario), Voisey's Bay (Labrador), Pechenga (Russia), Thompson (Manitoba), Raglan (Quebec), Kambalda and the Yilgarn komatiites (Western Australia), Jinchuan (China), with smaller deposits in China (Hong Qi Ling in Jilin Province and Karatungka in the Xinjiang Autonomous Region) (Lightfoot, 2007). PGE deposits are predominantly layered intrusions like the JM Stillwater (USA), Bushveld Complex (RSA), Great Dyke (Zimbabwe) and Lac de Iles (Canada, Barnes and Lightfoot, 2005; Eckstrand and Hulbert, 2007).

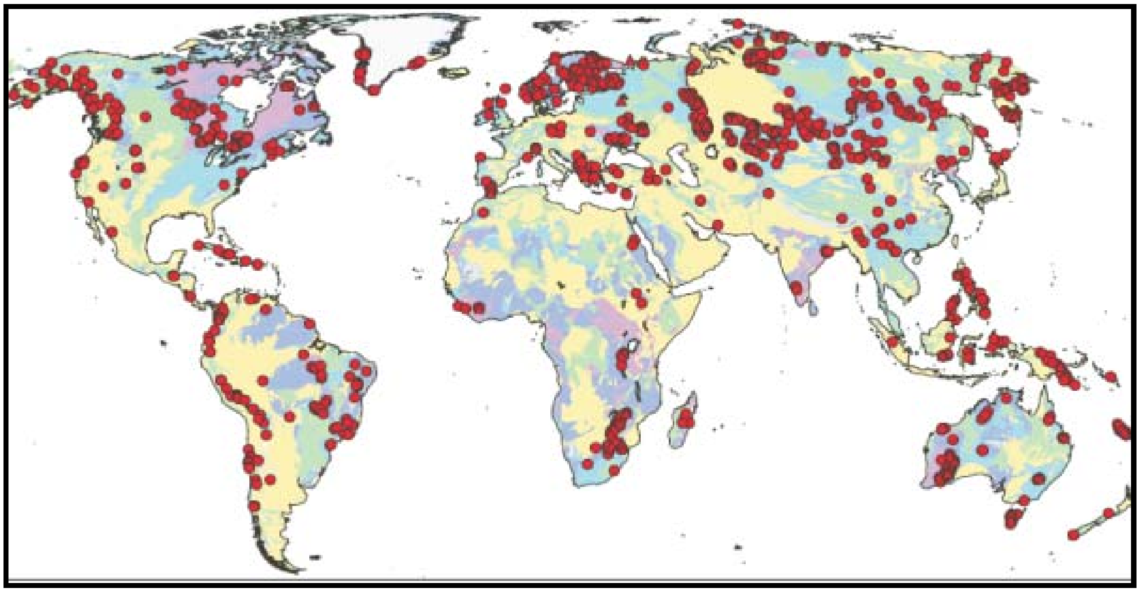

Figure 1: World's major magmatic Ni-Cu-PGE sulphide deposits and mining camps with over 100 000 tonnes of ore. Adapted from Eckstrand and Hulbert., (2007).

Most Ni-Cu sulphide ore deposits occur in clusters of deposits known as mining camps where, typically the grade of the ores is greater than 0.5 percent Ni. A cluster or mining camp generally contains more than 100,000 tons with individual ore deposits generally containing greater than 10,000 t Ni (Fig 2, Barnes and Lightfoot, 2005; Eckstrand and Hulbert, 2007).

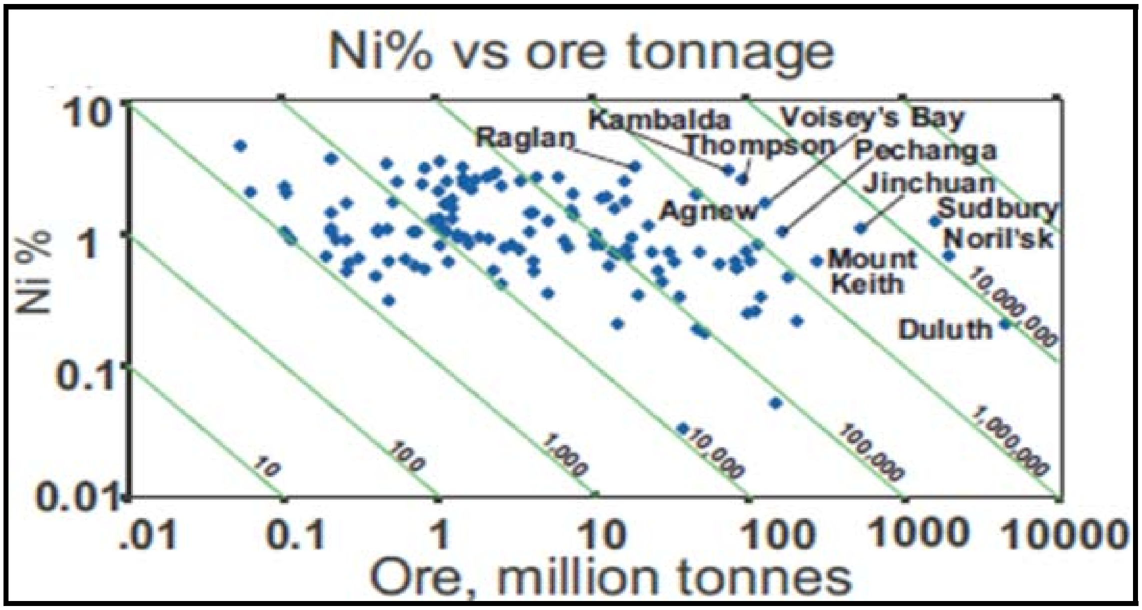

Figure 2: Ni ore production and reserves, from Eckstrand and Hulbert., (2007).

Zhongchang (N26.32728, E102.02540) and Yantiangou (N26.27919, E102.30019) are small magmatic Ni-Cu PGE deposits that occur in the Emeishan Large Igneous Province (ELIP) in the Panxi (**Pan**zihua- **Xi**chang) region, Sichuan Province, S-W China. The deposits occur in a cluster together with several other Ni-Cu-PGE deposits within close spatial proximity. These deposits are located about 40 km apart towards the northern-western margin of the central/ inner zone of the ELIP close to the Limahe Ni-Cu deposit.

The occurrence of these deposits alongside the major sulphide deposits and several other minor ones in terms of geological and structural setting suggests that they are coeval with the Emeishan continental flood basalts and were emplaced at ~260Ma (Zhou et al., 2008). Tang et al., 2007 describes these deposits as being spatially and temporally related to the flood basalts. Their mode of formation is not clearly understood; but could be as a result of in-situ sulphide segregation (Zhongchang) or by a sulphide bearing mush introduced into a plane of weakness (Yantiangou) according to classification of the sulphide deposits in the ELIP by Song et al., (2005).

The Zhongchang and the Yantiangou deposits are currently being mined on a small scale and exploration data gave the grades of the deposits as, Zhongchang (0.8% Ni, 1% Cu, 0.8 ppm Pt+Pd) and Yantiangou (0.6% Ni, 0.7% Cu, < 1 ppm Pt+Pd; Munteanu et al., 2013).

1.2 GEOLOGICAL SETTING OF Ni-Cu-PGE DEPOSITS

Most magmatic sulphide deposits occur in regions of lithostratigraphic structural weakness, near regional deep faults where large volume of mantle derived magma had access to continental crust (Barnes and Lightfoot., 2005; Song et al., 2011). These regions such as a rift zones and crust-penetrating fault zone served as conduits through which efficient transportation of sulphur-undersaturated magma occurred from the mantle to shallow crustal depths for emplacement (Schulz et al., 2010; Song et al., 2011).The deposition of these therefore, has been most commonly facilitated during periods of active regional tectonism, under mildly compressional to extensional tectonic conditions (Begg et al., 2010). The sulphide deposits and their host intrusions range in age from Archean to Middle Jurassic (Schulz et al., 2010).

The existence of such kinds of deposits along continental margins and subduction zones is not very common, possibly as a result of limited interaction with continental lithosphere, or simply from poor preservation of deposits along active margins (Begg et al., 2010). One such occurrence however is the Duke Island Complex in south-eastern Alaska, on a continental volcanic arc along an active subduction zone. Here, significant zones of sulphide mineralization are found primarily in the olivine clinopyroxenite unit of the complex, consisting of pyrrhotite, chalcopyrite, cubanite and pentlandite (Thakurta et al., 2012).

Examples of deposits associated with intra-continental magmatic settings are Noril'sk (Siberia, Russia), Duluth Complex (Minnesota, USA), Bushveld Complex (RSA), Stillwater Complex (Montana, USA). Deposits occurring on rifted continental margins are Thompson (Manitoba, Canada) and Cape Smith (Quebec, Canada); while those formed from magmatism related with greenstone belt formation are Kambalda (Western Australia) and Pechenga (Kola Peninsula, Russia, Begg et al., (2010).

Even though both Ni-Cu and PGE deposits are associated with mafic and ultramafic rocks, Ni-Cu sulphide deposits often occur in dynamic magmatic systems, such as lava channels and magma conduits, whereas PGE deposits commonly occur in larger layered intrusions (Li et al., 2001). Magmatic Ni-Cu-PGE sulphide deposits often occur in association with other magmatic ore deposits such as contact-type deposits, chromite deposits, and Fe-Ti-V (Schulz et al., 2010).

1.3 SCOPE AND OBJECTIVES OF THE STUDY

The Panxi region has been identified as one of the large igneous provinces of the world. It has great potential for mineral resource development as it hosts oxide and sulphide mineralization. Some amount of work has been done by different researchers and documented in literature. However this work is limited to deposits of Limahe, Jinbaoshan, Yangliuping, Baimazhai, Ban Phuc and Zhubu; and not much work extends to cover the Yantiangou and the Zhongchang deposits. This thesis intends to extend mineralogical and petrological studies to the two deposits and investigate their mineral chemistry and ore tenors, as well as to provide comparison to some of the data published in the literature.

The scope of this work is based on the Zhongchang and Yantiangou Ni-Cu- PGE deposits. Emphasis will be on investigation of petrology, mineral chemistry and the metal tenors of the deposits. Samples were taken from these deposits; nine samples from Yantiangou and eleven samples from Zhongchang, which will be investigated for petrology as well as mineralogy and mineral chemistry.

Petrological studies will be concerned with identifying main rock forming minerals, crystallization sequence and alteration. Mineral chemistry investigations will be based on the composition of the silicates (olivine, pyroxenes and plagioclase ± hornblende ± biotite), oxides (Cr-spinels, Fe-Ti oxides) and sulphides (pyrrhotite, pentlandite, chalcopyrite). The metal tenors will be calculated based on the content of Ni, Cu, Co, S, Pt and Pd from whole rock sample analyses.

1.4 THESIS OUTLINE

This thesis is composed of ten chapters. The first chapter is the introduction to the area of study and magmatic Ni-Cu deposits. Chapter two focuses on the regional geology, describing the extrusive and intrusive rocks of the ELIP, and the mineralization associated with the intrusions. The third chapter is on the genetic model of Ni-Cu-PGE deposits as presented in literature by various authors and researches. Chapter four outlines the methodologies used to obtain the data presented. Chapter five to seven present results on petrography, mineral chemistry and whole rock contents of ore elements (S, Ni, Cu, Co, Au, Pt, Pd and Rh), respectively. Descriptions on the observed features of the studied rocks are recorded and some formulated calculations are documented. Discussion in chapter eight uses the data presented in the three chapters on results, and attempts to provide explanations on the relationships between rock forming minerals, ore mineralogy and geochemistry to propose possible genetic models for the formation of Zhongchang and Yantiangou deposits. Chapter nine on exploration highlights techniques applicable to similar Ni-Cu-PGE deposits and the conclusions chapter (10) highlights the main points of the study, it is followed by the list of references. Appendices are attached at the end of the thesis.

CHAPTER 2 REGIONAL GEOLOGY

The Emeishan Large Igneous Province (ELIP) in Fig 3 comprises thick (2000–5000 m) sequences of dominant low-Ti tholeiitic lavas, subordinate lavas of picrites, trachytes tephrites, and rhyolites with associated pyroclastic rocks (Pirajno, 2013). The volcanic rocks erupted on Yangtze craton to the east and the Songpan- Ganzi terrain Tibetan Plateau to the west, covering an area of over 250 000 km^2 (Song et al. 2008), while numerous ultramafic, mafic and felsic intrusions also occur in the ELIP.

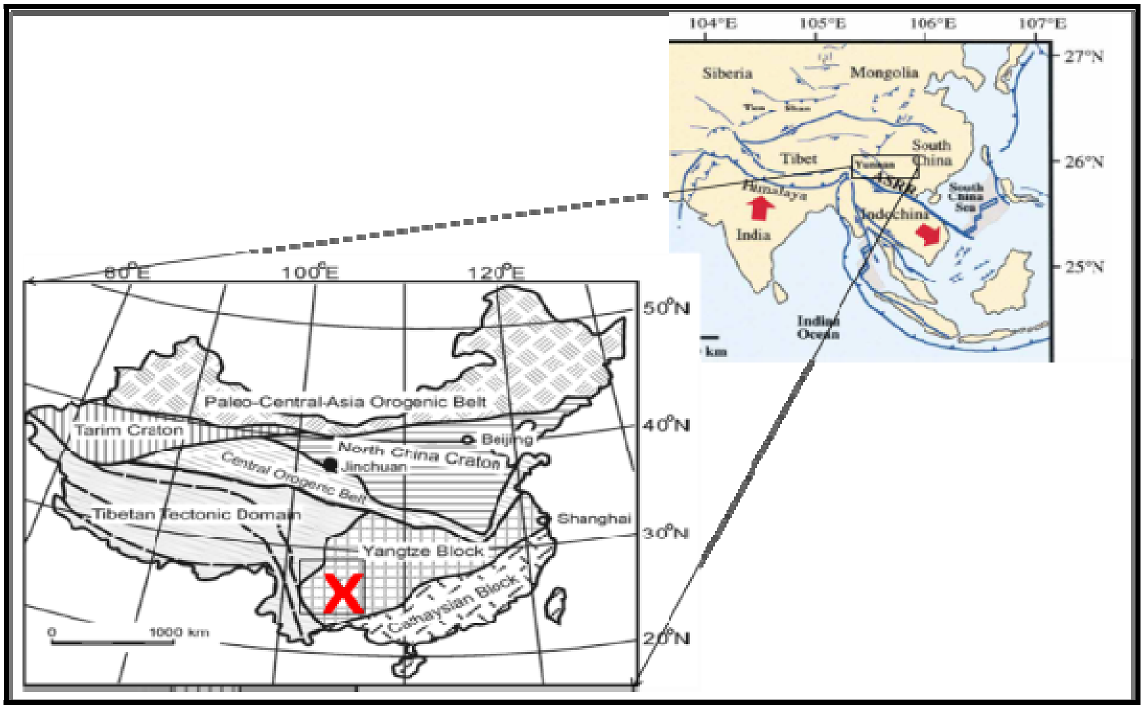

Figure 3: Location of the Emeishan Large Igneous Province marked with X. Modified after Zhang et al., (2009).

2.1 LITHOLOGIC AND STRATIGRAPHIC SEQUENCE

The basement (Kangding Complex) is a crystalline Proterozoic formation of granites, schists and gneisses (Wang and Zhou., 2006). Zhang et al., 2009 describe them as granulite-amphibolite facies metamorphic rocks and metasedimentary rocks intercalated with Neoproterozoic (~800 Ma) granites.

Overlying the crystalline basement is a late Middle-Permian shallow water carbonate succession comprising the Quixia Formation and the Maokou limestone Formation (Peate and Bryan 2008).

The limestones comprise bedded to massive fossiliferous limestone units which have been divided into three different biostratigraphic units based on the inherent fossil material, and can be correlated throughout most of southern China (He et al., 2003). They are from the bottom to the top, *Neoschwagerina simplex*, *Neoschwagerina craticulifera-Afghanella schencki*, and *Yabeina-Neomisellina* zones as the topmost. The thickness of the limestone package ranges from 250-600m with an average of about 350m (Peate and Bryan 2008; He et al., 2003; Figures 4 5).

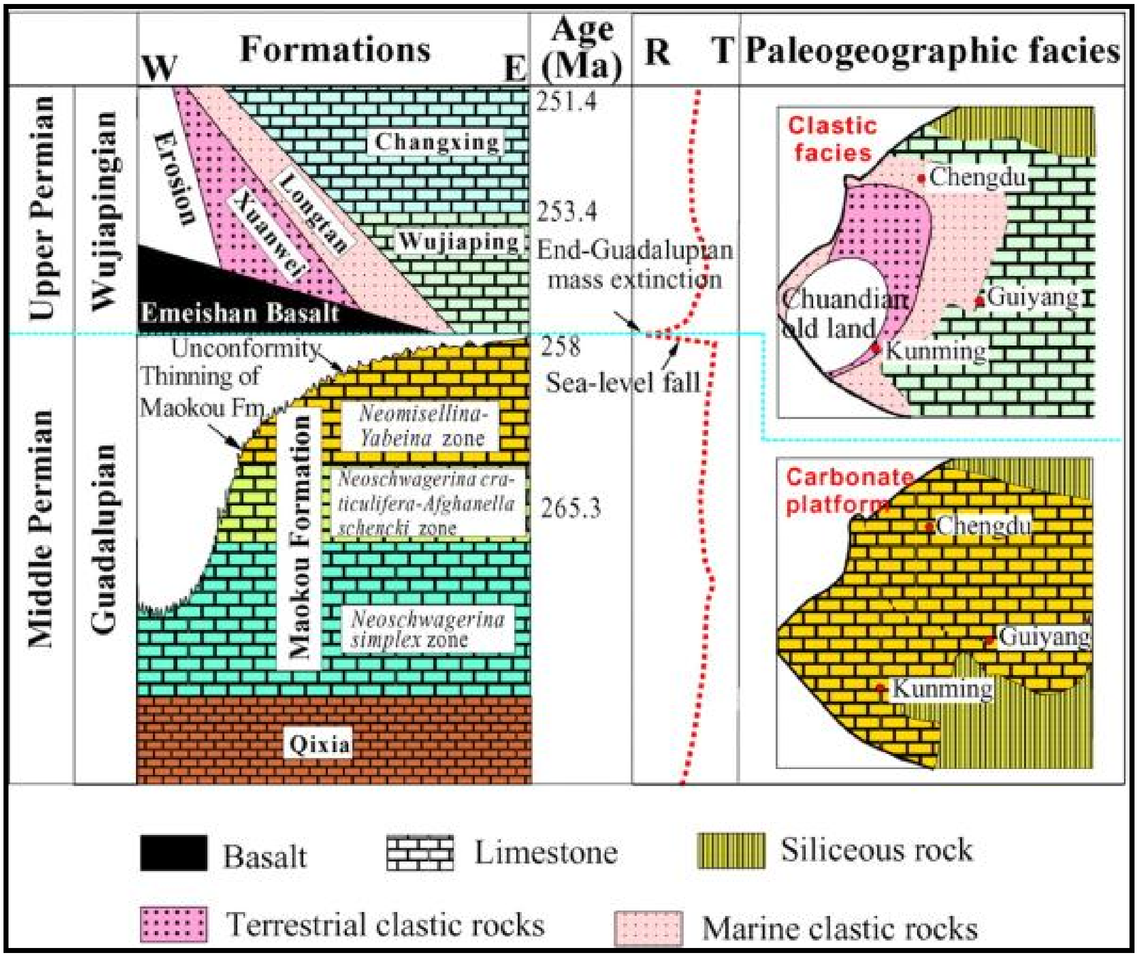

Figure 4: Stratigraphic sequence of the Permian Formations preceeding the ELIP, and paleogeographic pattern across boundary between middle Permian and Upper Permian rocks in Emeishan Large Igneous Province, Xu et al., (2004).

Differential thinning in a west-east cross section (He et al, 2003; He et al., 2006) and preferential erosion of the upper limestone biostratigraphic units of the Maokou limestone gives evidence to the mantle plume theory that is believed to have formed the flood basalts (Peate and Bryan 2008).

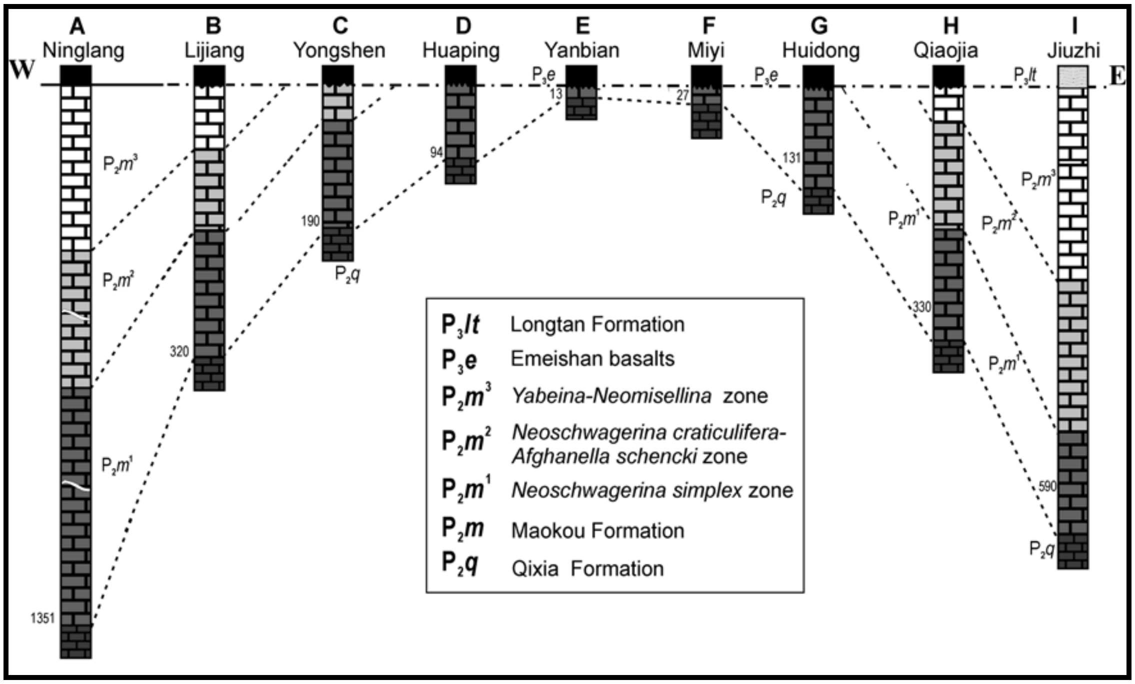

Figure 5: Biostratigraphic correlation of the Maokou Formation in the ELIP along west-east oriented traverse. Number next to sections represent the thickness of the formation. Vertical scale is the same for each section. Adapted from Xu et al., (2007).

The Maokou Limestone Formation is in turn overlain by late Permian Emeishan flood basalts with SHRIMP zircon U–Pb age of approximately 260 Ma (Zhou et al., 2008) A subaerial erosional-unconformity represented by a basal conglomerate marks the contact between the Middle Permian Maokou limestone and the late Permian flood basalts. The subaerial uncomformity is marked by palaeo-weathering and karst paleotopographic features preserved from the domal uplift and extending to the outer areas of the dome (Pirajno, 2013; Xu et al., 2007). This paleokarst unconformity was in turn covered or infilled by the Emeishan basalt and tuffs, suggesting that uplift and erosion occurred prior to the eruption of the ELIP (He et al., 2010).

The volcanic successions of the ELIP are overlain by Late Permian/ Triassic to Quartenary clastic sedimentary rocks (sandstone, siltstone, limestone and conglomerates, Xiao et al.,

2003) of the Xuanwei, Longtan and Wujiaping Formation (Pirajno, 2013; He et al., 2003; Xu et al., 2007). Basal conglomerates and relict gravels along the unconformity are usually cemented by basaltic lavas, tuff and pyroclastics (He et al., 2003). Provenace analysis on the basal gravels of the unconformity suggest the source to be the uppermost layers of the Maokou Formation eroded during and or following the uplift (Xu et al., 2007).

The ELIP (Fig 6) is divided into three approximately concentric zones corresponding to crustal thickness and the degree of crustal uplifting before the Emeishan eruptions (He et al., 2003; Xu et al., 2004) from the central to the outer zone with progressive thinning of the crust away from the plume head (Shellnut and Iizuka, 2012).

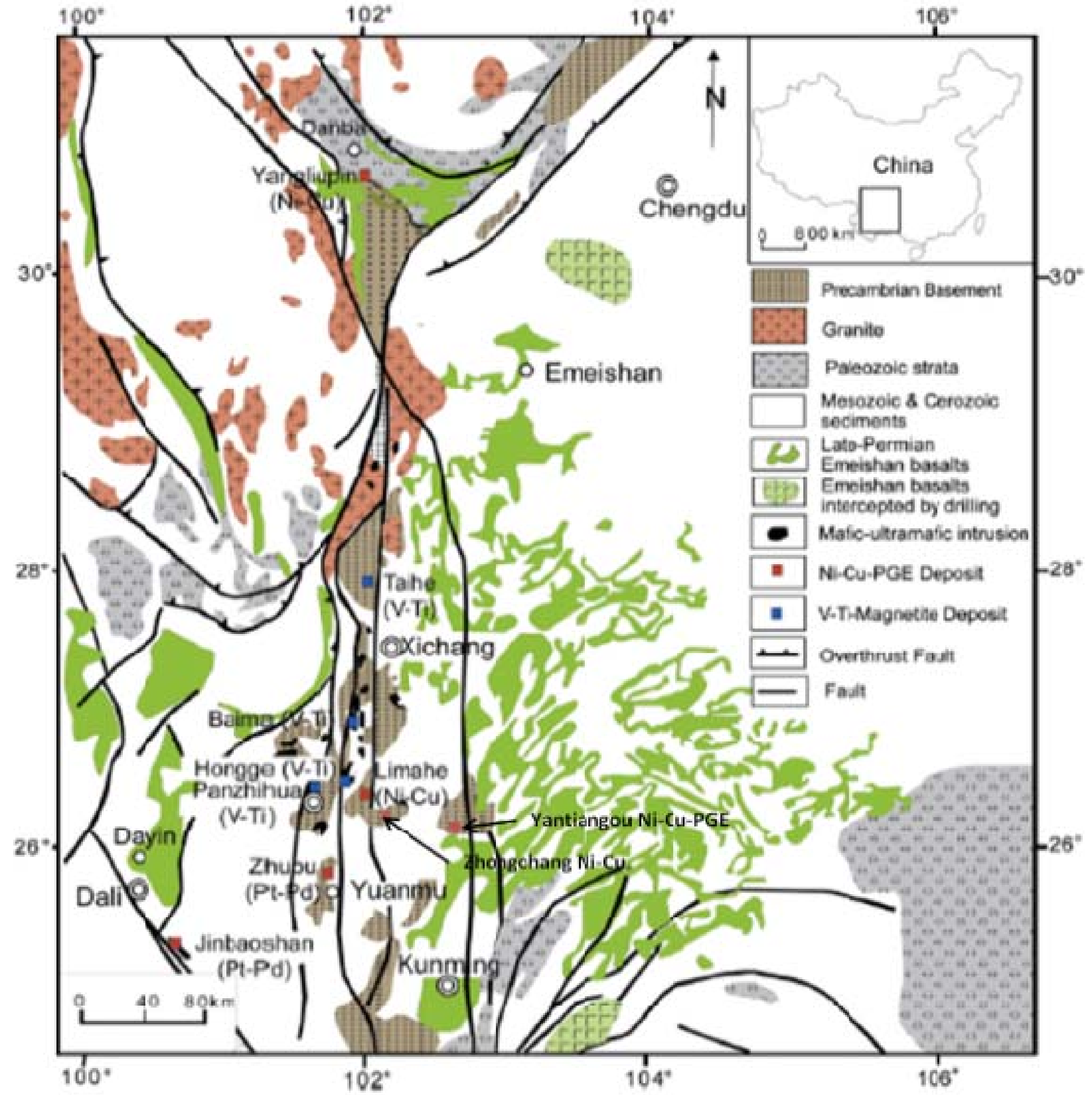

Figure 6: Distribution of the Emeishan continental flood basalt and some coeval mafic- ultramafic intrusions hosting Ni-Cu-PGE sulphides and V-Ti oxides. (Modified after Tao et al., 2010).

The central zone of the ELIP comprises discontinuous outcrops of a thick sequence of continental flood basalts with mafic-ultramafic extrusive rocks (Song et al., 2008, Munteanu et al., 2013). The occurrence of numerous large layered gabbroic intrusions, smaller ultramafic intrusions and syenitic-granitic intrusions is a prominent feature of the central zone. The outer zone comprises a relatively thin flood basalt sequence (less than 1000 m) and small mafic- ultramafic intrusions (Song et al., 2008).

The thickness of the flood basalts varies from over 5km in the west to about a few hundred meters in the east (He et al., 2003), and a decrease in age of the basalts has been noted from the west to the east (He et al., 2003; Munteanu et al., 2013).

2.2 EXTRUSIVE ROCKS

Three separate volcanic suites of the flood basalts have been identified in the ELIP (Fig 7) and have been described as having distinct sequences that can be identified as individual cycles (CGGJC 1986, p 29 in Munteanu et al., 2013). The volcanic sequences consists mainly of massive tholeiitic and alkaline mafic lavas with associated pyroclastic volcanic breccia and tuff, porphyritic basalts, trachites and rhyolites (Wang and Zhou, 2006; Pirajno, 2013). Alkali basalts have been documented in the eastern part, a second major stage occurs throughout the province comprising of porphyritic pyroxene to plagioclase bearing and fine grained basalts; and a third late stage comprises bimodal basalt- trachyte and basalt- rhyolite suite (Zhang et al., 2006). Ultramafic volcanic classified as picrites and komatiites have also been noted on the western part of the Panxi region, near the centre of the dome (Munteanu., et al 2013).

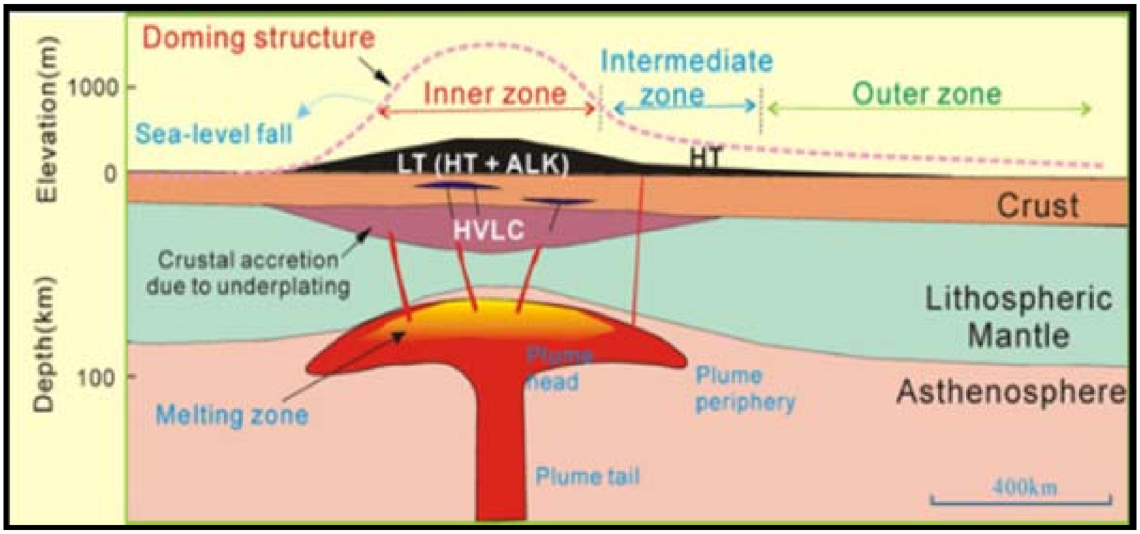

Figure 7: Surface uplift, generation of Emeishan basalts, and crustal accretion due to upwelling of mantle plume (Xu et al., 2004). HVLV- high velocity lower crust; HT- high-Ti basalt; LT- low-Ti basalt; ALK- alkaline series.

The flood basalt cycles seem to vary in terms of the Ti- content, between high Ti and low Ti compositions as observed in Zhang et al., (2006); Xiao et al., (2004); Xu et al., (2010). There is a noted bimodal assemblage of rocks in the Panxi region in terms of mafic and felsic intusions, where felsic rocks were either derived from fractionation of the basaltic magmas or by magma mixing and or contamination with crustal rocks (Shellnutt et al., 2011).

2.2.1 High Ti and Low Ti Basalts

The western part of the ELIP lava succession is dominated by the LT lavas with minor HT lavas occurring in the uppermost sequence overlying the LT lavas. The eastern part of the ELIP comprises exclusively the HT lavas (Xu et al., 2001; Ali et al., 2005). Analyses of rare earth elements (Sm/Yb ratio and Nd isotope values) suggests that the LT and HT basalts resulted from magmas generated at different depths of mantle melting and variable thickness of the lithosphere beneath the western and the eastern parts of the ELIP during emplacement, resulting in different partial melts and degrees of crustal assimilation, and therefore showing variable isotopic signatures (Xu et al., 2001; Xu et al., 2007; Wang et al. 2007). The low-Ti series underwent significant crustal contamination indicated by negative Nb and Ti anomalies, favouring sulphide mineralization as opposed to oxide bearing intrusions with positive Nb and Ti anomalies.

The data presented by Xu et al., (2004) indicates that the low-Ti lavas were generated at 60-100 km depths and mantle temperatures in excess of 1500°C, and required 16% partial melting, while the high-Ti lavas were generated at 75-100 km depths, mantle temperature of less than 1500°C and at a partial melting of 1.5%.

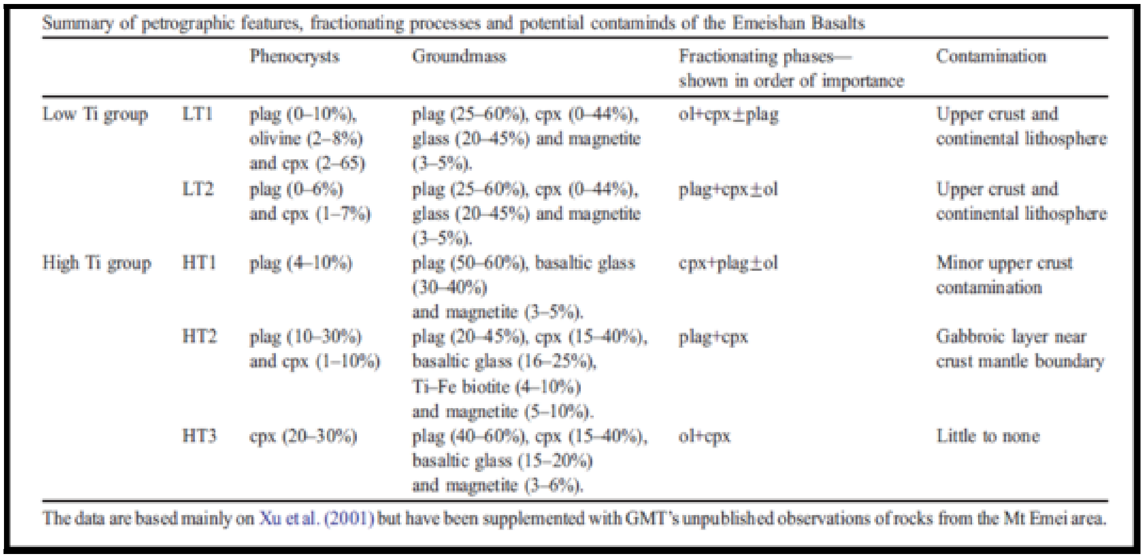

Summary of petrographic features, fractionating processes and potential contaminds of the Emeishan Basalts

		Phenocrysts	Groundmass	Fractionating phases—shown in order of importance	Contamination
Low Ti group	LT1	plag (0–10%), olivine (2–8%) and cpx (2–65)	plag (25–60%), cpx (0–44%), glass (20–45%) and magnetite (3–5%).	ol+cpx±plag	Upper crust and continental lithosphere
	LT2	plag (0–6%) and cpx (1–7%)	plag (25–60%), cpx (0–44%), glass (20–45%) and magnetite (3–5%).	plag+cpx±ol	Upper crust and continental lithosphere
High Ti group	HT1	plag (4–10%)	plag (50–60%), basaltic glass (30–40%) and magnetite (3–5%).	cpx+plag±ol	Minor upper crust contamination
	HT2	plag (10–30%) and cpx (1–10%)	plag (20–45%), cpx (15–40%), basaltic glass (16–25%), Ti–Fe biotite (4–10%) and magnetite (5–10%).	plag+cpx	Gabbroic layer near crust mantle boundary
	HT3	cpx (20–30%)	plag (40–60%), cpx (15–40%), basaltic glass (15–20%) and magnetite (3–6%).	ol+cpx	Little to none

The data are based mainly on Xu et al. (2001) but have been supplemented with GMT's unpublished observations of rocks from the Mt Emei area.

Figure 8: Summary of petrographic features and potential contaminants of the Emeishan Basalts. After Ali et al., (2005).

Therefore, the lithospheric signature observed in most LT magmas has been attributed to crustal assimilation during the evolution of the LT magmas (Fig 8). Owing to them being directly above the plume head, it is proposed that the LT lavas were generated in the plume axis region where the geotherm was higher and the lithosphere was thinner. The temperature in this axial region produced a high degree of partial melting of the mantle and continued on to assimilate the crust into the magma. HT basalts formed where the geotherm was lower, away from the axial area of the plume, and below much thicker lithosphere. The lower geotherm produced a low degree of partial melt which generated minimal amount of crustal assimilation during ascent (Xu et al., 2007).

The majority of εNd(T) values of Emeishan basalts range between -5 and +6 . The 'high-Ti' basalts have εNd(T) values between -3.6 and +4.8 which overlaps completely with the range of 'low-Ti' basalts (εNd(T)= -10.2 to +6.4). These values support the argument that 'high-Ti' and 'low-Ti' Emeishan basaltic rocks are derived from the same source and that the compositional differences are related to differing degrees of partial melting with or without assimilation of continental crust rather than to a two-source-assimilation model (Shellnutt and Jahn, 2011).

The compositions of the basalts as shown in Fig 9 defines a continuous trend of basalts from LT to HT, opposed to magma generated from different sources (Ho et al., 2011).

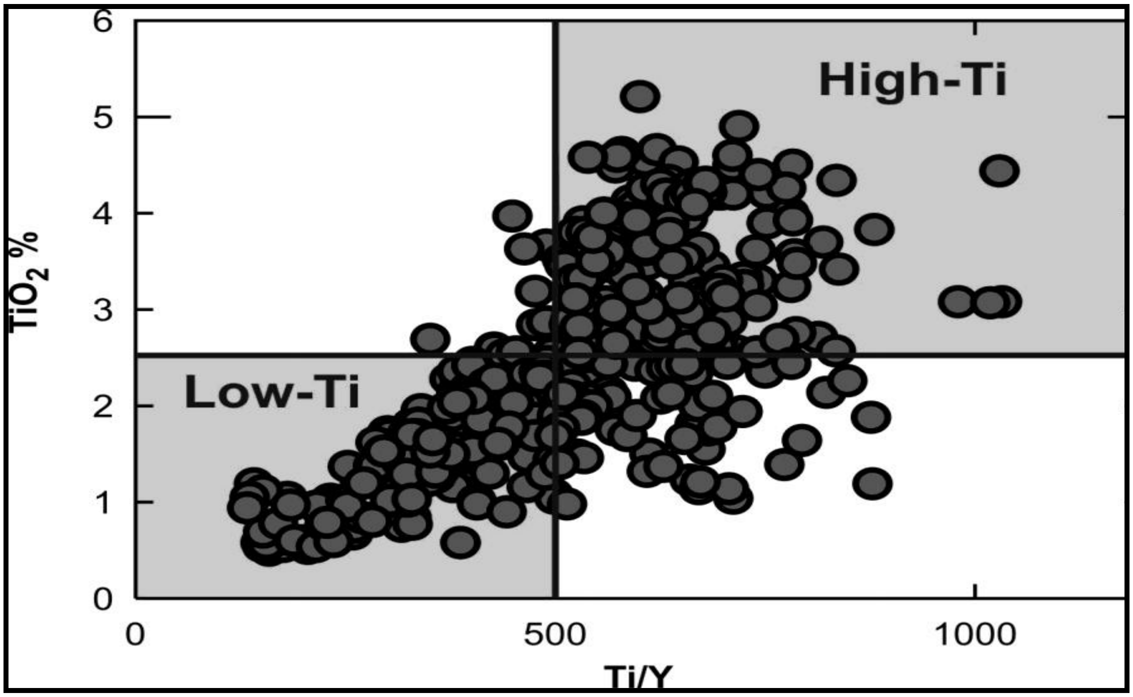

Figure 9: Plot of compositions of the Emeishan basalts (Munteanu et al., 2013). Data from Xu et al. (2001), Xiao et al. (2004), Song et al. (2008), Zhou et al (2006), Fan et al. (2008).

A different view from same source origin of the basalts is based on geochemical studies which indicate distinct mantle sources (Chung and Jahn, 1995; Xu et al., 2001, 2004; Fan et al., 2008). These views suggest that the LT basalts originated from subcontinental lithospheric mantle while the high-Ti magma was developed from a deep mantle plume under variable melting conditions (Chung and Jahn, 1995; Xu et al., 2001, 2004; Fan et al., 2008). Meanwhile, Shellnutt and Jahn, (2011) suggest that the basalts were derived from a compositionally and isotopically heterogeneous source formed by mixing between different components (e.g. sublithospheric mantle, lithospheric mantle, and subducted material) and further modified by crustal assimilation as a passive process which bore no major influence on the final composition of the basalts.

2.2.2 Picrites and Komatiites

These high temperature, low viscosity ultamafic extrusive units occur in the western part of the province, over the inferred centre of the plume head (Xu et al., 2007) around Lijiang and Dali localities (Kamenetsky et al., 2012). These high magnesium lavas are believed to be the products of undifferentiated primary magmas (Munteanu et al., 2013), and are considered to represent melting of hotter-than normal asthenosphere due to the presence of a mantle plume

(Chung and Jahn, 1995; Chung et al., 1998; Song et al., 2001; Ali et al., 2005). The occurrence of picrites in the inner zone is consistent with a hotter mantle beneath the plume centre than beneath the plume periphery (Xu, et al 2004).

Picrites are defined as having >18 wt % MgO with 1-2 % total alkalis and komatiites as having > 18 wt % MgO with < 1% total alkalis according to the IUGS classification (Kerr and Arndt, 2001 in Fig 10). Petrogenetically related basalts containing 12-18 % MgO are described as komatiitic (Sproule et al, 2003). Although high Mg (25-32%) komatiites occur exclusively in the Archean greenstone terrains, low Mg (18-25%) komatiites occur, albeit rarely, in regions of Proterozoic and younger age (Sproule et al, 2003; Zhang et al, 2006). The picritic/komatiitic flows are composed of a fine grained unaltered and probably originally glassy matrix with a highly porphyritic texture containing 7-15 % modal phenocrysts of forsteritic olivine, plus minor diopsidic clinopyroxene (Zhang et al., 2005; 2008).

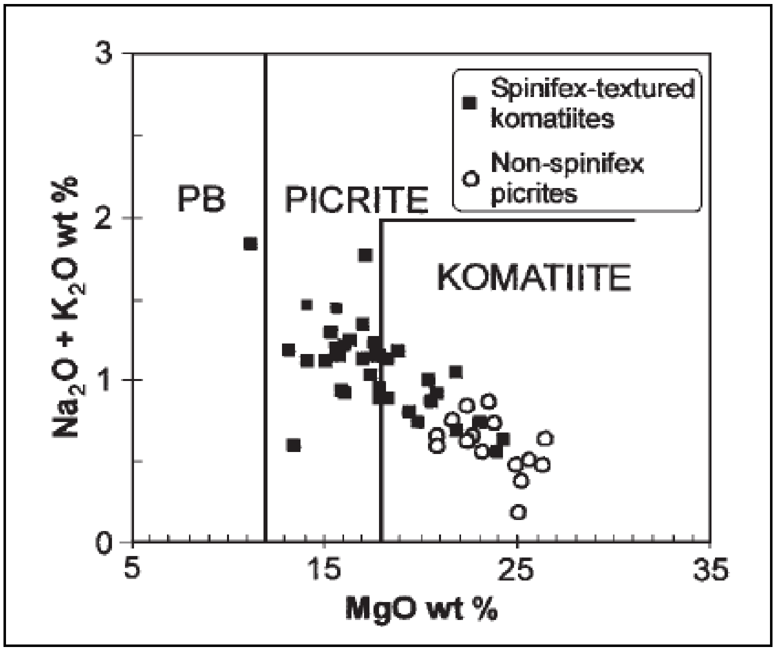

Figure 10: Plot of total alkalis vs MgO showing the classification fields proposed for high-Mg rocks by the IUGS subcomission (Le Bas. 2000, Adapted from Kerr and Arndt., 2001).

2.3 INTRUSIVE ROCKS

Mafic- ultramafic layered complexes, dykes and sills, as well as some felsic intrusions occur in the ELIP (Pirajno, 2013).The mafic- ultramafic complexes are located along north- south trending faults which occur close to the inferred domal uplift/ central part of the ELIP. The faults have resulted in the exposure of Precambrian basement and the Emeishan mafic-ultramafic complexes from the lower levels (Pirajno, 2013).

The compositional variations in the rocks of the ELIP have been attributed to possible distinctly different sources, mantle plume, asthenosphere and or lithospheric mantle; or from a common source that underwent variable degrees of mantle melting and variable levels of crustal contamination. Non-mineralized intrusions are discussed below, while the mineralized intrusions are discussed under mineralization.

2.3.1 Granitic Plutons

These intrusions consist of variable compositions from peralkaline to peraluminous and metaluminous varieties (Shellnutt and Iizuka., 2012). The origin of these rocks remains controversial; Xu et al., (2010) and Shellnut et al., (2011) present three possible modes of formation. Models presented are; fractionation from mantle- derived basaltic magmas; magma mixing between crustal melts and primary basaltic magmas; or from partial melting of basaltic rocks in the lower crust or in the upper mantle. A ‘Daly Gap’ noted by Shellnutt et al., (2009), highlights that normal fractional crystallization of magma from mafic to intermediate to felsic rocks is not observed in the rocks of the ELIP. Rocks of intermediate composition are rarely found with the mafic/ ultramafic intrusions and the granitoid intrusions and therefore the normal fractional crystallization model of magma is deemed unsatisfactory.

Peralkaline and metaluminous rocks display mantle isotopic signatures and are derived from the ELIP mantle plume source, while the peraluminous granites have isotopic signature indicating derivation from melting basement rocks (Shellnut, 2007).

The granitic intrusions consist mainly of homogenous, micro-granular to coarse grained rocks containing quartz, alkali feldspar, plagioclase, hornblende, and mica (Ganino et al., 2008). The distribution of granitic plutons in the ELIP is presented in Fig 11.

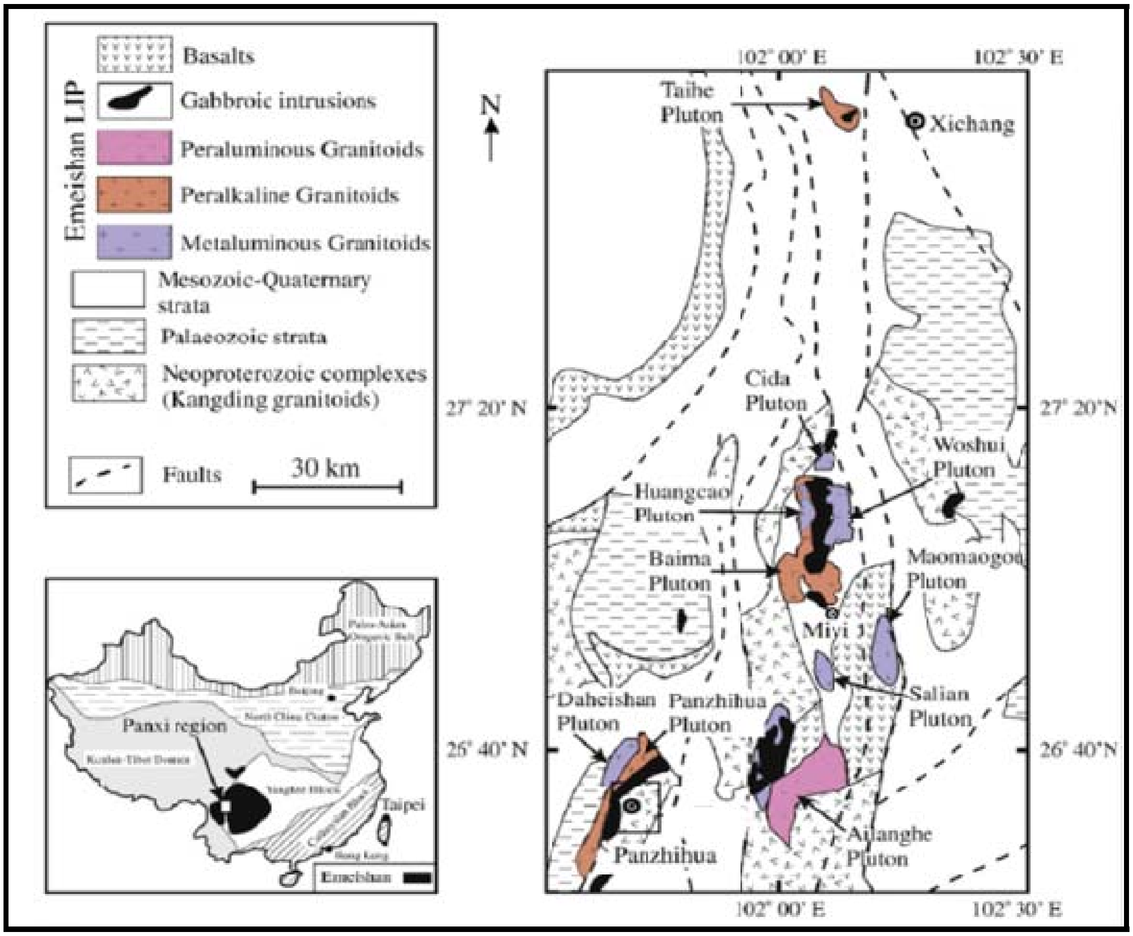

Figure 11: Distribution of granitic intrusions in the ELIP, (Shellnutt et al., 2011).

2.3.2 Dykes and Sills

Mafic to ultramafic dykes and sills have been mapped in the Panxi region, exposed by uplift and erosion along north-south trending faults (Ganino et al, 2008). Diabase dykes and sills with a similar age and geochemistry to the Emeishan flood basalts also occur in the region, e.g. the low-Ti Yanyuan diabasic dyke and high-Ti Shadou diabasic sill (Fan et al., 2008), while mafic diabase/ olivine dykes are seen cutting across granitic plutons (Zhao et al., 2010).

2.4 MINERALIZATION IN THE ELIP

Mineralized mafic- ultramafic intrusions are exposed along north-south striking faults and range from 10 km^2 to 100km^2 in the study area (Zhang et al., 2009). The intrusions can be divided into two types (Fig 12). These are small ultramafic sills and dykes that generally consist of peridotite, olivine, pyroxenite and gabbro and they often host magmatic Cu-Ni-PGE bearing sulphide deposits. A second type of intrusive bodies comprises large mafic layered intrusions that are host to the giant Fe-Ti-V oxide deposits. There exist also transitional type of intrusions which consist of Fe-Ti-V ore bearing gabbro in the upper part and Cu-Ni-PGE sulphide ore bearing peridotite and pyroxenite in the lower part. These intrusions have been dated at 251-263 Ma (e.g., Lo et al., 2002; Zhou et al., 2002; 2008), which is roughly consistent with the age of the flood basalts (Zhang et al., 2009).

Magmatic ore bodies in the Emeishan Large Igneous Province include the Ni-Cu-PGE sulphides mineralisation at Baimazhai, Yangliuping and Limahe, and the PGE dominated deposits Dayanzi and Jinbaoshan deposits. The gabbroic intrusions that host the Fe-Ti-V oxide deposits are also somewhat enriched in PGE (Pirajno, 2013).

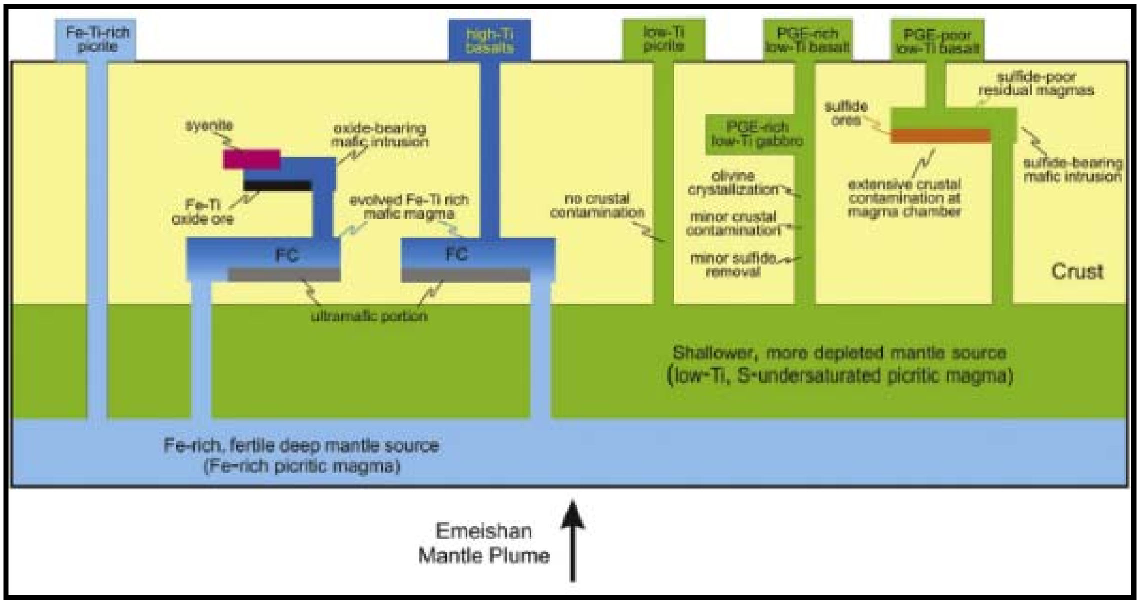

Figure 12: An integrated model for the ELIP magmatism that produced various rock types and associated deposits. High- Ti basalts experienced fractionation of olivine and chromite under S-undersaturated conditions and are associated with oxide bearing intrusions. Low- Ti rocks formed by olivine dominated fractionation under S- undersaturation or sulphide saturation, (Zhou et al., 2013).

2.4.1 Fe-Ti-V Mineralization

Five major Fe-Ti-V oxide deposits occur in the ELIP hosted in large layered mafic intrusions. They make up a 200 km-long belt (Zhong et al., 2005; Pang., 2008) in the central western portion of the province. These are Panzhihua, Hongge, Baima, Taihe and Xinjie and they are associated and aligned along major N–S trending faults in the middle zone (Zhong et al., 2005). Xinjie and Hongge are however examples of transitional type intrusions that host Fe-Ti-V oxide deposits and Cu-Ni-PGE sulphide deposits at different stratigraphic levels (Zhong et al., 2005; Zhang et al., 2009).

These oxide mineralization bearing intrusions represent the largest resource of its kind in China. The Panzhihua deposit alone contains 1333 million ton ore reserves of 43 wt% FeO, 12 wt% TiO_2 and 0.3 wt% V_2O_5, which makes China a major producer of these metals (Pang., 2008).

Other deposits being mined are Hongge, Baima, and Taihe. Two smaller deposits, Anyi and Mianhuadi are also currently being mined and they occur outside of the region previously believed to exclusively host Fe-Ti-V deposits (Zhou et al., 2013).

The Fe-Ti-V oxide-bearing intrusions are emplaced in the Neoproterozoic Dengying Formation, composed mainly of limestone, or in the Palaeoprotorezoic Hekou Formation, composed of meta-sedimentary-volcanic rocks (Xing et al., 2012). The ore occurs as massive and semi-massive conformable masses in lower parts of layered mafic–ultramafic intrusions (Pang et al., 2010) while rhythmic layering of oxide-rich and oxide-poor layers commonly alternate in the upper parts comprising plagioclase, clinopyroxene, olivine and magnetite (Xing et al., 2012).

The formation of these deposits is thought to be consistent throughout the province due to type similarities (Shellnutt and Zhou., 2007). These are thought to have formed through the separation of an immiscible oxide melt and crystallization from gabbroic magma (Zhou et al., 2013; Howarth et al., 2013) due to their close association with syenitic plutons and high-Ti flood basalts (Zhou et al., 2013).

Shellnutt and Jahn (2011), suggested formation of the deposits through settling and sorting of dense cumulous Fe-Ti oxide in magma as well as in situ, on contact crystallization of titanomagnetite. Ganino et al. (2008) and Zhang et al., (2009) proposed that the formation of Fe-Ti oxide ores resulted from early crystallization of parental Fe–Ti-rich melt, and that magnetite will segregate to the bottom if crystallized early due to its high density as demonstrated by the occurrence of massive titanomagnetite masses in the lower parts of the intrusions. Pang et al., (2010) identified the occurrence of rare Cr-bearing titanomagnetite (Cr_2O_3=1.2-10.7 wt %) in the intrusions as consistent with early crystallization of Fe-Ti oxides.

2.4.2 Ni-Cu-PGE Mineralization

The Emeishan Large Igneous Province hosts a number of magmatic sulphide deposits in small mafic –ultramafic intrusions in the central and outer zones in the northern and southern margins (Song et al., 2009). These bodies have variable metal contents and are made up of peridotite to pyroxenite with cumulus olivine and cumulus to intercumulus pyroxene with accessory chromite inclusions and grade into gabbro and diorite (Munteanu et al., 2013).

Four genetic types of magmatic sulphide mineralization have been identified in the Emeishan large igneous province. These are: 1). Ni-Cu-(PGE) sulphide deposits produced by in-situ sulphide segregation; 2). PGE-enrich layers within layered intrusions; 3). Ni-Cu sulphide mineralization related to sulphide-bearing mush; and 4). PGE sulphide mineralization distributed throughout ultramafic rock. The distribution of the sulphide mineralization is associated with the dynamic activity of the mantle plume (Song et al., 2005).

Song et al., (2008; 2009) divided the sulphide intrusions as follows:

- rich in Ni, Cu and PGE, such as Nantianwan, Yangliuping and Qingkuangshan containing sulphide ores with more than 10 vol.% sulphides (0.1-6.2 wt.% Ni, 0.03-11 wt.% Cu) and moderate PGE contents (0.1–5 ppm Pt, 0.01–1.8 ppm Pd, 0.5 ppm Ir);
- rich in Ni and Cu but PGE poor such as Limahe, Baimazhai, Qingshuihe, and Hetaoshu with sulphide-rich ores containing more than 10 vol.% sulphides (0.1–4 wt.% Ni, 0.02–6.5 wt.% Cu) but extremely poor in PGE (<0.2 ppm Pt and <0.3 ppm Pd, <0.007 ppm Ir);, and
- rich in PGE but Ni and Cu poor such as Jinbaoshan, Zhubu and the Yingfeng deposits bearing low sulphide contents (~1 to 2 vol.%) and very high Pt and Pd (0.3 to 10 ppm) and Ir (0.02 to 0.5 ppm).

Ore forming minerals in magmatic sulphide deposits are principally pyrrhotite ($Fe_{1-x}S$ (x=0-0.2)), pentlandite ($(Fe, Ni)_9S_8$), chalcopyrite ($CuFeS_2$) with PGEs contained in some sulphides, arsenides, tellurides, antimonides, bismuthinides and as alloys (Schulz et al., 2010). Cobalt (Co) is found in pentlandite and most deposits also contain 1- to 15-% magnetite (Munteanu et al., 2013).

CHAPTER 3 ORE GENETIC MODEL

Magmatic Ni-Cu-PGE sulphide ores are formed by the equilibration of immiscible magmatic sulphide and komatiitic to basaltic magma (Naldrett, 2004). These deposits can be classified into three types based on variable factors that induce sulphide saturation. The different modes are fractional crystallization, crustal contamination (Li et al, 2001), and magma mixing (Piña et al., 2011). These processes act to induce sulphide saturation in magma upon intrusion and together with magma chamber dynamics, subsequent physical and chemical processes (e.g. changes in chamber geometry or loss in velocity of magma), act to form ore deposits (Lightfoot, 2007).Magmatic ores are characterised by chalcophile elements that strongly partition into a sulphide liquid that segregates from magma (Li et al, 2001).

Naldrett (2004) and Li et al., (2001) note that magmatic Ni-Cu-PGE sulphide deposits can be divided into two major groups, the Ni-Cu deposits which are rich in sulphide with ore containing (20-90) % sulphide, which have PGE as a by product, and the PGE deposits which are sulphide poor, with ore containing (0.5-5) % sulphide with Ni and Cu occurring as by products. Dynamic magmatic systems that experience repeated surges and replenishments of magma promote development of economic deposits through increased interaction between sulphide liquid and silicate magma, therefore, concentrating and making available chalcophile elements to sufficient levels for reaching economic grades (Schulz et al., 2010).

In order for an ore deposit to form, magma must reach sulphide saturation. When the immiscible sulphide droplets segregate from the melt they scavenge Ni, Cu and PGE. Normal fractionation process of mafic- ultramafic magmas forms only small quantities of immiscible sulphide, consequently, other factors are required more often than not to increase the sulphide quantities and produce economic metal tenors (Schulz et al., 2010). Controls that play an important role in the formation of ore deposits that are intrinsic to the magma composition are temperature, viscosity, volatile content (Arndt et al., 2005). External controls of the Ni-Cu-PGE deposit formation are the geodynamics of magmatic systems such as the conduit system that provides pathways to emplacement mode of emplacement as well as the degree of interaction with sulphur rich crustal rocks (Lambert et al., 1998). High temperature low viscosity magma that incorporate crustal rock through high temperature melting and turbulent flow e.g komatiites and tholeiitic picrites are more capable of forming Ni-Cu-PGE deposits.

Lower-temperature, volatile rich alkali picrites and basalts have less ore forming potential (Arndt et al., 2005).

The enrichment of minerals to economic proportions ultimately depends on: composition of the parental magma; preferential partitioning of the different elements into sulphide/ silicate; the degree and stages of sulphur saturation in the melt; and the effective mass of silicate magma with which a given mass of sulphide has equilibrated defined by Campbell and Naldrett (1979) as the R-factor.

R = mass of silicate melt / mass of sulphide melt

Low R-factors occur in environments with low silicate to sulphide ratio as in dynamic magma chambers, and result in attainment of relatively low metal concentrations. These are associated with higher proportions of sulphide minerals and low PGE concentrations. High PGE concentrations are attained in high R- factor settings as when sulphide liquid segregates in a large chamber (Li et al., 2001; Maier et al., 2004)

3.1 SOURCE OF MAGMA

Ni-Cu and PGE will tend to be retained in the mantle during partial melting under sulphur saturated conditions because of their very high sulphide/ silicate melt partition coefficients (Keays and Lightfoot 2010). At least 25% partial melting is required in mantle with 250 ppm sulphur to produce sulphur undersaturated and PGE undepleted primary magma (Song et al., 2009; Maier., 2005). These magmas are rise up due to lower densities than the unmolten surrounding rocks (Arndt et al., 2005).

The PGE contents in sulphide ores are strongly dependent on metal compositions in the parental silicate magmas and the ratios between sulphide liquid and silicate magma, defined as R-factor (Campbell and Naldrett., 1979). However, PGE abundances and R factors may vary for each pulse of parental magma involved in the magmatic system. In addition, contents of Ni, Cu, and PGE in the sulphide ores may be affected by the differentiation of the sulphide melt (Song et al., 2008, 2009).

Primary magmas derived from a high degree of partial melt (>25-30%) are fertile in Ni, Cu and PGE (Li et al., 2001). These will often be sulphur undersaturated as they rise into the crust and through fractional crystallization, contamination with the crustal material, assimilation of sulphide bearing sedimentary rocks, may attain sulphide saturation. The sulphide rich fraction will scavenge chalcophile elements, Ni, Cu and PGE in according to their respective partition coefficients.

3.2 TRANSPORTATION MECHANISM

Interaction of the magma with crustal rocks during ascent and / or emplacement plays a pivotal role in formation of magmatic sulphide deposits. Sulphur incorporation from outside the magma can induce sulphur saturation early in order to produce immiscible sulphide liquid. The stage at which sulphide immiscibility occurs is critical in that some metals will partition to the silicates, therefore, it is important for sulphide immiscibility to occur before crystallization of the silicates. This will facilitate partitioning of metals into the sulphides instead of silicates for example; the tendency of nickel to partition to olivine which can deplete Ni before interaction with sulphide liquid.

Interaction of sulphides with sufficient amount of magma is also important in concentrating chalcophile elements to economic levels. This can be enhanced through efficient flow dynamics; through turbulent versus laminar flow which increases interaction between sulphur and metals in a magma and a dynamic magma system increases interaction between sulphur and new surges of undepleted magma. These processes will act to increase silicate to sulphide liquid ratios as chalcophile elements partition preferentially into sulphide liquid than into silicate melt (Mathez, 1999; Barnes and Maier, 1999).

Fractional crystallization of silicates in magma can induce sulphide saturation as the volume of silicates to sulphur in the melt is reduced (Li et al., 2001).

3.3 ELEMENT PARTITIONING

Distribution or partition coefficient is described as the measure of the preference for an element (such as Ni, Cu, Pt, etc.) to enter a particular physical phase (such as a sulphide liquid, in preference to a silicate liquid, Li et al., 2001).Partition coefficient between a sulphide melt and a silicate melt is calculated as:

$D^{sul/sil}$ = concentration of element in sulphide melt/ concentration of element in silicate melt.

- Where D<1, the elements are *incompatible* and concentrate in the residual melt (e.g. K, Rb, Li, Sn, W, Ta).
- Where D>1, elements are *compatible*, crystallisation causes depletion in the residual melt.
- D depends on valency, co-ordination state, and ionic radius, (Mungall et al., 2005).

Partitioning between a sulphide melt and a silicate melt is dependent on temperature (T), oxygen fugacity ($f\,O_2$) and sulphur fugacity ($f\,S_2$) (Li et al., 2001).

Sulphur dissolves in silicate magma from ~1100°C followed by segregation of an immiscible Fe- rich sulphide liquid (FeS) from 1050°C (Fig 13). Sulphur dissolution and immiscibility are also dependent on oxygen fugacity (fO_2) and sulphur fugacity (fS_2) (Mungall et al., 2005). Crystallization of Fe-rich solid, monosulphide solid solution (Mss) occurs from 950°C, enriched in Fe, Co, Rh, Ru, Ir & Os while the residual liquid becomes progressively enriched in Ni, Cu, Pt, Pd and Au (Barnes et al., 1997). Cu trapped in the Mss exsolves out as chalcopyrite at lower temperatures, which migrates to grain boundaries and any excess sulphide liquid forms a Cu-rich liquid from which crystallises an Fe-poor intermediate solid solution (Iss). The partition coefficients for all the metals increase with bulk sulphur content as well as sulphur content of Mss (Li et al., 1996).

Ni is incompatible with mss at high temperatures and thus will be enriched in the residual sulphide liquids under normal $f\,O_2$ and $f\,S_2$. It is then incorporated into the mss towards sulphide magma solidus, resulting in Ni depletion in lower temperature mss cumulates (Mungall et al., 2005). Co is found in pentlandite and substitutes for Ni for up to a percent level (Barnes and Lightfoot., 2005).

The Fe-poor intermediate solid solution (iss) cools to form Cu-rich assemblages of chalcopyrite and bornite. Upon cooling of the mss, some of the PGE that are held in sulphide crystal structure are expelled, forming discrete minerals including sulphides, arsenides, tellurides, antimonides, and alloys. Platinum and gold occur primarily in discrete small PGM, ranging in size from tenths to tens of microns. Significant quantities of palladium can be held in solid solution in pentlandite (Zientek, 2012; Mungall et al., 2005). Any excess sulphur remaining forms late pyrite.

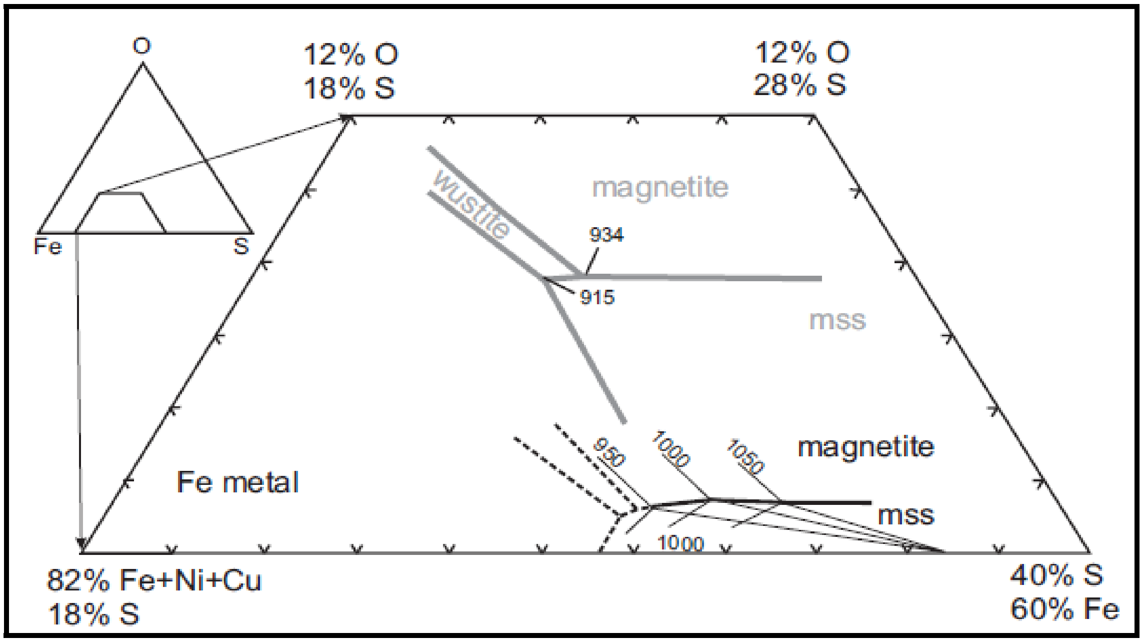

Figure 13: Fe–Ni–Cu–S–O system with typical magmatic compositions (wt %). Under normal conditions of sulphide segregation from basaltic magmas, the sulphide magma will have a composition close to the magnetite–mss cotectic. The magnetite–mss cotectics shown correspond to the Ni- and Cu- free subsystem Fe–S–O (grey line; Naldrett, 1969) or to the five-component system containing about 5 wt% each of Ni and Cu (black line; Mungall et al. 2005). Isothermal liquidus surfaces shown schematically for 950, 1000, and 1100°C (Mungall., 2005).

Partition coefficients for Ni and Cu between sulphide and silicate liquids are of the order of hundreds to thousands and in the orders of tens of thousands for the PGE (Mungall, 2005). The extremely high partition coefficient for PGE will lead to a significant drop/ depletion of PGE in the silicate melt even at small amounts of sulphide segregation (Zhang et al. 2005). Ni partitioning increases with partial melting and will continue to partition into the olivine even after all of the sulphide liquid has been consumed. Cu increases with partial melt until all of the sulphide liquid is consumed and subsequently drops with increasing partial melt. As the melt volume increases the concentration of Cu in the melt is diluted (Li et al., 2001). In addition to copper, nickel, PGE, and gold, sulphide ores contain minor amounts of silver, and metalloids such as arsenic, antimony, bismuth, and tellurium (Zientek, 2012).

3.4 ORE DEPOSITION

Sulphide deposition must be an effective process where sulphides are concentrated and restricted in a location where their abundance is sufficient to form an economic deposit (Maier et al., 2001). Structural traps, where the flow velocity of magma is reduced, form important sites for the collection of sulphides. Accumulation of sulphides is controlled by irregularities in the footwall such as potholes, cracks and undulating topography as areas where dense sulphides can settle down. Loss of velocity when a magma enters a large chamber from a narrow conduit also results in concentration of sulphides (Barnes and Lightfoot., 2005). Failure of restricted accumulation may result in a large volume of silica hosting the sulphides and the grade being uneconomic (Barnes and Lightfoot., 2005).

Ni sulphide deposits can be divided into massive, net textured or disseminated based on the sulphide content in the silicate matrix (Fig 14). Massive ores generally exceed 66% modal percent and tend to occur at the base of intrusion in depressions due to their high density. Net textured ores comprise 33-66% modal sulphide content forming an interconnected matrix in the host, while disseminated ores contain 1-33% sulphide and individual grains are not interconnected in the host rock (Barnes and Lightfoot., 2005; Schulz et al., 2010). Brecciated ores also form along contacts with the footwall and hangingwall comprising fragments of both the intrusion and the wallrock (Naldrett, 2004).

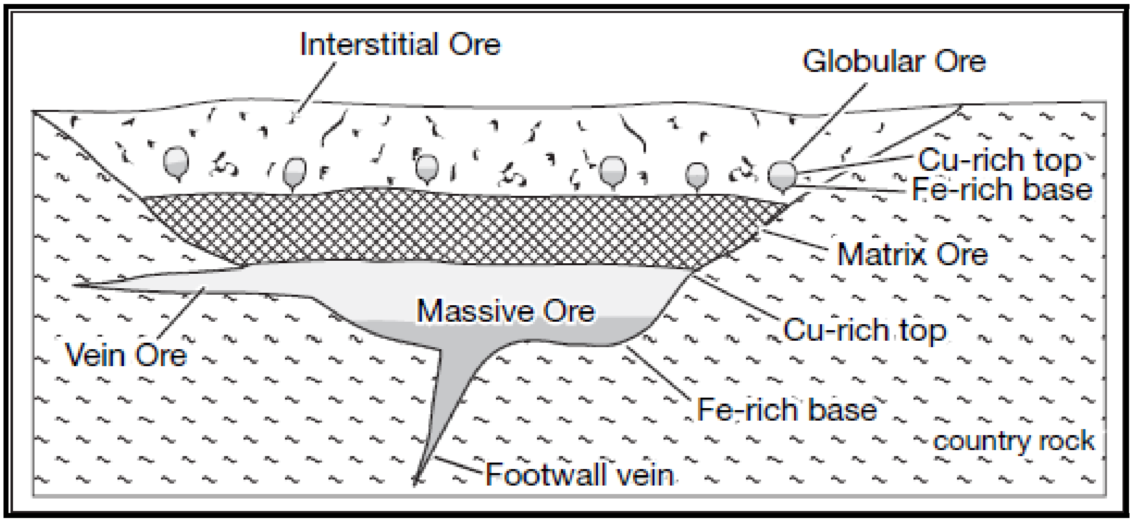

Figure 14: Idealised sketch of the relationship between massive, matrix, disseminated and vein sulphides (modified after Barnes et al., 1997b). Barnes and Lightfoot., (2005).

CHAPTER 4 METHODOLOGY

4.1 PETROGRAPHY

Petrographic analyses were conducted on thin sections under an optical microscope. Transparent minerals were studied under transmitted light, while opaque minerals were studied under reflected light. Composite lighting (transmitted + reflected) was used in identifying the silicates intimately associated with or hosting the sulphides. Photomicrographs were taken with the use of a Leica camera mounted microscope.

4.2 MINERAL CHEMISTRY

The composition of silicates, sulphides and oxides were measured with the electron microprobe equipment. EPMA (Electron Probe Micro-Analyser) data acquisition was performed at Rhodes University, Department of Geology, on a Jeol JXA 8230 Superprobe, using 4 WD spectrometers. The analytical conditions employed were: acceleration voltage 15 kV, probe current 20 nA and spot beam size (< 1 micron). Qualitative analysis (WDS total scan) used 50 ms dwell time, at 50 microns step. For each element, the quantitative analysis runs at 10 sec counting time on peak and 5 sec on each upper and lower background, respectively. Natural standards were used for measuring the characteristic X-rays. The ZAF matrix correction method was employed for quantification.

For element concentration below 5%, a large diffracting crystal with high sensitivity was used for quantitative analysis. The ZAF matrix correction method was used for quantification.

4.3 MINERAL CLASSIFICATION

The classification, determination and plotting of mineral compositions (i.e end members) was conducted using MinPet software (version 2.02) from microprobe analyses. The Ni and forsterite contents in olivine were used to determine the Mg # of the parental magma and the onset of fractional crystallisation of the olivine or sulphides. This was based on calculations on mineral probe data. All mineral and element analyses are calculated on an anhydrous basis.

4.4 WHOLE ROCK GEOCHEMISTRY

The contents of Ni, Cu, Co, S, Pt, Pd, were measured by ICP-OES and emission spectrometry in the Sichuan Bureau for Geology and Mineral Resources, China. Based on these contents, the metal tenors were calculated and used to estimate the depleted or undepleted natures of the parental magmas relative to the mantle. The mantle-normalised values of the metals (Ni, Cu, Pt, Pd) and the Cu/Pd ratios were also used as indicators of pre-emplacement sulphide saturation events in the evolution of the parental magmas. The plots were generated using Microsoft excel and Igpet software.

CHAPTER 5 PETROGRAPHY

5.1 ZHONGCHANG DEPOSIT

The Zhongchang deposit consists of mafic- ultramafic rocks emplaced into the Protorezoic dolomites and schists of the Huili group. It is funnel shaped with concentric gabbro, pyroxenite and peridotite zones from the outside to the centre. The Ni-Cu-PGE mineralization is hosted along the pyroxenite- peridotite contact, which is a transitional contact (Fig 15).

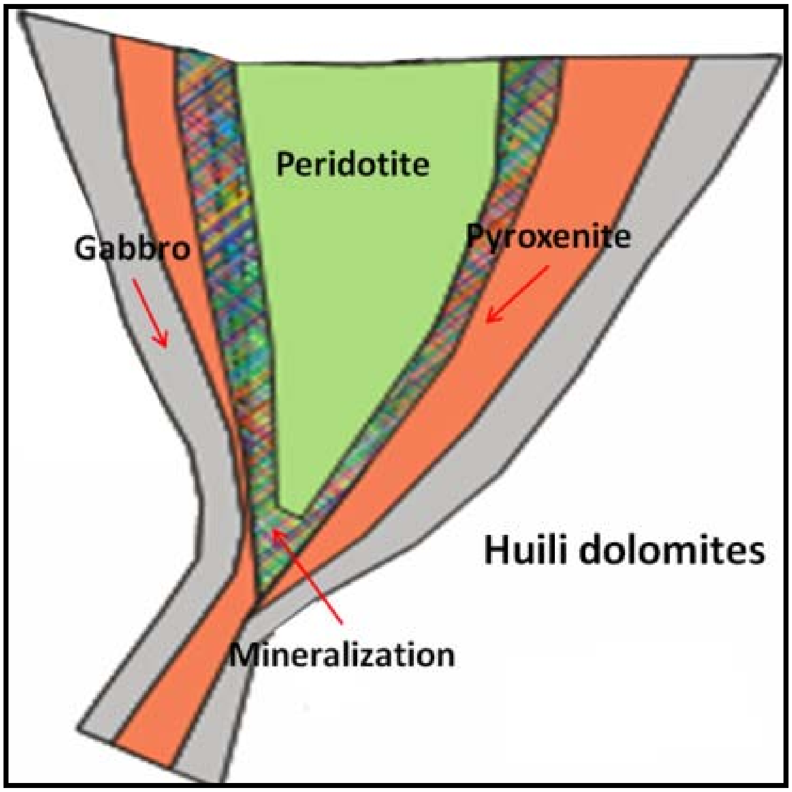

Figure 15: Schematic illustration of the Zhongchang deposit with concentric gabbro, (Sichuan Geological Bureau., 2013).

The rock forming minerals show slight alteration in some areas with the majority of the minerals showing no alteration. In the peridotite, olivine shows slight serpentinization while pyroxenes have been altered to hornblende along the margins. Primary hornblende also occurs in the peridotite and pyroxenite as euhedral crystals. The presence of these altered minerals suggests reaction with H_2O during emplacement or at a later stage.

5.1.1 SILICATE MINERALOGY

5.1.1.1 Peridotite

Peridotite is represented by samples **ZC1-3 & 10**. It occurs as a medium to coarse grained rock with equigranular texture (Fig 16). It comprises ~40-50% olivine formed as large grains or as smaller inclusions in clinopyroxene. There is an increase in grain size of olivine with decreasing pyroxene content in the peridotite. Clinopyroxene constitutes 30-40% of the rock volume and exists as medium sized grains (0.5-2mm). Hornblende and accessory chrome spinel, magnetite and ilmenite oxide minerals form 5-10% of composition and biotite occurs in trace quantities. These minerals occur interstitially to olivine and clinopyroxene.

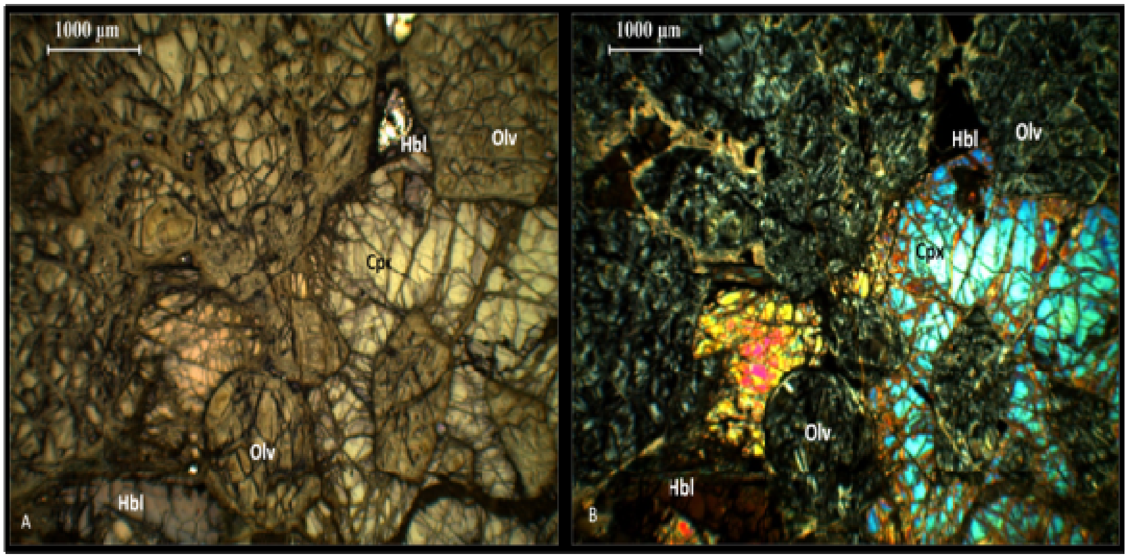

Figure 16: Photomicrograph of sample ZC 3- Zhongchang peridotite with olivine (olv), clinopyroxene (cpx), hornblende (hbl), a taken under parallel polars and b under crossed polarized light.

5.1.1.2 Pyroxenite

Pyroxenite occurs as a medium grained rock consisting of olivine, clinopyroxene, plagioclase feldspar, hornblende and biotite (Fig 17). It comprises 40-50% clinopyroxene occurring as medium sized to large grains (0.5-5mm) with large poikilitic grains forming inter-locking triple junctions. Olivine forms 10-20% as inclusions in clinopyroxene and has fine-medium sized grains. Hornblende occurs as euhedral grains and along margins with oxide minerals while anhedral plagioclase comprises ~30% of the composition. Accessory minerals are chrome spinel, magnetite, ilmenite, and biotite. Sample **ZC 6** represents the pyroxenite samples.

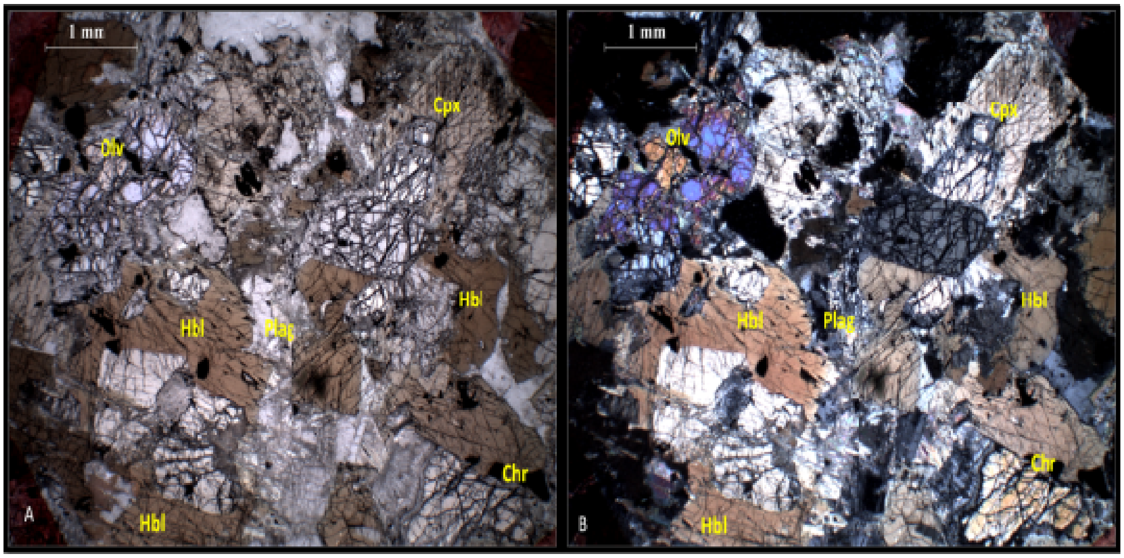

Figure 17: Sample ZC 6 displays medium grained Zhongchang showing adculmulate textured hornblende pyroxenite. Mineral present are olivine (olv), clinopyroxene (cpx) hornblende (hbl), minor ilmenite (ilm) and opaque minerals, a in plane polarized light and b, observed with crossed polarized light.

5.1.1.3 Gabbro

Gabbro occurs as the outermost zone of the intrusion as a medium to fine grained rock made up of feldspar, hornblende and pyroxene. These occur in almost equal modal proportions in the rock (Fig 18). Olivine forms 10-12% modal composition with the rest of the composition made up by accessory minerals. Feldspars have been altered to sericite in places and replaced by carbonates (calcite). Hornblende occurs as euhedral grains and as anhedral grains interstitial to pyroxene and feldspar. Carbonate minerals occur as euhedral grains with accessory oxides and mica forming the remainder of the rock. Pyroxene alteration results in formation of secondary anhedral interstitial hornblende. **Gabbro samples are ZC 4, 6, 7-9 &11**.

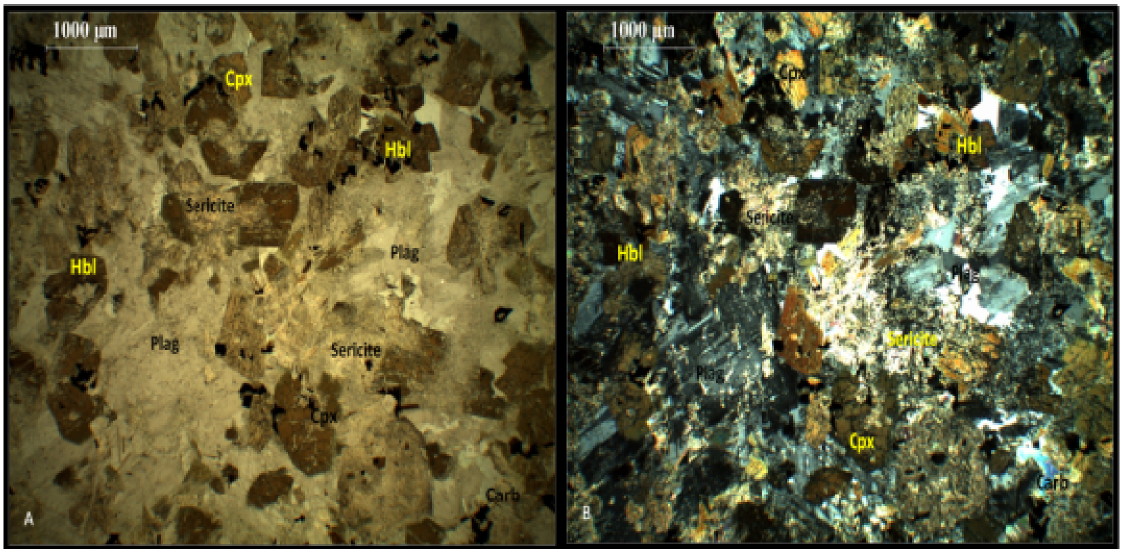

Figure 18: Coarse grained gabbro form Zhongchang (ZC 9) with plagioclase (Plag) , clinopyroxene (Cpx), hornblende (Hbl) and carbonate (Carb) grains. Sericite exists as fine grains where plagioclase has been altered and replaced, a in plane polarized light and b, in cross polarized light.

Figure 19 displays antiperthite exsolution of K-feldspar in plagioclase and grid twinning.

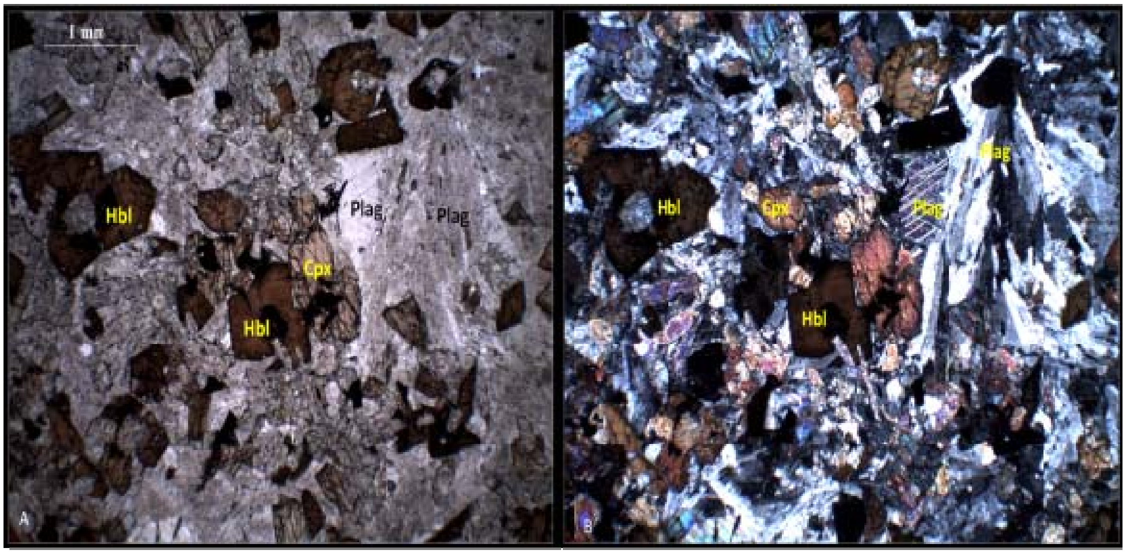

Figure 19: Granophyric textured gabbro with radial elongate plagioclase crystals and alkali feldspars displaying characteristic grid twinning in sample ZC 8, a in plane polarised light and b, in cross polarized light.

Plagioclase and pyroxene are partly altered containing secondary epidote; secondary chlorite also occurs between plagioclase crystals and carbonate in Fig 20.

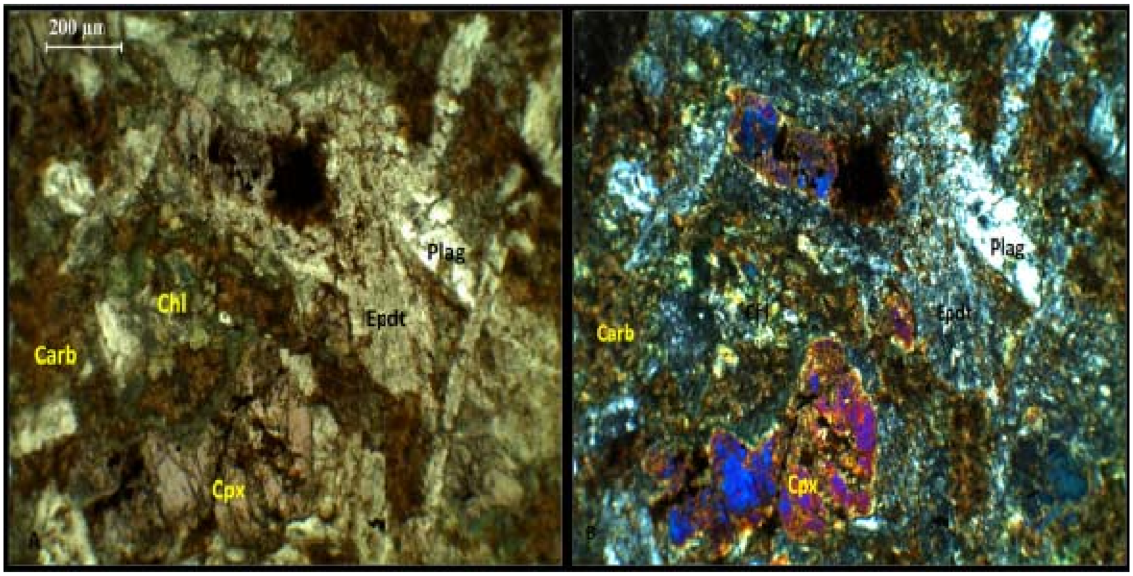

Figure 20: ZC 8 showing epidote on plagioclase and chlorite and carbonate alteration, a in plane polarized light, b under cross polars.

Very fine grained massive gabbro (Fig 21) occurs on the marginal facies. It consists of pyroxene, plagioclase, hornblende set in a fine matrix of secondary carbonate incorporated from the wallrocks. Pyroxene and feldspar grains occur as narrow elongate laths with interstitial carbonate, hornblende and oxide minerals.

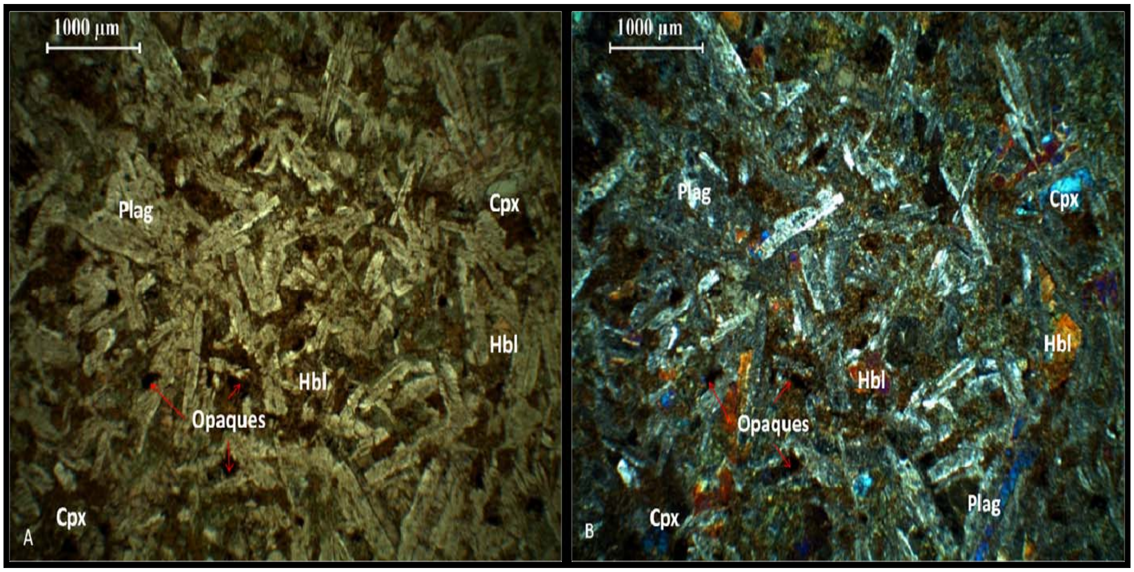

Figure 21: ZC 4 Microcrystalline gabbro/ microgabbro with euhedral elogate plagioclase and clinopyroxene laths in a hornblende and carbonate groundmass, a in plane polarized light and b, in cross polarized light.

Alteration is observed in some of the gabbro samples (ZC 5 and ZC 7) with hornblende forming elongated euhedral crystals (Fig 22). The plagioclase in these samples is almost completely sericitized and quartz from late stage fractionation is developed interstitial to the plagioclase. Carbonate minerals occur as replacement minerals to the pyroxenes which are not common in these samples.

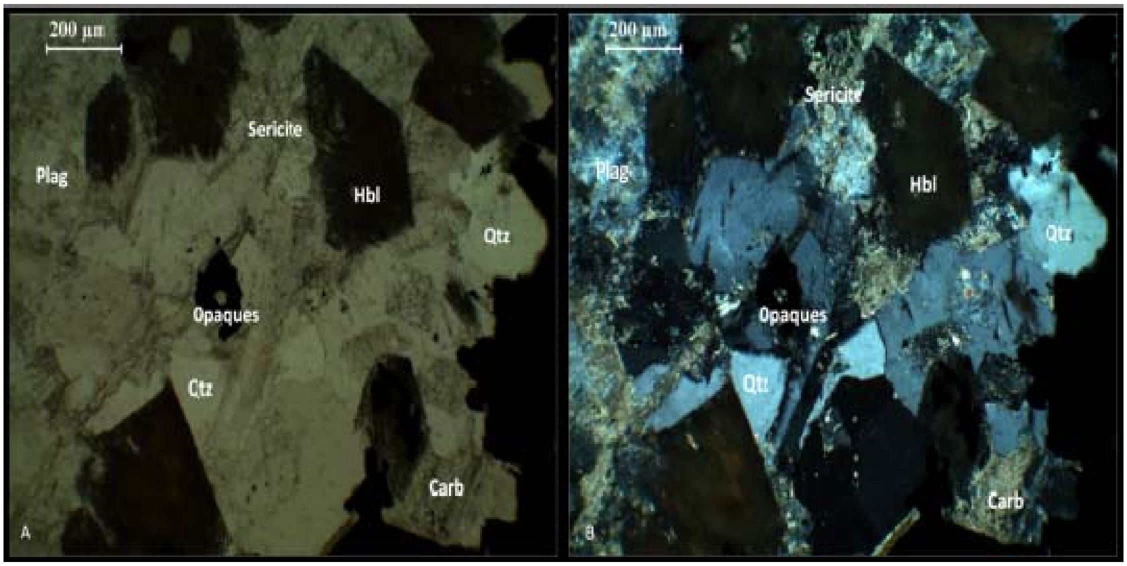

Figure 22: Sample ZC 5 with altered gabbro with hornblende (Hbl), plagioclase (Plag) , quartz (Qtz) and sericite. Annealing of minerals especially hornblende suggesting high T ductile transformation, a in plane polarized light and b, under cross polars.

5.1.2 ORE MINERALOGY

Sulphides occur interstitially to the other minerals in olivine and clinopyroxene. Main sulphide minerals are chalcopyrite, pyrrhotite and pentlandite with smaller amounts of lead and silver. PGE occur in trace quantities as Pt and Pd bismuthinides, arsenides and tellurides. Oxide minerals are also present in trace quantities; these are magnetite, ilmenite and chrome spinel.

Oxide minerals occur as accessory fine grained crystals in the form of ilmenite, magnetite and chrome spinels. These are enclosed in the olivine and pyroxene silicates or along silicate margins. Illmenite also forms exsolution lamellae along magnetite cleavage lines. The sequence for oxide formation appears to be chromite, magnetite and last, ilmenite.

Sulphide minerals occur as coarse, blebby and globular textured grains as well as large interstitial grains (Fig 23). These occur mainly as chalcopyrite> pyrrhotite> pentlandite, and pyrite crystals are not common. The sulphides are associated with olivine, clinopyroxene and hornblende; the mineralization sequence suggests early silicates crystallized before sulphides. Oxide minerals occur together with sulphide minerals although in smaller quantities.

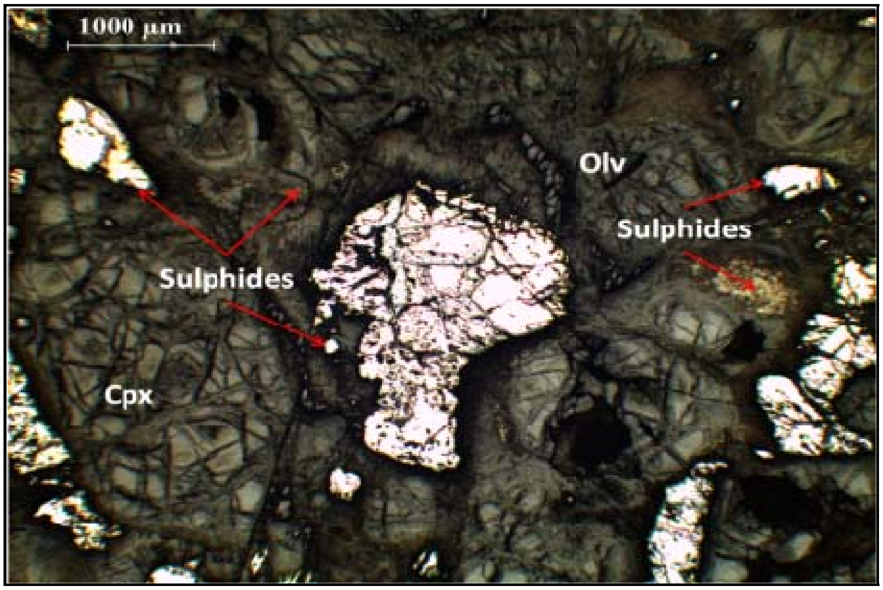

Figure 23: Photomicrographs of ZC 3 with sulphide mineralization occurring interstitially to olivine and clinopyroxene. Apparent blebby and globular texture of the sulphides is observed here. Picture taken in under composite lighting to show sulphides (opaque minerals) composited with transmitted light to show transparent minerals (silicates).

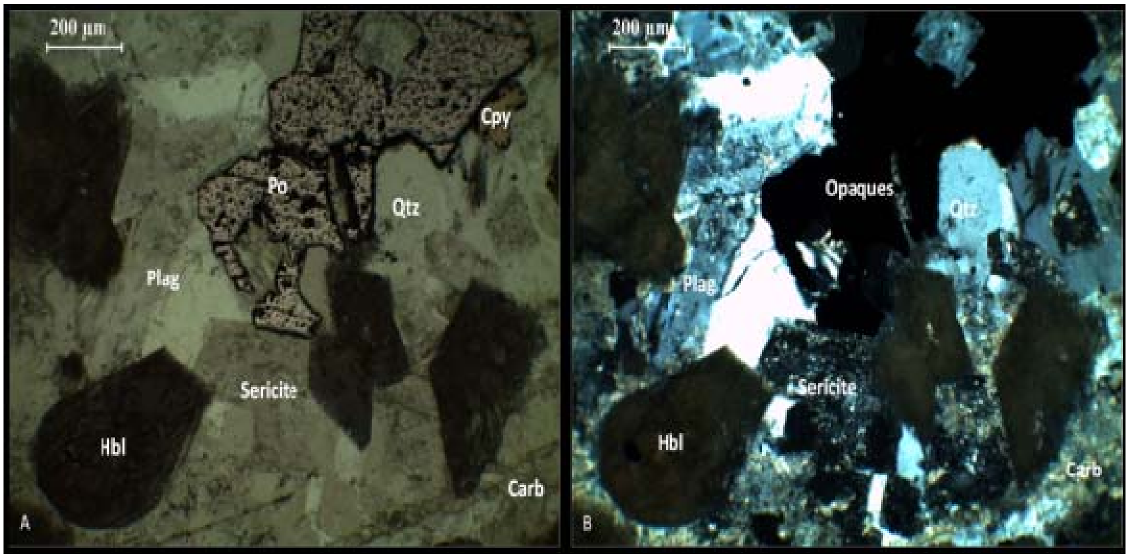

Figure 24: Sample ZC 5 with pyrrhotite and chalcopyrite occuring interstitially to sericitised plagioclase and interstitial secondary quartz, a, large crystal of Po (pyrrhotite) with smaller Cpy (chalcopyrite) grain seen under composite light in a, b in transmitted light with crossed polars shows sulphide grains as opaques minerals.

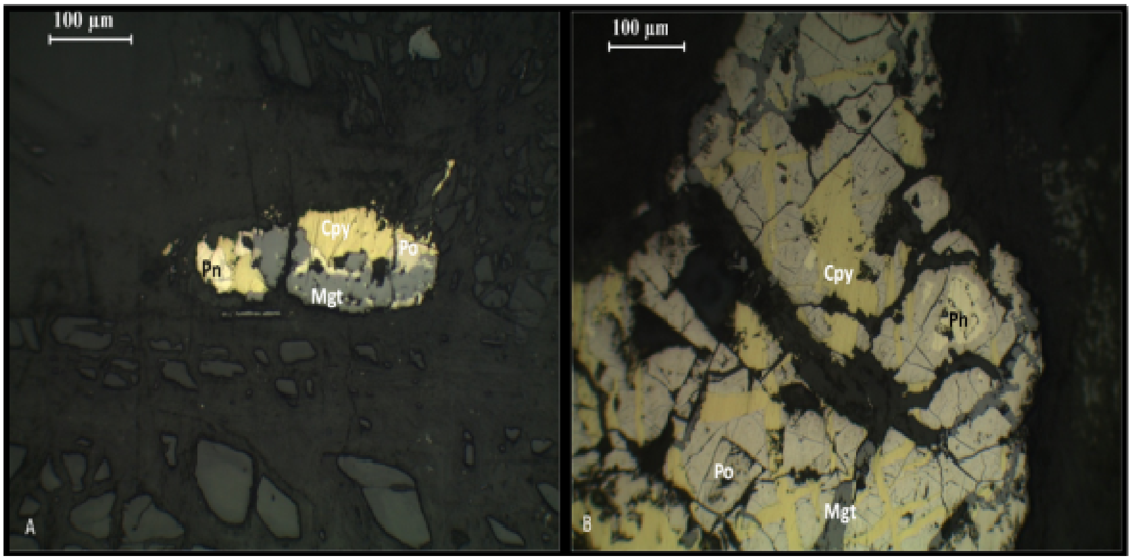

Figure 25: Pentlandite (Pn) seen with Pyrrhotite (Po), Chalopyrite (Cpy) and Magnetite (Mgt) under reflected light.

Chalcopyrite forms large anhedral grains >1000 µm and encloses smaller grains of pyrrhotite and pentlandite. Pyrrhotite forms subhedral to anhedral grains of up to >500 µm. Pentlandite occurs as small (>100µm) anhedral inclusions in chalcopyrite but is mostly associated with pyrrhotite (Figs 24, 25 & 26). Pyrrhotite is dominant in some sulphide grains (Fig 26 d), with surbodinate chalcopyrite Magnetite displays early phase coalescence as in occurs within sulphide grains, and some of it could be a product of pyrrhotite alteration.

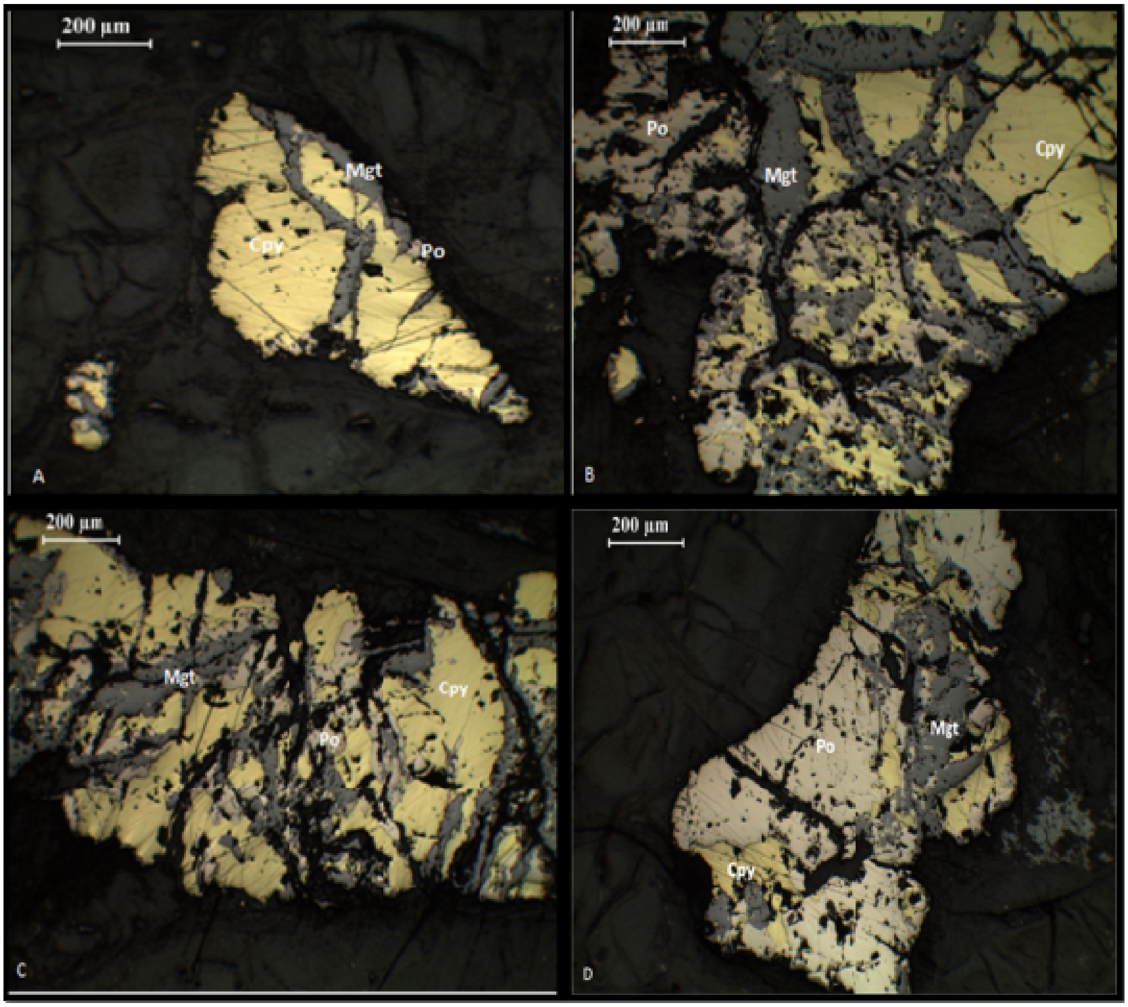

Figure 26: Sulphide mineralization in Zhongchang observed in reflected light indicating Cpy (chalcopyrite) as the dominant sulphide followed by Po (pyrrhotite) in a pinkish shade. Magnetite (Mgt) growths observed along sulphide fracture lines.

5.2 YANTIANGOU DEPOSIT

The Yantiangou deposit (Fig 27) is hosted in a 100-150m thick ultramafic dyke that extends for 600-700m length on the surface. The orebody dips in a North West direction and was emplaced into the Protorezoic quartz phyllite/schists of the Huili group. It consists of medium to fine grained peridotite with chilled margins along the contacts with the country rock.

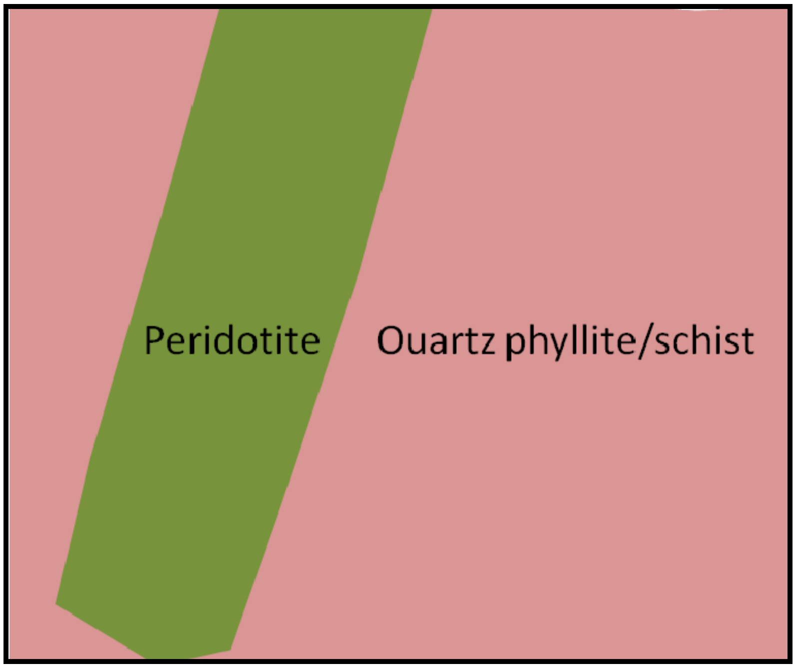

Figure 27: Yantiangou deposit schematic illustration the mineralization is hosted in the ultramafic dyke intruding the quartz phyllite country rock (Sichuan Geological Bureau., 2013).

The peridotite consists of olivine and clinopyroxene as primary minerals, biotite and hornblende in primary and secondary forms, as well as chlorite and carbonates occurring as alteration and replacement minerals (Fig 28). Sulphide minerals occur as small disseminated grains inside the silicates but primarily occur within biotite. The contact zone of the orebody with the country rock comprises olivine and pyroxene megacrysts set in a very fine grained clinopyroxene and replacement carbonate matrix Major sulphide minerals are pyrrhotite, pentlandite, and chalcopyrite, with smaller amounts of pyrite and galena. Traces of PGE, Pt and Pd occur as bismuthinides, arsenides and tellurides. Oxide minerals occur in trace quantities, these are magnetite, ilmenite and chrome spinel.

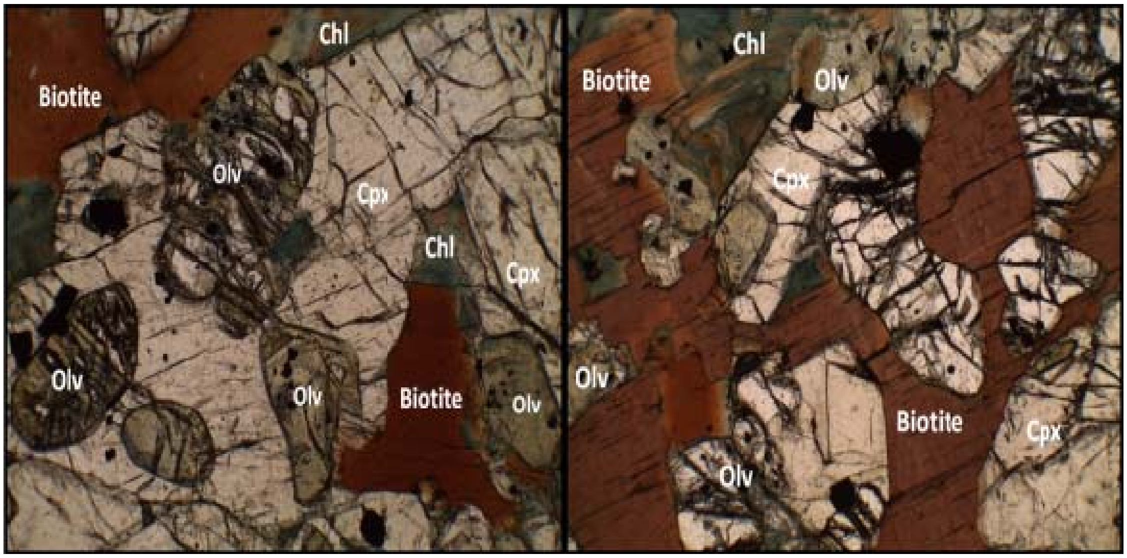

Figure 28: YTG 5, Mineral paragenetic sequence showing crystallization sequences with olivine, clinopyroxene and biotite. Minor opaque minerals occur as inclusions (× 100 magnification).

5.2.1 SILICATE MINERALOGY

The peridotite occurs as medium to coarse grained crystalline cumulate of olivine, pyroxenes, biotite, and hornblende (Fig 29). Olivine occurs as large to medium sized grains as well as small inclusions in the clinopyroxene. It forms ~40% modal composition. Clinopyroxene occurs as the dominant pyroxene with diopside as the main constituent. Minor orthopyroxene (clinoenstantite) occurs in the peridotite as a primary constituent and has secondary pigeonite exsolution. Grains of clinopyroxene are quite large exceeding 5mm in length and forming a poikilitic texture, they compose ~30% of the rock. These megacrysts form triple equilibration junctions and display slight serpentinisation in places (YTG 7), see Fig 32.

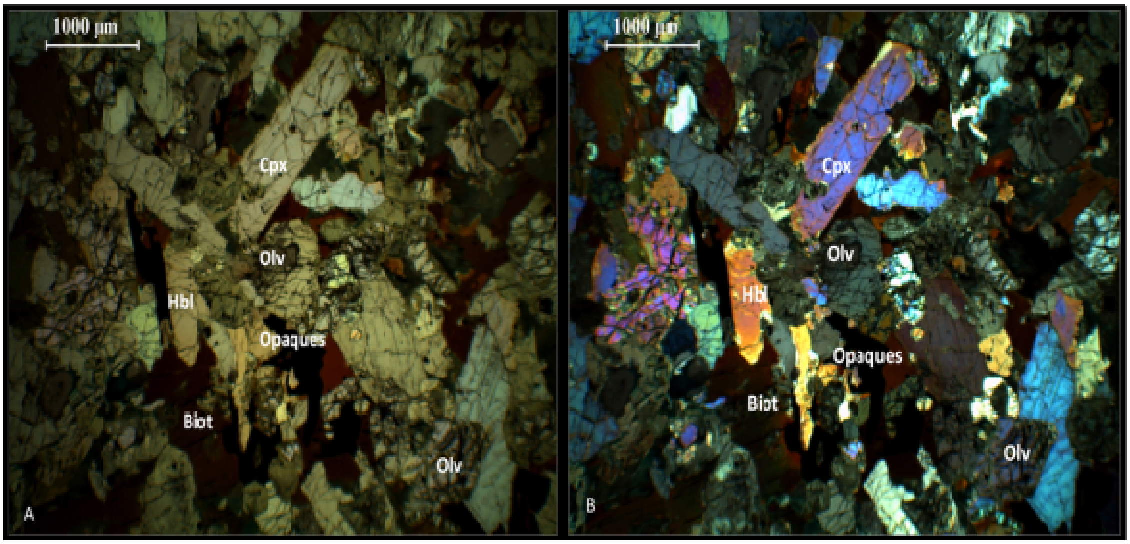

Figure 29: Yantiangou peridotite with olivine (Olv), clinopyroxene (Cpx), hornblende (Hbl), biotite and oxides in YTG 2.

Hornblende occurs interstitially filling spaces between olivines and clinopyroxenes, it constitutes about 10% of the rock. Biotite mica is very prevalent in the Yantiangou peridotite forming large flakes with interstitial hornblende (Fig 30). The plagioclase is mainly potassic alkali feldspar which is associated with the biotite and less hornblende. Minor spinel and oxides occur as accessory minerals, and sulphide mineralization is present albeit highly disseminated.

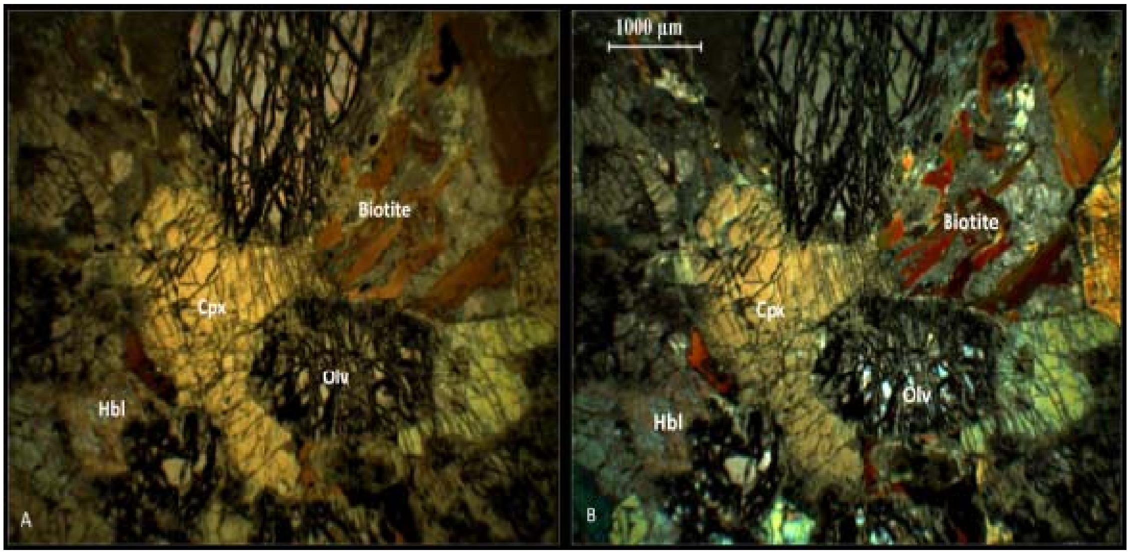

Figure 30: Biotite macrocrysts over 3mm in length observed with hornblende (Hbl) and carbonate (Carb) in YTG 8 peridotite. Clinopyroxene (Cpx) with olivine (Olv) core indicates olivine reaction with melt to form pyroxene along outer margin of olivine.

The uniform equi-granular texture (Fig 31) is observed in most of the Yantiagou peridotite with uniform small sulphide dissemination indicate emplacement of a crystal sulphide bearing mush as opposed in situ sulphide segregation.

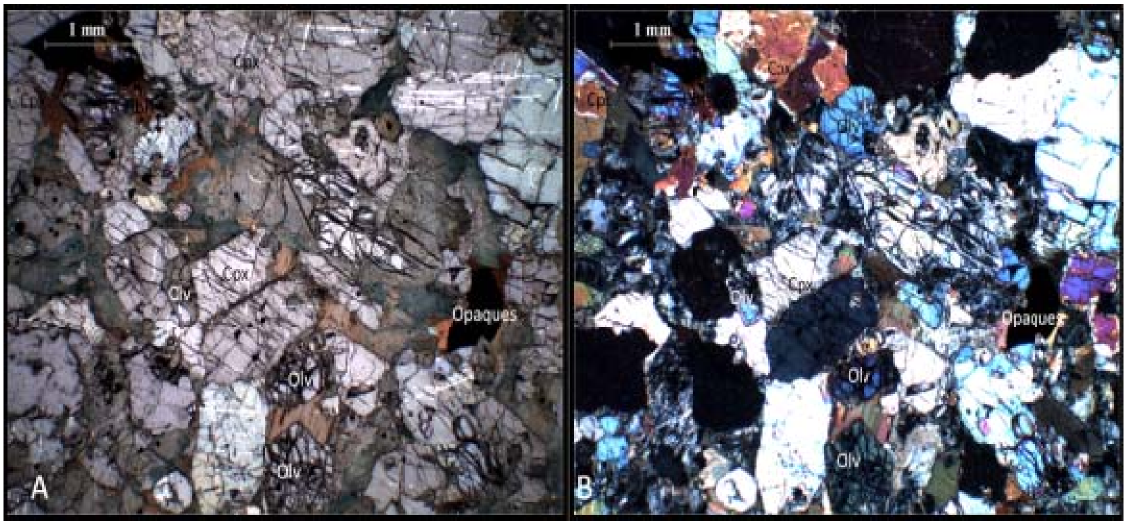

Figure 31: Crystalline equigranular textured peridotite with pervasive hornblende and annealing texture between the silicate grains in YTG 6.

The clinopyroxene grains in Fig 35 below show Ostwald ripening annealing textures and 120◦ triple junctions indicating mineral equilibrium at grain boundaries. Olivine grains at the centre indicate reaction with the melt to form clinopyroxenes and biotite is chloritized along the margins due to hydration.

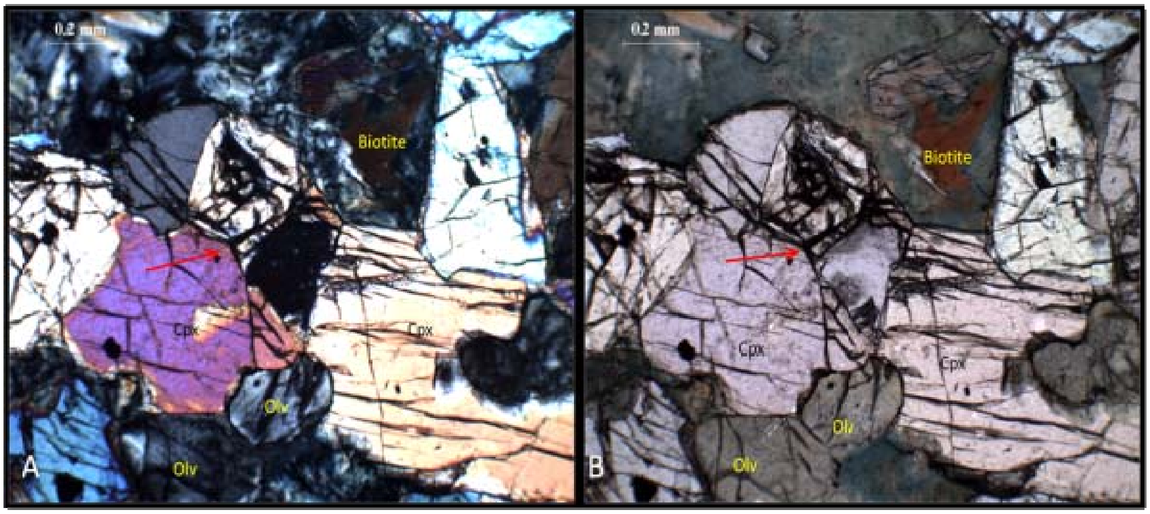

Figure 32: YTG 5, large pyroxene grains with interlocking triple junctions. Fig a, under crossed polarized light and b, in plane polarized light. Olivines reaction with melt to form pyroxene. Green chloritization occurring around biotite as a result of late- stage hydration of biotite.

The peridotite along the margins of the Yantiangou intrusion is chilled due to quenching upon contact with quartz phyllites of the wallrock. Prophyritic texture set in an aphanitic recrystallized glassy matrix suggests crystal growth occurred before emplacement. The microcrystalline glassy matrix contains olivine, hornblende, pyroxene and interstitial oxide (magnetite and ilmenite) microcrysts. The contact rocks also contain sodic alkali feldspar and as a result, not much biotite is observed in these rocks (Fig 33).

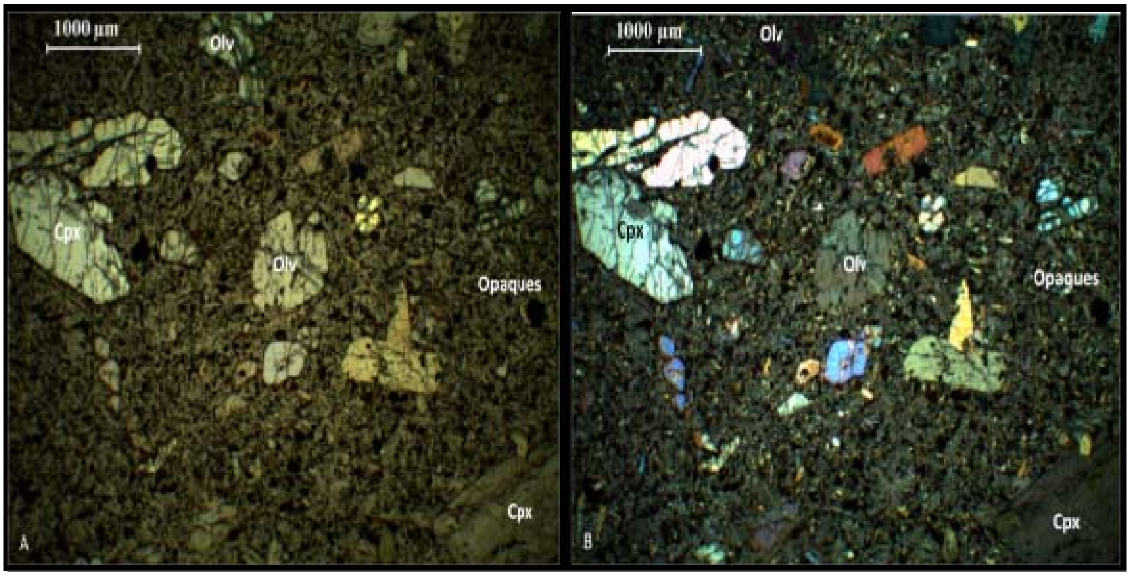

Figure 33: Porphyritic texture in YTG 4 of phenocyrsts of clinopyroxene (cpx) and olivine (olv) in an aphanetic groundmass. Cpx crystals show a euhedral form with a preferred direction of growth, a in plane polarized light and b in cross polarized light.

5.2.2 ORE MINERALOGY

Sulphide mineralization in the Yantiangou deposit is intimately associated with biotite and less so with hornblende, olivine and pyroxene (Figs 34 35). It occurs as disseminations throughout the dyke type intrusion and displays no sign of in situ sulphide segregation. Mineral assemblages observed are pyrrhotite, chalcopyrite and very minor pentlandite (Figs 36 37). Pyrite occurs in some high sulphur minerals. Magnetite occurs with sulphide mineralization but to a small extent, chrome spinel also occurs within biotite.

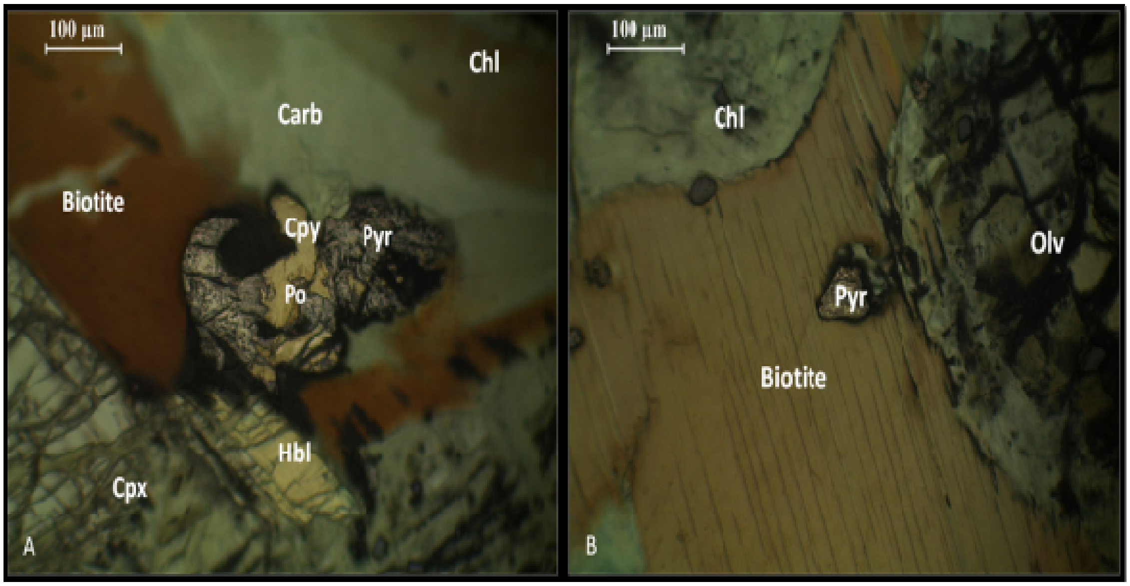

Figure 34: Sulphide mineralization associated with biotite and hornblende. Biotite displays chloritization and carbonate replacement taken under reflected light and some transmitted light for colour (composite light). Sulphide minerals occur as small disseminations of pyrite (Pyr), chalcopyrite (Cpy), and pyrrhotite (Po).

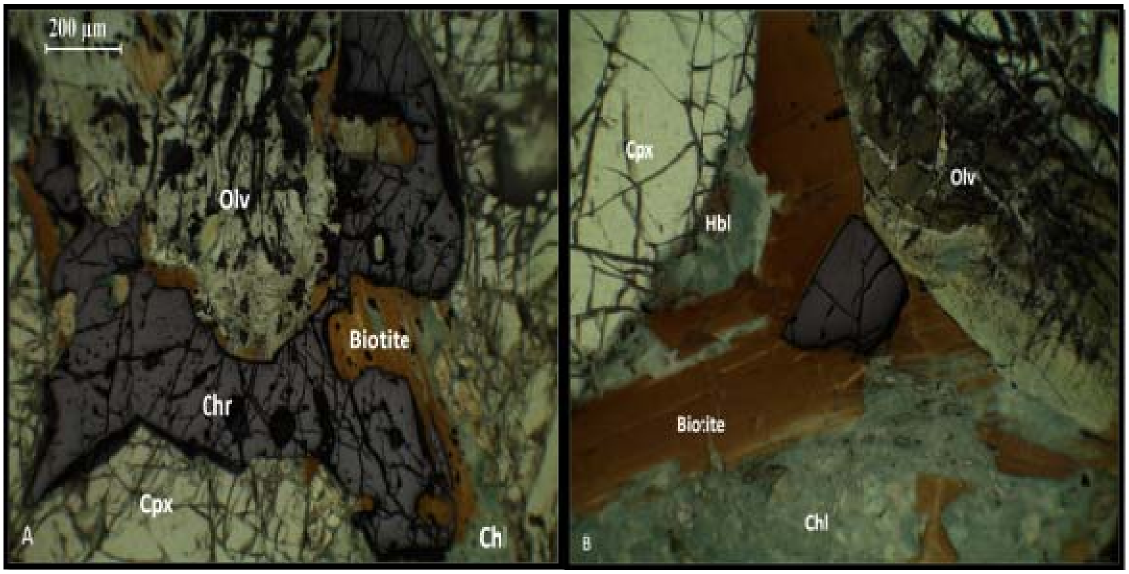

Figure 35: a. Large irregular shaped chrome spinel in biotite, olivine (Olv) and clinopyroxene (Cpx), b. euhedral shaped grain of chrome spinel in biotite. Scale same as a. Pictures taken under composite lighting.

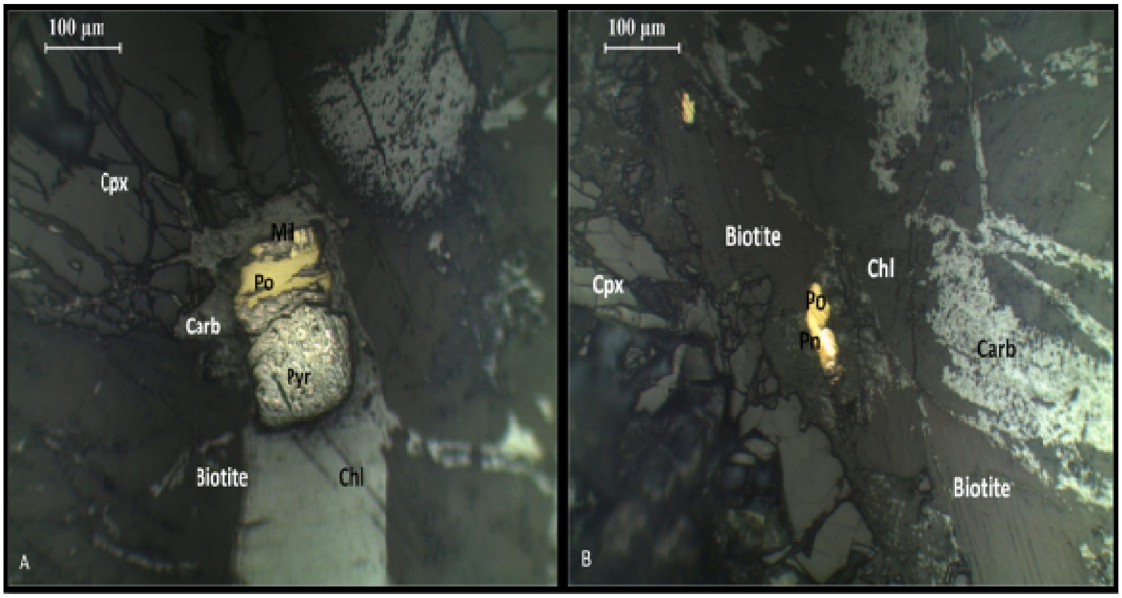

Figure 36: Fig a shows pyrrhotite (Po) and millerite (Mil) with pyrite (Pyr) inside chlorite under reflected light. Fig b shows pyrrhoitite (Po) and pentlandite (Pn) in biotite under reflected light.

Millerite occurs as inclusions in pyrrhotite and pyrite. Chalcopyrite occurs in larger anhedral grains ~100 µm in size while the other sulphides are less than ~ 20µm (Figs 39 &40).

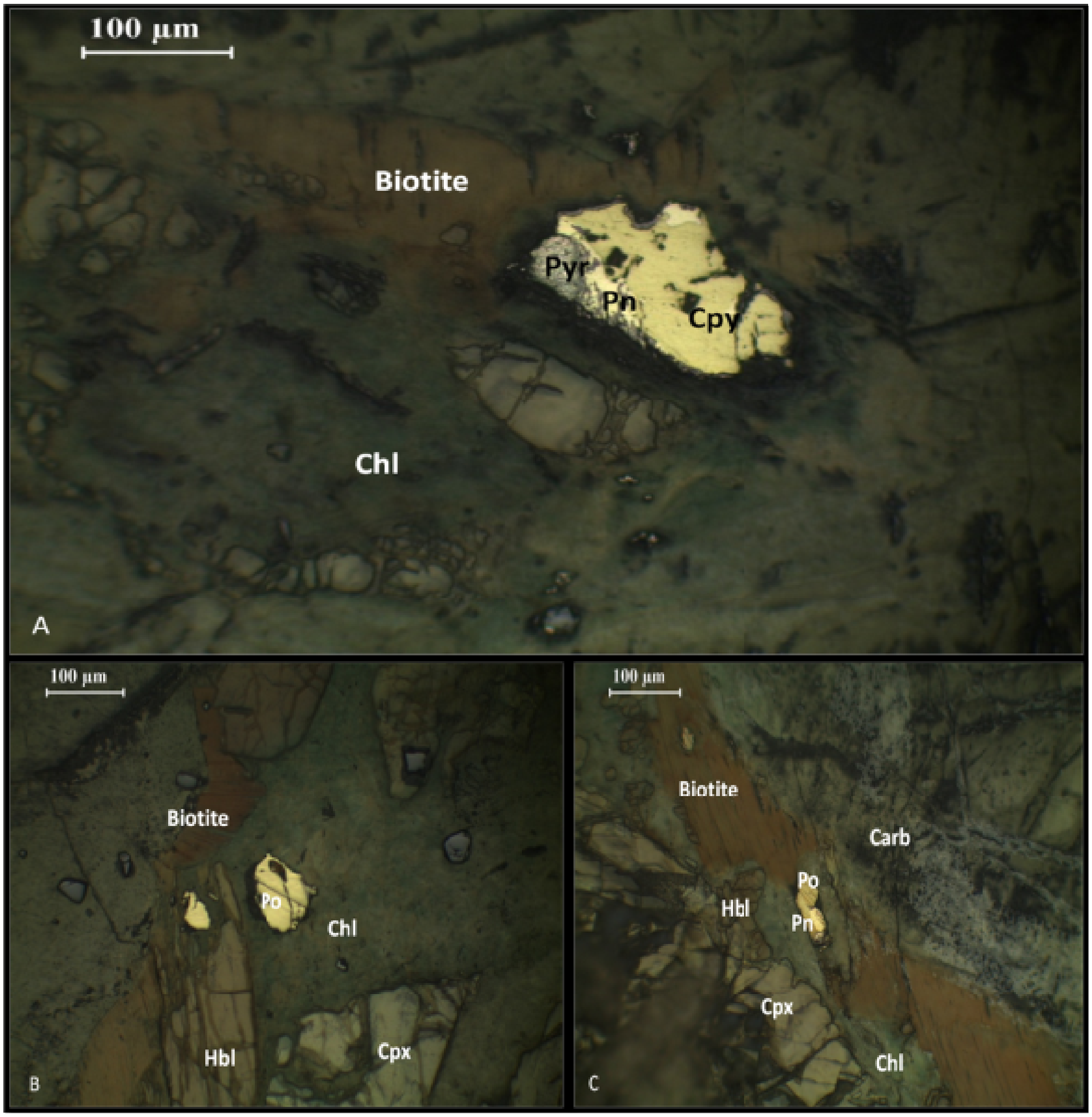

Figure 37: a. Chalcopyrite (Cpy), pyrite (Pyr) and pentlandite (Pn) sulphide minerals in biotite and chlorite, b. pyrrhotite (Po) and pentlandite (Pn) in biotite and chlorite with replacement carbonates and hornblende, c. pyrrhotite (Po) in biotite, hornblende and chlorite. Pictures were taken under composite light.

CHAPTER 6 MINERAL CHEMISTRY

6.1 ZHONGCHANG

Backscatter electron microprobe images indicate the inclusion of oxide mineral phases in silicates. Figures 38 and 39 below show oxides in clinopyroxene and olivine. Exsolution patterns of illmenite are observed in magnetite along cleavage lines in the pyroxenite and gabbro.

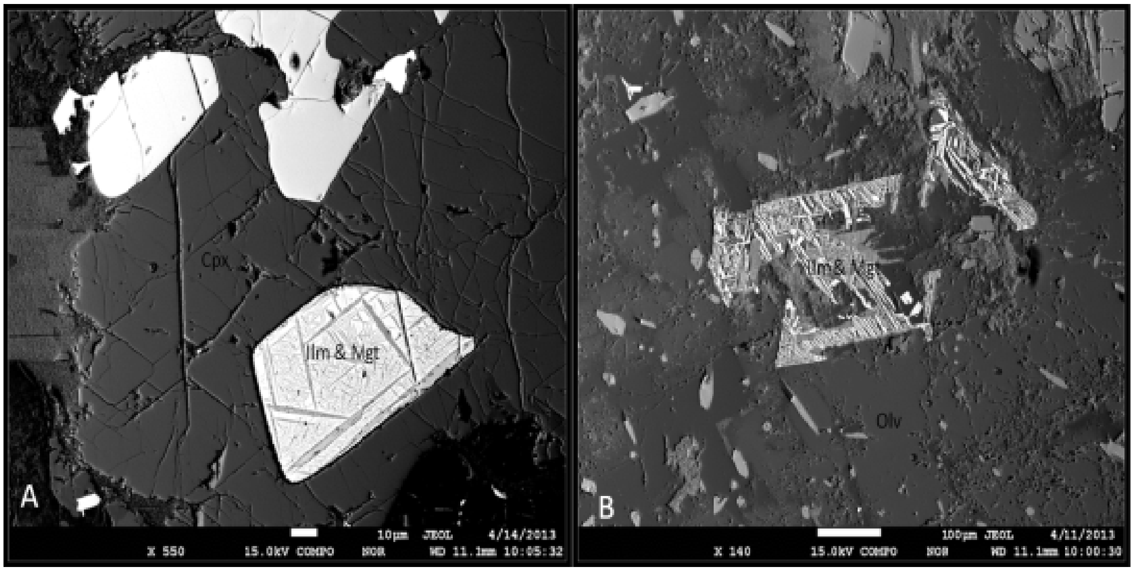

Figure 38: a, Ilmenite (Ilm) exolutions along magnetite (Mgt) cleavage lines in a Cpx (Clinopyroxene) crystal in ZC 6 pyroxenite, and b, skeletal magnetite cleavage and ilmenite growths in olivine in ZC 11 gabbro.

The oxide minerals occur as inclusion in the silicates, magnetite is developed within the olivine and pyroxene. Chromite occurs as euhedral crystals; usually the chromite crystallizes earliest in mafic-ultramafic magmas (Fig 40). Illmenite is developed along cleavage lines of magnetite as intergrowths or exsolution lamellae. The observed crystallization sequence for the oxides is therefore chromite- magnetite and lastly, ilmenite. The silicates crystallized later and enclosed the oxides. Oxide minerals are observed to occur in greater abundance in gabbro and in lesser amounts in peridotite and pyroxenite.

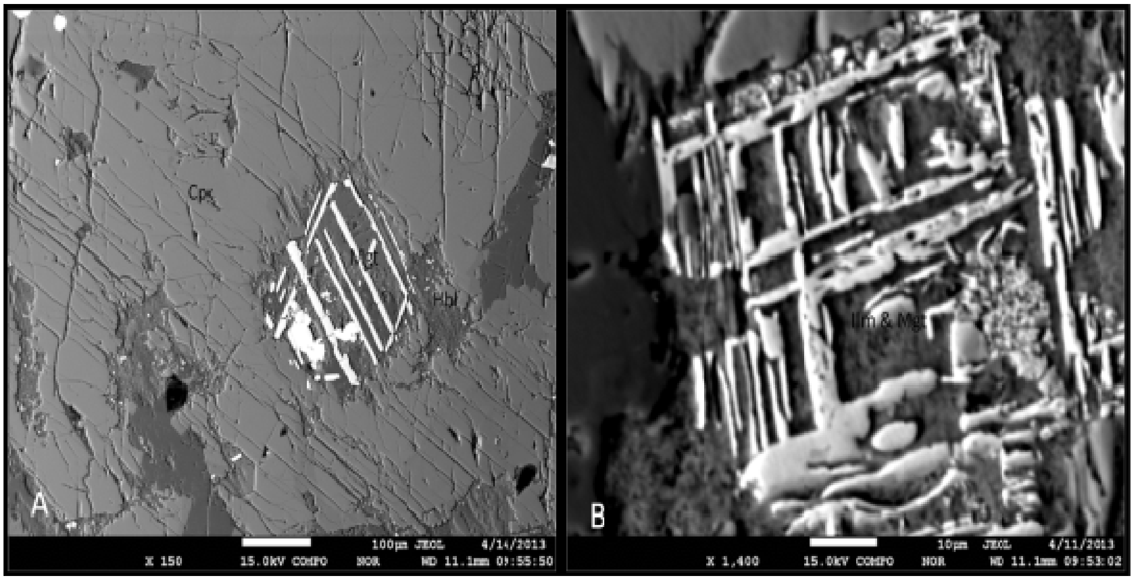

Figure 39: a Microprobe image of magnetite skeleton in hornblende in ZC 6 pyroxenite, and b, in ZC 11 gabbro

The inclusion of sulphide minerals in silicates is also evident in electron backscatter images. Figures 40b and 41 indicate sulphides included in clinopyroxene and olivine. Platimun group metal inclusions are observed as inclusions in sulphides in Fig 40 b. Analysis of PGM’s indicated that they are form tellurides and bismuthinites on most occasions. Pb is present as tellurides. A plot of microprobe analyses of michenerite, a palladium-bismuth telluride is shown in Fig 42.

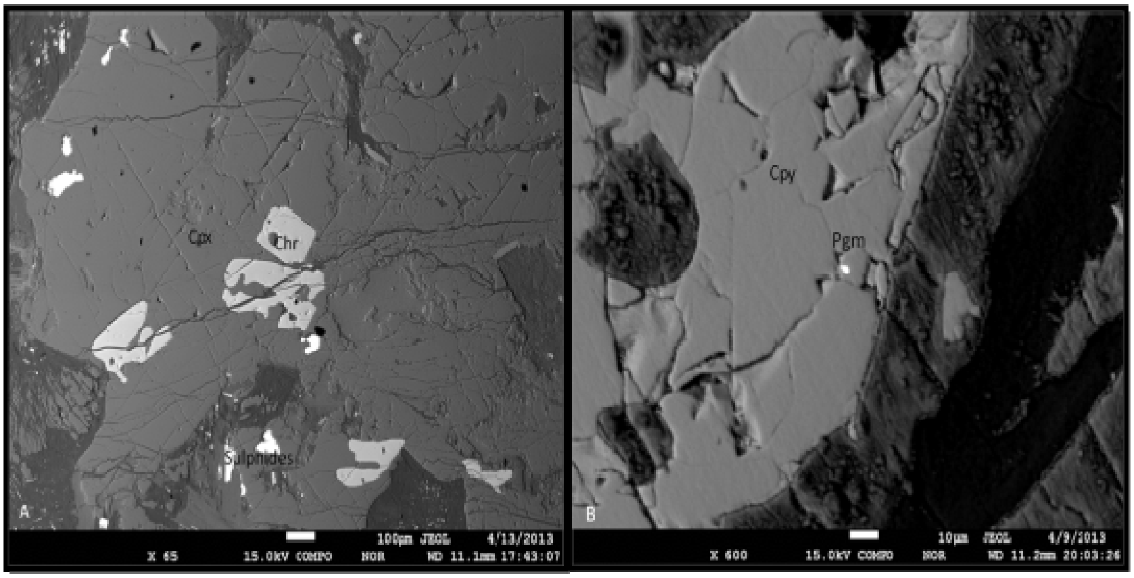

Figure 40: a, Chrome spinel in Clinopyroxene (Cpx) in ZC 10 pyroxenite sample and b, small PGM grain in Chalcopyrite (Cpy) in ZC 2 peridotite sample.

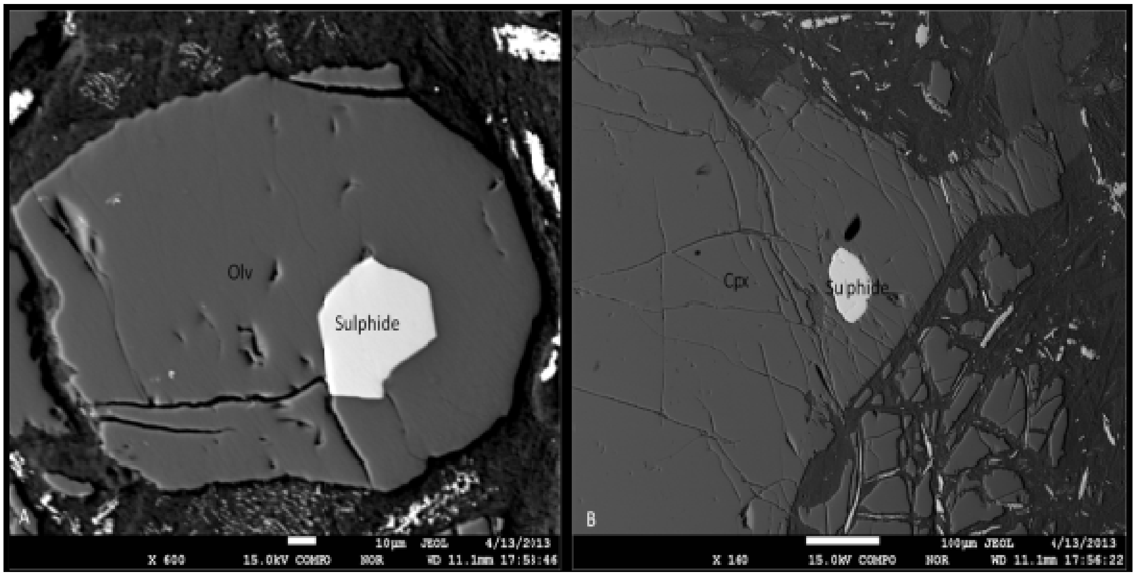

Figure 41: a, A sulphide inclusion in olivine (Olv) and b, sulphide inclusion in clinopyroxene (Cpx)

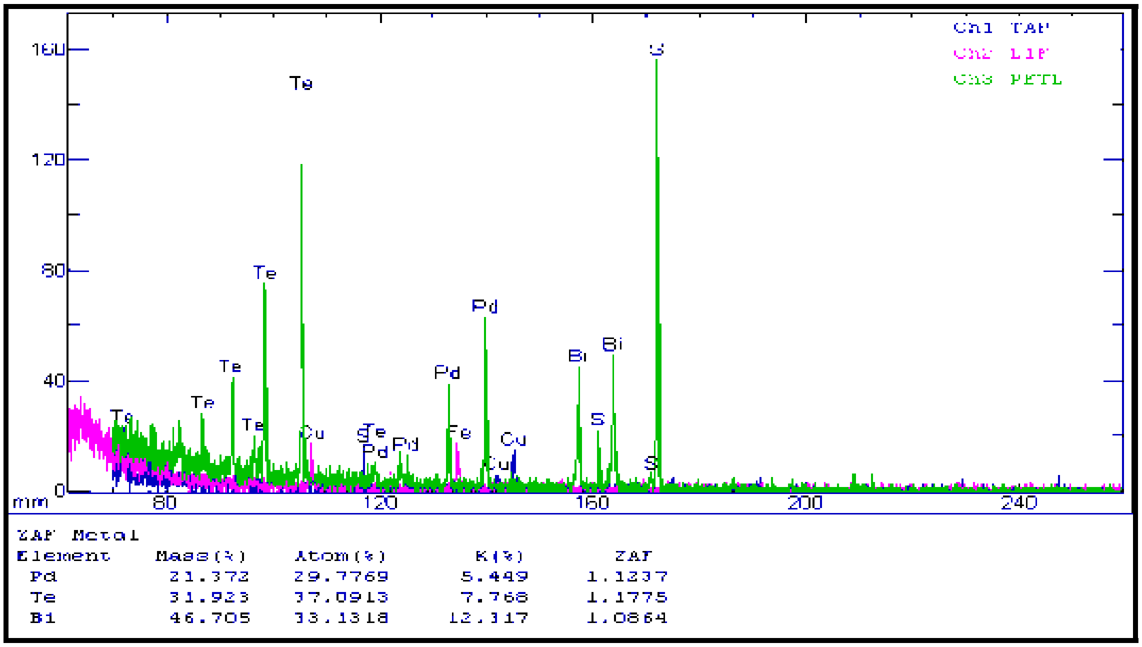

```
ZAF Metal
Element      Mass(%)    Atom(%)      K(%)      ZAF
 Pd          21.372     29.7769      5.449     1.1237
 Te          31.923     37.0913      7.768     1.1775
 Bi          46.705     33.1318     12.317     1.0864
```

Figure 42: Microprobe analysis of PGM grain showing Pd-Bi-Te phases (Michenerite).

The partitioning of PGM into tellurides and bismuthinides indicates PGE partitioning in a state of S-undersaturation.

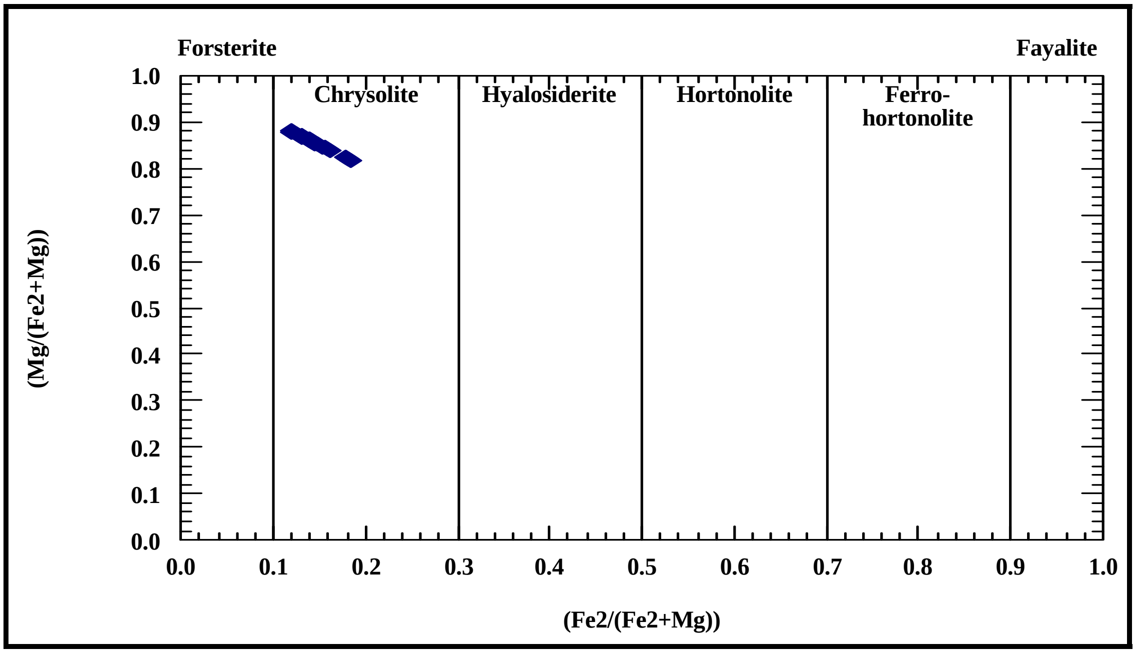

Figure 43: Zhongchang olivine plot, all points plot in the high Fo (80-90%) field. (Richard., 1995)

Olivine is more enriched in Mg as opposed to Fe shown here by samples plotting higher up the Forsterite axis and lower along the Fayalite axis (Fig 43). This low fayalite: forsterite ratio indicates a sulphur under-saturated magma resulting in early crystallization of olivine in normal magmatic fractionation, and late sulphide segregation as a result of late sulphide saturation. The olivines plot between Fo $_{82\text{-}87.}$

Clinopyroxenes from the Zhongchang intrusion with majority of points plotting along augite and diopside margins in Fig 44. The composition for the pyroxenes range from $En_{46}Fs_{8}Wo_{46}$ to En_{48} Fs_{8} Wo_{44} on average. Enrichment in Mg and Ca solid solution members with less Fe content is observed in the ternary diagram (after Morimoto et al. 1988).

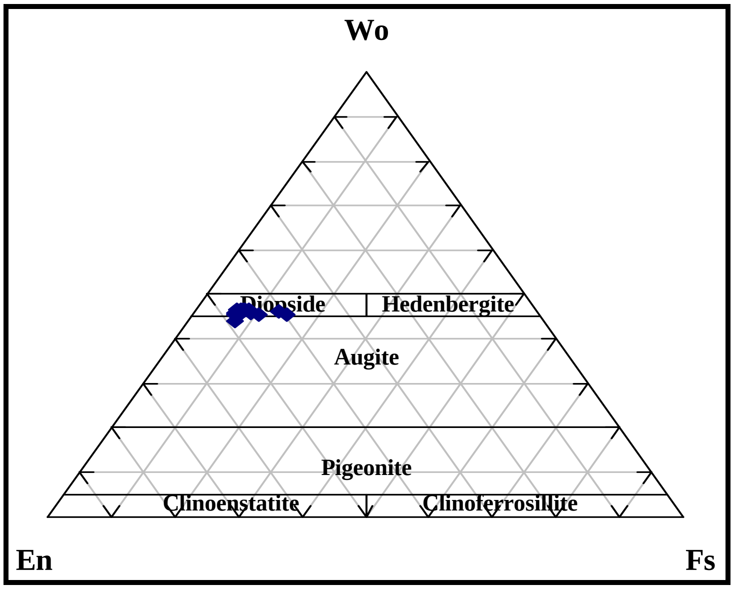

Figure 44: Zhongchang Pyroxene with all samples plotting along the diopside/ augite margin (After Morimoto et al., 1988).

The feldspar composition for the Zhongchang rocks is principally sodic plagioclase to potassic alkali (Fig 45). Samples reporting high orthoclase content are ZC 8 and 11 of gabbroic composition.

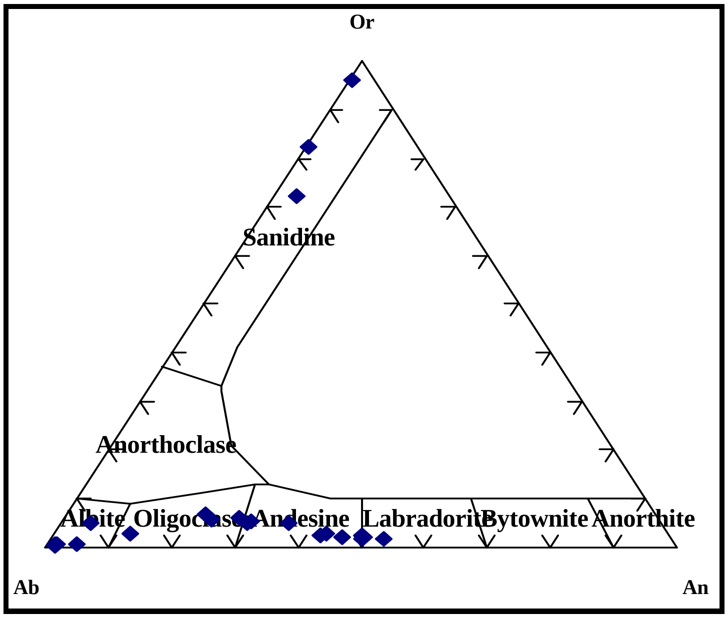

Figure 45: Zhongchang Feldspar, Na rich plagioclase feldspars with K- rich feldspar (After Smith., 1974)

The composition of the feldspars ranges from $An_2Ab_{98}Or_0$ to An_1 $Ab_{17}Or$ $_{82}$ indicating a broad spectrum of alkali composition from Na- rich feldspar to K-rich feldspar. All feldspars contain less than 50% anorthite.

6.2 YANTIANGOU

Crome spinels form the dominant oxide in Yantiangou with lesser amounts of magnetite. The magnetite is interwoven with sulphides as inclusions in silicates while chrome spinels exist as discrete mineral grains inclusions. Galena (PbS) also occurs in the Yantiangou sulphides (Fig 46).

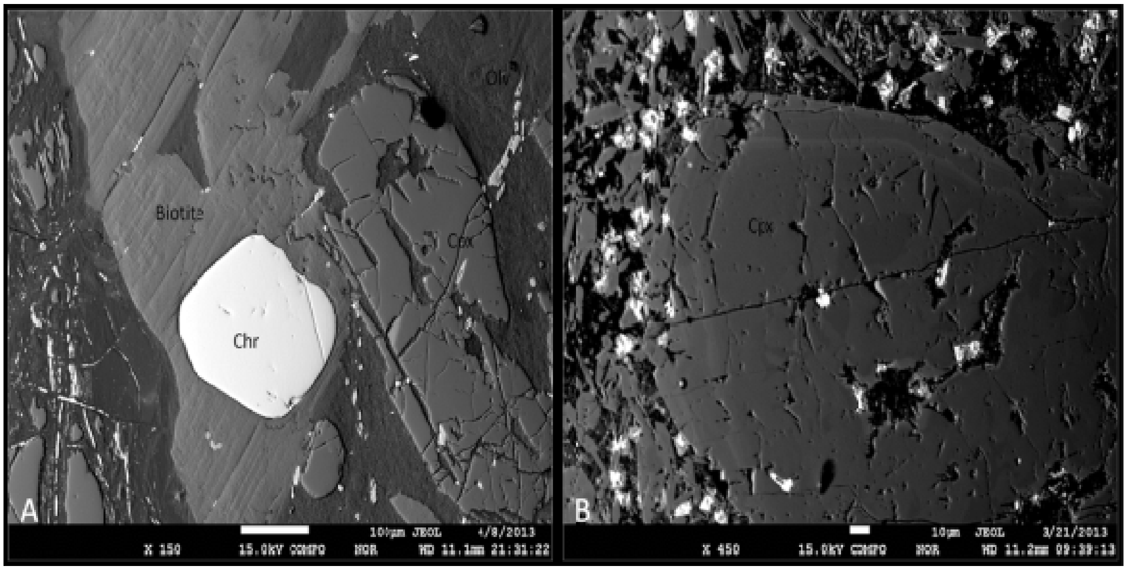

Figure 46: a, YTG 8-Chrome spinel inclusion in biotite and b, clinopyroxene phenocryst displaying concentric zoning. Sample YTG 3 (peridotite).

Sulphide compositions measured by electron microprobe show composition of PGM including sperrylite ($PtAs_2$) in Figs 47 48. Pyrite is present in sulphides with more than 60% S with millerite (NiS) in the pyrite. The presence of pyrite indicates hydrothermal circulation in the rock which suggests a late magmatic event.

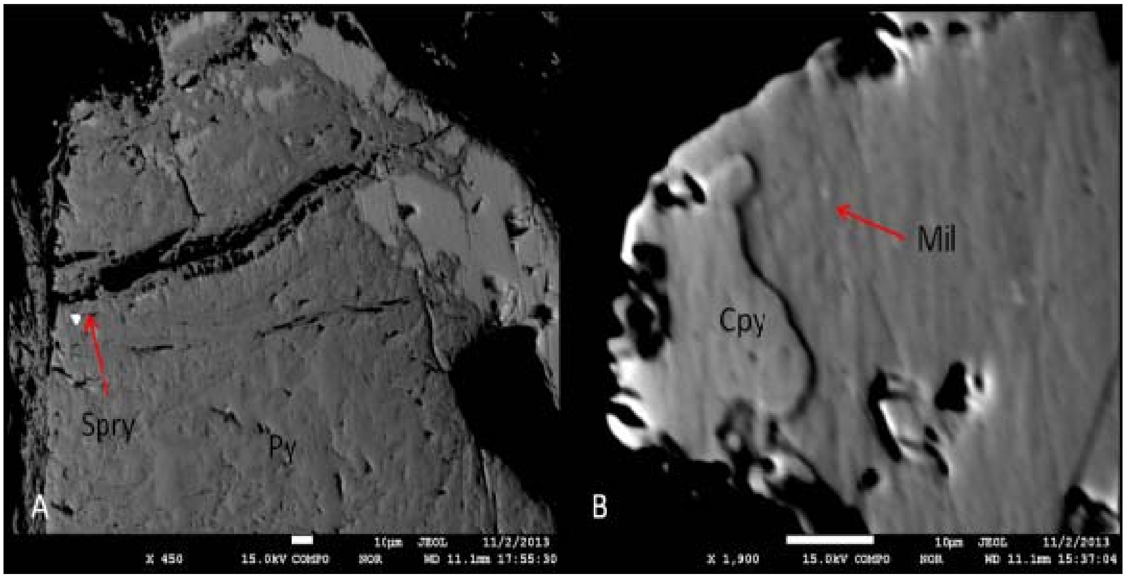

Figure 47: a, Sperrylite (Spyr) inclusion in Pyrite (Py) and b, Millerite (Mil) inclusion in Chalcopyrite (Cpy).

Platinum partitioned into arsenides in pyrite indicates late stage hydrothermal alteration took place in Yantiangou.

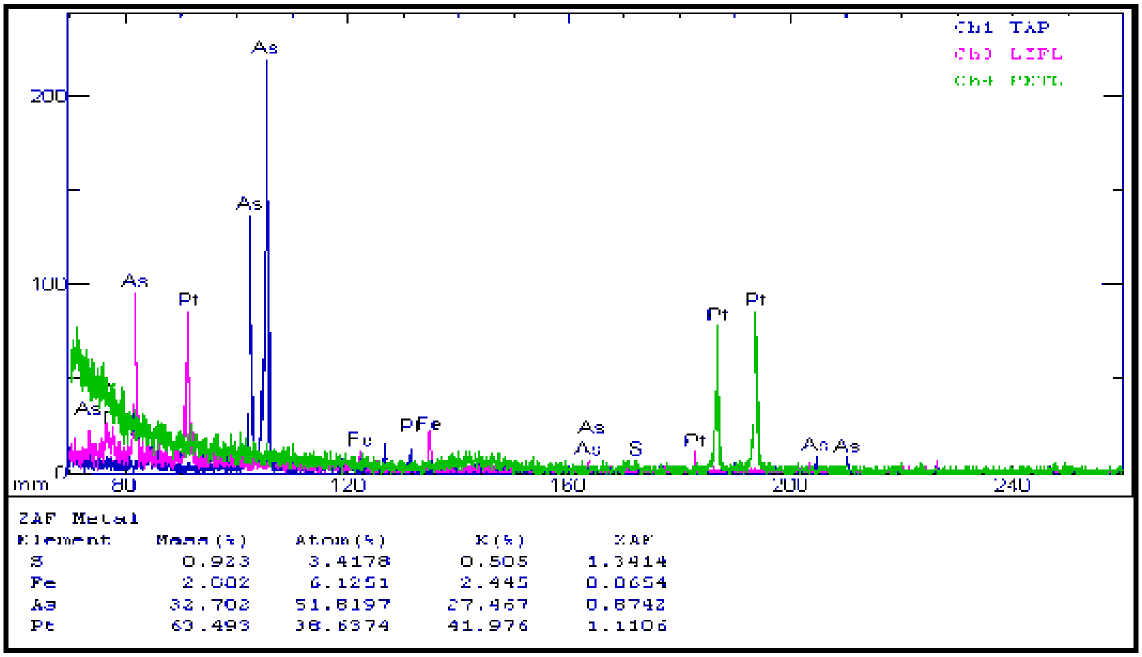

```
ZAF Metal
Element     Mass(%)   Atom(%)     K(%)      ZAF
 S           0.923    3.4178     0.505    1.3414
 Fe          2.002    6.1251     2.445    0.0654
 As         32.702   51.8197    27.467    0.8742
 Pt         63.493   38.6374    41.976    1.1106
```

Figure 48: Speryllite microprobe analysis with As, and Pt as main constituents.

Microprobe electron images indicating sulphides and spinel inclusions in biotite in Figure 49 indicate the crystallization of sulphides and oxides prior to silicates.

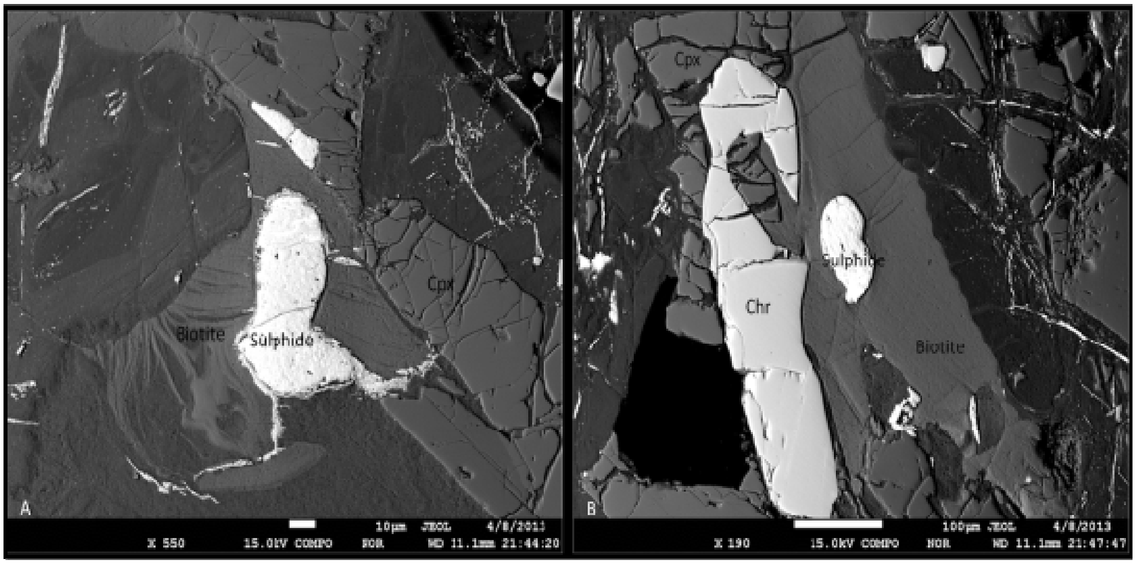

Figure 49: a, Sulphide inclusions in biotite and b, Chrome spinel and sulphides in biotite.

Olivine is more enriched in Mg as opposed to Fe shown here by samples plotting higher up the Forsterite axis and lower along the Fayalite axis (Fig 50). The low fayalite: forsterite ratio indicates a sulphur under-saturated magma resulting in early crystallization of olivine under normal magmatic fractionation, and late sulphide segregation as a result of late sulphide saturation. The olivines plot between Fo $_{(72\text{-}89)}$.

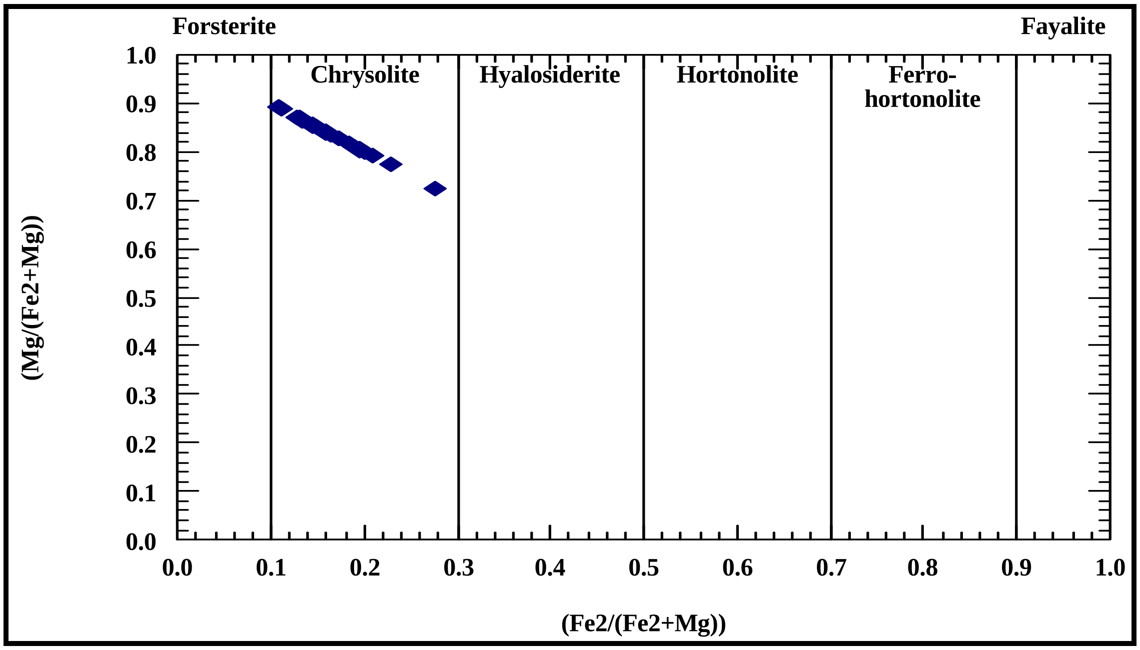

Figure 50: YTG olivines with Fo content of 70-90%. (Richard., 1995).

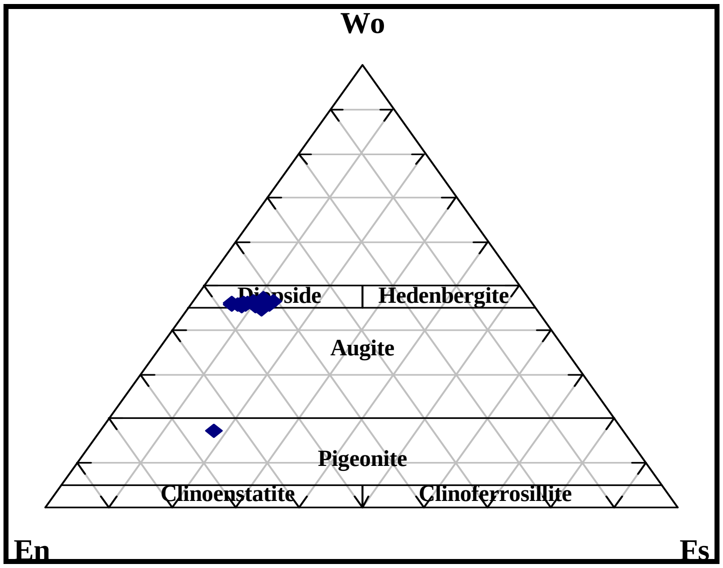

Figure 51: Yantiangou pyroxene plotting principally as diopside (After Morimoto., 1988)

Pyroxenes from the Yantiangou intrusion (Fig 51) plot in the diopside field. The compositions vary between $En_{42}Fs_{11}Wo_{47}$ and $En_{48}Fs_7Wo_{45}$. The pigeonite displays a textural variation under the microprobe with some apparent exsolution.

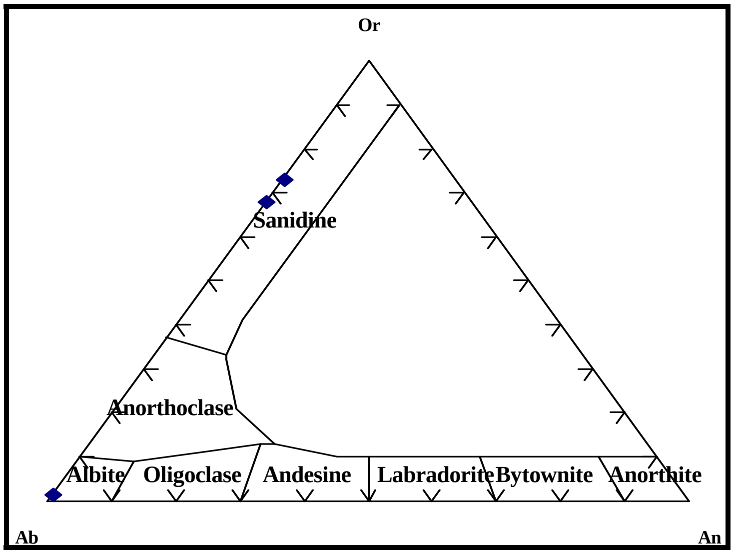

Figure 52: Yantiangou alkali feldspars (After Smith., 1974)

Alkali feldspar solid solution series from contact- aureole with quartz phyllite (Fig 52), formed as a result of contact metamorphism with the dyke intusion. The feldspars have a very low anorthite content and plot between $Ab_{98}An_0Or_2$ and Ab_{26} An_1 Or_{73}.

6.3 Ni IN OLIVINE

Ni in olivine is plotted using microprobe analyses to determine the amount of Ni that partitioned into olivine prior to sulphide saturation.

Li et al (2001) indicate that olivine crystallization before sulphide saturation will result in a decrease in Ni concentration with an increase in FeO/MgO ratio, i.e the fayalite/ forsterite ratio in olivine. The Ni in olivine will increase proportional with MgO or forsterite.

The average Ni content in olivine for Zhongchang (Fig 53) goes up to 0.12% /(1200 ppm).

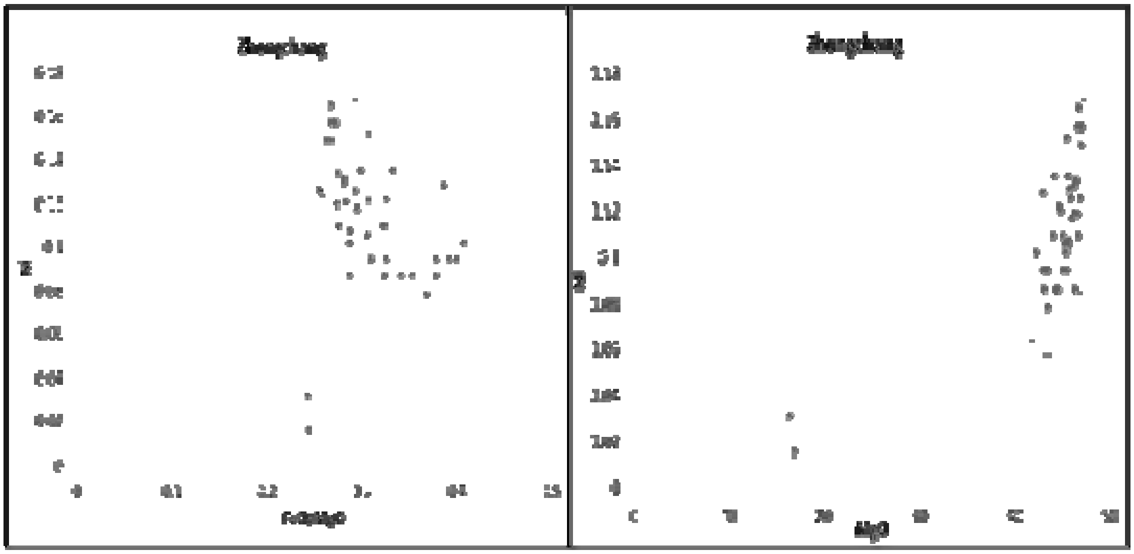

Figure 53: Zhongchang Ni vs FeO/MgO and Ni vs MgO plots indicating the extent of Ni partitioning into olivine.

The average Ni content in olivine for Yantiangou deposit (Fig 54) goes up to 0.17%/ (1700 ppm).

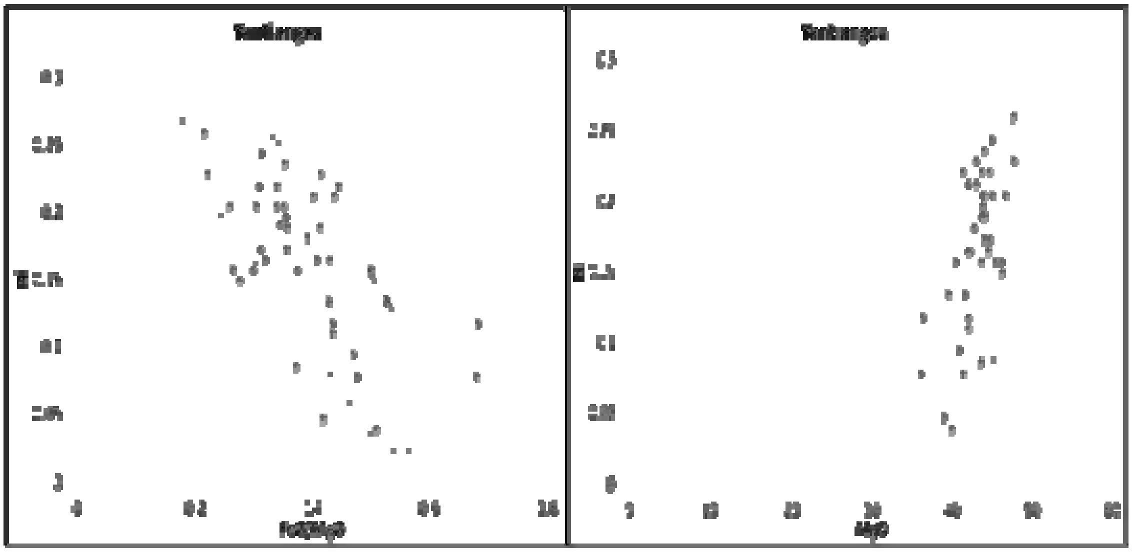

Figure 54: Yantiangou Ni vs FeO.MgO and Ni vs MgO plots indicating the partitioning of Ni into olivine.

CHAPTER 7 WHOLE ROCK GEOCHEMISTRY

7.1 BULK ROCK ANALYSES

Table 1: Bulk rock analyses results for ZC (Zhongchang) and YTG (Yantiangou)

Sample	$(Pt)/10^{-9}$	$(Pd)/10^{-9}$	$(Au)/10^{-9}$	$(Rh)/10^{-9}$	$(Co)/10^{-6}$	$(Cu)/10^{-6}$	$(Ni)/10^{-6}$	$(TS)/10^{-6}$
ZC1	554	140	43.0	1.51	280	11894	7615	39415
ZC2	405	208	118	1.61	163	6295	3024	15404
ZC3	189	132	108	1.96	186	7911	4859	37301
ZC4	1.83	3.90	2.12	1.20	34.8	131	169	423
ZC5	1.82	2.19	3.60	1.73	29.9	64.1	26.3	5150
ZC6	4.00	1.61	5.80	1.19	85.9	116	444	2220
ZC7	1.18	0.89	2.53	1.73	39.0	41.2	28.3	1631
ZC8	1.01	1.35	2.00	1.82	38.0	21.8	25.2	2295
ZC9	1.20	1.14	1.53	1.52	42.0	21.8	28.6	1042
ZC10	4.30	3.20	10.50	1.33	103	396	720	3126
ZC11	1.17	1.01	4.50	1.77	45.7	39.5	44.7	1601
YTG1	18.0	14.9	3.70	1.45	93.7	228	802	1420
YTG2	90.0	10.8	27.2	1.79	110	2092	1244	7385
YTG3	6.10	2.11	4.50	1.10	62.0	371	329	680
YTG4	3.30	1.46	2.78	1.86	56.6	195	287	468
YTG5	6.40	2.45	0.69	1.35	78.5	82.7	582	725
YTG6	7.50	7.90	1.70	1.53	87.9	201	710	1269
YTG7	7.90	1.78	0.42	1.54	87.0	170	665	1314
YTG8	6.70	1.91	3.70	1.89	95.4	232	831	1571
YTG9	41.0	3.20	7.70	1.15	158	4171	3575	15811

7.2 METAL TENORS

Tenor calculations are used to determine the concentrations of metals in the sulphide portion of the ore, as most sulphide ore include other constituents that are non sulphide such as oxides (chromites) and silicates (olivine) (Barnes et al., 1988). Oxides and silicates also control the distribution of Ni-Cu-PGE, but only contribute to diluting the sulphide component since the metals cannot be beneficiated from them.

Whole rock analyses give the amount of metals in relation to the total rock composition with sulphides, oxides and silicate as a whole. Calculation of metal tenors in the sulphide portion (absolute concentrations) therefore assists in giving the amount and composition of the sulphide liquid and the composition of the parental magma which are the major controls in the genesis of Ni-Cu-PGE deposits (Li et al., 2001). The ratios of the elements relative to each other and relative to sulphur following absolute concentrations can be used to determine the petrogenesis of the rocks (Barnes and Lightfoot., 2005).

Most metals are assumed to be present in the sulphide fraction of the rock and calculations to establish the metal abundances in the rock is conducted to 100% sulphide to determine the metal tenor of the sulphide. The assumptions made are that the chalcophile metals are predominamtly hosted by the sulphides and that sulphur has not been added or removed from the samples by metamorphism or alteration, ie the rocks retain the original suphur content as at the time of sulphide formation (Barnes and Lightfoot., 2005).

This procedure (Fig 55) is based on the theory of sulphide liquid segregating from silicate magma following the Fe- rich mss between 1100 and 950°C and Cu- rich iss between at <950°C as explained in the ore genetic model section (Chapter 3) to form pyrrhotite, chalcopyrite and pentlandite(Barnes and Lightfoot., 2005). As this assemblage represents the major mineral assemblage observed in magmatic sulphide deposits, the sum of these three minerals is taken to represent the total percentage of sulphides in the sample. This calculation ignores minor metals that exist together this assemblage eg pyrite, cubanite and PGEs occuring outside the sulphide structure as alloys and other mineral compounds whose presence has been shown to have little effect on the result of the calculation (Li et al., 2001).

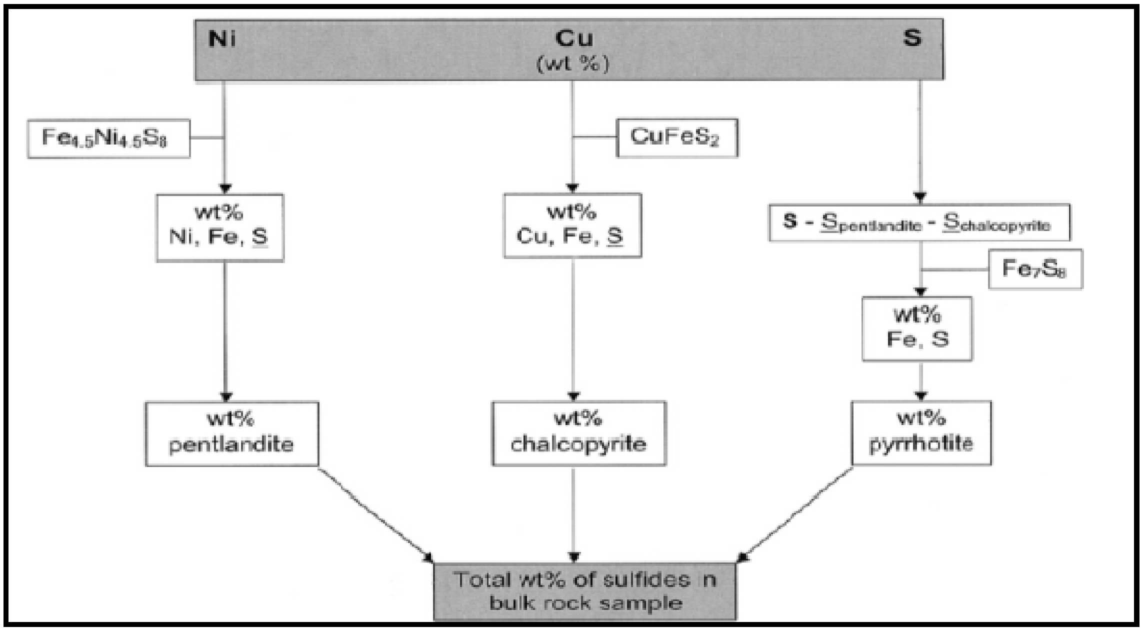

Figure 55: Procedure of estimating sulphide content in rock sample using whole rock assay. Li et al., (2001).

Whole rock assay values of Ni and Cu in the sample and mineral composition to calculate the amount of pentlandite with mineral formula $(Fe, Ni)_9S_8$ and and chalcopyrite with mineral formula ($FeCuS_2$). The remaining sulphur is then used to calculate the percentage of pyrrhotite (Fe_7S_8) in the sample. The metal value of the assay divided by total percentage of sulphides in the sample represented by the sum of all three will represent their concentration in 100% sulphide (Li et al., 2001).

Barnes and Lightfoot (2005), present a formula for calculating the concentration of an element in the sulphide as:

$$\mathbf{C_{(100\%\ sul)} = C_{wr} \times 100/(2.527 \times S + 0.3408 \times Cu + 0.4715 \times Ni)}$$

Where:

$C(100\%\ sul)$ = concentration of an element in 100 percent sulphides,

C_{wr} = concentration of the element in the whole rock, and;

S, Cu, and Ni = concentration of these elements in the whole rock, in wt percent.

Barnes and Francis, 1995 which states that:

$$\mathbf{C_s = C_r/W}$$

Where:

Cs = concentration of an element in the sulphide fraction of the rock,

Cr = concentration of the element in the whole rock and;

W = weight fraction of the elements present in the whole rock.

The complete method of calculation is presented in Appendix 5.

The results from both methods are presented in the table 5 for comparison.

Background Values used based on measured and microprobe data are as follows:

Table 2 Whole rock background values for tenor calculations

Background Values		**Cu**	**Ni**	**Samples**
YTG	Per	83	582	All YTG samples
ZC	Gabb	22	30	ZC 4,5,6,7,8,9 & 11
ZC	Per	116	450	ZC 1, 2,3 & 10

Table 3: Tenor values for Zhongchang and Yantiangou based on methods by Barnes and Frances., 1995 and Barnes and Lightfoot., 2005

		After Barnes and Frances., 1995					After Barnes and Lightfoot., 2005				
Sample	Rock type	Total S in rock wt %	Cu tenor %	Ni tenor %	Pt tenor ppb	Pd tenor ppb	Total S in rock wt %	Cu tenor %	Ni tenor %	Pt tenor ppb	Pd tenor ppb
ZC1	Peridotite	10.70	11.01	6.70	5179.92	1309.01	10.70	11.12	7.12	5177.81	1308.47
ZC2	Peridotite	4.22	14.63	6.10	9590.88	4925.68	4.22	14.90	7.16	9587.04	4923.72
ZC3	Peridotite	9.90	7.88	4.46	1910.01	1333.97	9.90	7.99	4.91	1909.18	1333.40
ZC4	Gabbro	0.12	9.32	11.85	1563.19	3331.39	0.12	11.20	14.40	1562.60	3330.13
ZC5	Gabbro	1.30	0.32	0.00	139.77	168.19	1.30	0.49	0.20	139.70	168.11
ZC6	Gabbro	0.58	1.60	7.09	685.62	275.96	0.58	1.98	7.60	685.33	275.84
ZC7	Gabbro	0.41	0.46	0.00	285.99	215.70	0.41	1.00	0.69	285.85	215.60
ZC8	Gabbro	0.58	0.00	0.00	174.20	232.85	0.58	0.38	0.43	174.12	232.73
ZC9	Gabbro	0.26	0.00	0.00	455.94	433.15	0.26	0.83	1.09	455.72	432.94
ZC10	Peridotite	0.81	3.45	3.33	529.65	394.16	0.81	4.88	8.87	529.41	393.98
ZC11	Gabbro	0.41	0.43	0.36	288.45	249.01	0.41	0.97	1.10	288.32	248.89
YTG1	Peridotite	0.37	3.89	5.89	4814.18	3985.07	0.37	6.11	21.44	4812.09	3983.34
YTG2	Peridotite	1.96	10.22	3.37	4580.30	549.64	1.97	10.64	6.33	4578.33	549.40
YTG3	Peridotite	0.18	15.87	0.00	3361.49	1162.74	0.18	20.44	18.14	3360.03	1162.24
YTG4	Peridotite	0.12	9.19	0.00	2703.36	1196.03	0.12	15.98	23.48	2702.14	1195.49
YTG5	Peridotite	0.18	0.00	0.00	3495.57	1338.15	0.18	4.51	31.79	3493.89	1337.50
YTG6	Peridotite	0.33	3.57	3.87	2269.57	2390.62	0.33	6.08	21.47	2268.56	2389.55
YTG7	Peridotite	0.34	2.57	2.46	2332.13	525.47	0.34	5.01	19.63	2331.06	525.23
YTG8	Peridotite	0.41	3.61	6.02	1620.16	461.87	0.41	5.62	20.09	1619.46	461.67
YTG9	Peridotite	4.27	9.56	7.00	959.24	74.87	4.28	9.75	8.36	958.85	74.84

The variations observed in the calculated results of the tenors below are due to application of background values under Barnes and Frances for different deposits and their lithologies based on microprobe and whole rock data. Gabbroic rocks are less mineralised in Zhongchang as opposed to periditotes, while one backgound values was applied to Yantiangou as there is only peridotite hosting mineralization in that deposit.

The Barnes and Lightfoot method on the other hand applies constant values across the deposits and rock untis for calculation of the tenors. While this method has proved to be very accurate in in calculating tenors, it can be misleading as no controls are put in place it tends to overestimate values that are especially below the background. It is not reccommended to be used for rocks with very low sulphide content containing less than 1% modal sulphides as low suphide content minerals are prone to sulphur redistribution during wearthering and metamorphism.

Samples with less than 1% sulphur the error of calculation is higher as a bigger proportion of the metals is in silicates and not sulphides. The less sulphide in the rock the bigger proportion of metals in the silicates.

7.3 NORMALIZATION TO MANTLE

Chalcophile elements can be presented on mantle normalised graphs with the intention of comparing their distribution relative to one another (Barnes and Lightfoot., 2005). These mantle-normalized metal patterns of can be applied to evaluating the effects of partial melting, crystal fractionation and sulphide saturation in mafic and ultramafic rocks (Pasava et al., 2003). These factors are evaluated based on the different partition coeffecients of the PGE and Ni-Cu into sulphides.

During partial melting of the mantle material, the level of partial melting will determine the amount of sulphur incorporated in the melt or remaining in the mantle. Too little melting will leave most of the sulphur in the mantle, and given the partition coeffecients of PGE's, which is up to tens of times more than that of copper and nickel, the magma produced will be PGE depleted as a consequence of their partitioning and remaining in the mantle sulphides (Barnes et al., 1998). Rocks forming from this magma will be depleted in PGE relative to copper and nickel which will form trough-shaped graph patterns. Rocks forming from the segregation of magma enriched in PGE will have arch shaped patterns (Barnes et al., 1988). Mantle-derived magmas from which Ni-Cu deposits form tend to be depleted in PGE relative to Ni and Cu.

The elements below are arranged in order of decreasing melting points (Barnes et al., 1985).

Table 4: Primitive mantle values

Primitive Mantle Values (Barnes and Lightfoot., 2005)						
Ni (ppm)	Rh (ppb)	Pd (ppb)	Pt (ppb)	Co (ppm)	Au (ppb)	Cu (ppm)
1960	0.95	4	7	105	1	30

Table 5: Trace element mantle normalized values for Zhongchang and Yantiangou.

Sample	Rock Type	Ni	Rh	Pt	Pd	Au	Cu
ZC1	Peridotite	3.885	1.589	79.143	35.000	43.000	396.480
ZC2	Peridotite	1.543	1.695	57.857	52.000	118.000	209.825
ZC3	Peridotite	2.479	2.063	27.000	33.000	108.000	263.690
ZC4	Gabbro	0.086	1.263	0.261	0.975	2.120	4.372
ZC5	Gabbro	0.013	1.821	0.260	0.548	3.600	2.138
ZC6	Gabbro	0.226	1.253	0.571	0.403	5.800	3.850
ZC7	Gabbro	0.014	1.821	0.169	0.223	2.530	1.372
ZC8	Gabbro	0.013	1.916	0.144	0.338	2.000	0.728
ZC9	Gabbro	0.015	1.600	0.171	0.285	1.530	0.727
ZC10	Peridotite	0.367	1.400	0.614	0.800	10.500	13.202
ZC11	Gabbro	0.023	1.863	0.167	0.253	4.500	1.317
YTG1	Peridotite	0.409	1.526	2.571	3.725	3.700	7.616
YTG2	Peridotite	0.635	1.884	12.857	2.700	27.200	69.720
YTG3	Peridotite	0.168	1.158	0.871	0.528	4.500	12.369
YTG4	Peridotite	0.146	1.958	0.471	0.365	2.780	6.507
YTG5	Peridotite	0.297	1.421	0.914	0.613	0.690	2.756
YTG6	Peridotite	0.362	1.611	1.071	1.975	1.700	6.699
YTG7	Peridotite	0.339	1.621	1.129	0.445	0.420	5.663
YTG8	Peridotite	0.424	1.989	0.957	0.478	3.700	7.749
YTG9	Peridotite	1.824	1.211	5.857	0.800	7.700	139.020

The mantle normalised diagrams of the Zhongchang peridotites show enrichment of metals as compared to the gabbros (Fig 56). This indicates that the peridotites experienced higher amounts of metal partitioning than the gabbros and therefore higher mineralization content. The general trend for the Yantiangou deposit shows an only slight metal enrichment. This shows that metal partitioning was very low due to either low sulphur content or low metal content of the parental magma. This is apparent in the low volume of disseminated sulphides in a large volume of rock that retain PGE's.

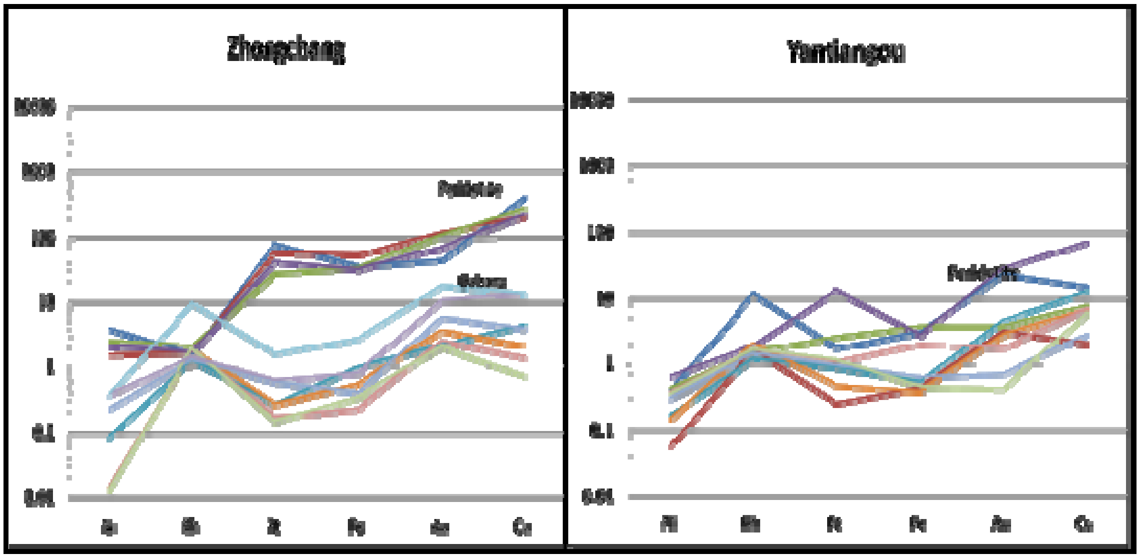

Figure 56: Mantle normalised plots of Zhongchang gabbro and peridotite as well as Yantiangou.

On average values plotted in Fig 57, Zhongchang peridotite and Yantiangou have enriched metal values with respect to the mantle. Zhongchang peridotite shows higher enrichment values than the Yantiangou peridotite. The Zhongchang gabbro is depleted, displaying below mantle values for almost all metals.

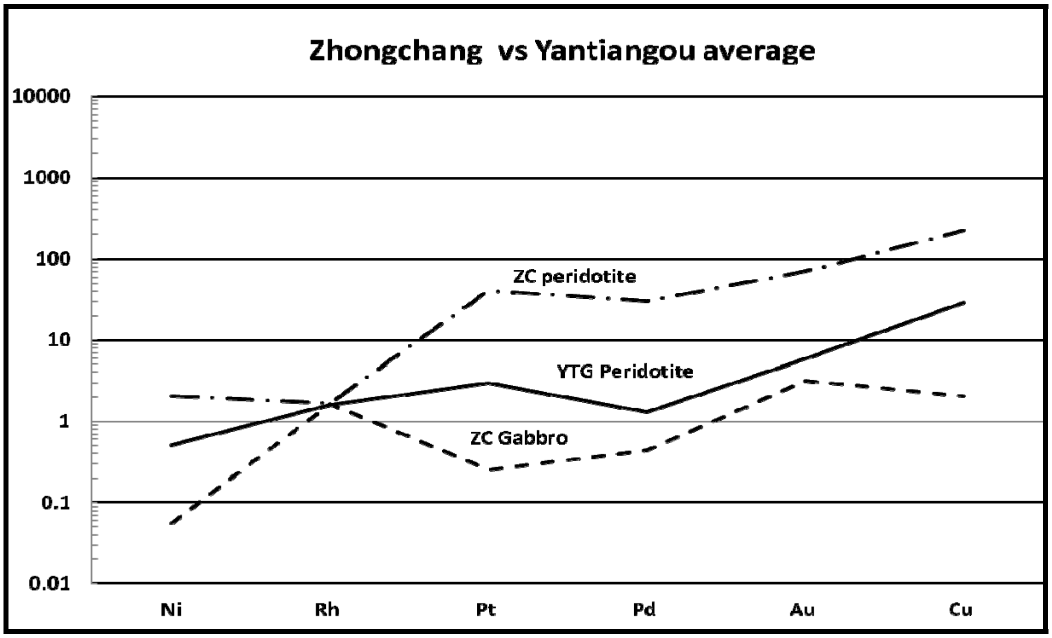

Figure 57: Comparison of mantle normalised values between Zhongchang gabbro, peridotite and Yantiangou which is entirely peridotite.

7.4 Cu/Pd RATIOS

In terms of the depletion of the rocks in the Zhongchang deposit, the gabbros and peridotites show similar amount of depletion with respect to mantle values. The higher Pd content for the peridotites which are mineralized, indicates accumulation of sulphides as opposed to the lower Pd content in the gabbros which are barren (Fig 58).

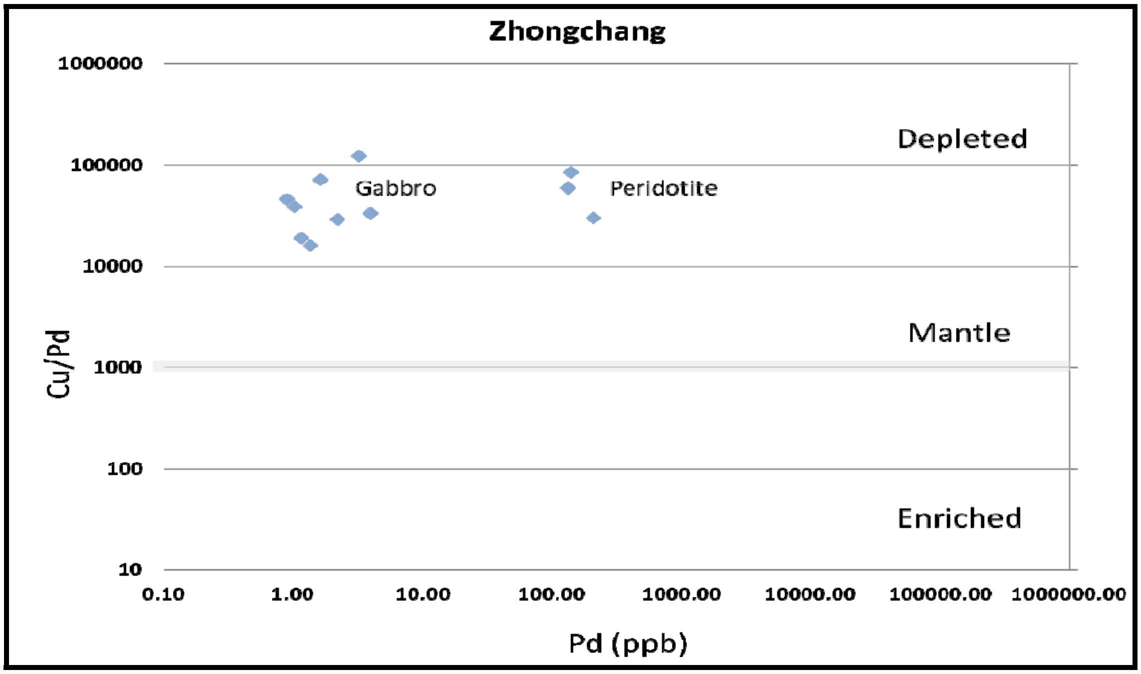

Figure 58: Cu/Pd plot of Zhongchang showing depleted nature of the magma relative to parental magma.

Yantiangou peridotites have experienced sulphide saturation and segregation. The peridotites are depleted relative to the mantle. The slight variations in the lower Pd and relatively higher Cu/Pd values can be attributed to earlier differentiation of some PGE rich sulphides (Fig 59).

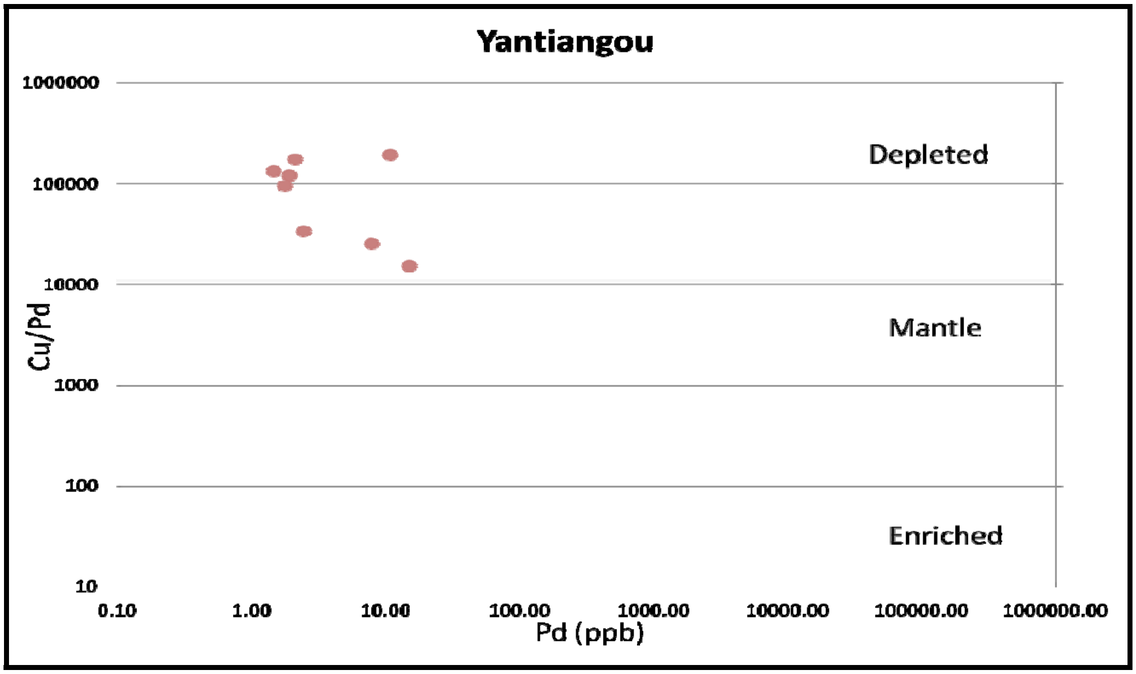

Figure 59: Cu/Pd plot of Yantiangou showing depleted nature of the magma relative to parental magma.

CHAPTER 8 DISCUSSION

8.1 ZHONGCHANG DEPOSIT

8.1.1 Petrography and petrogenesis

Ultramafic rocks in the Zhongchang deposit are formed by olivine, clinopyroxene, hornblende and minor biotite. Alkali feldspars and quartz are developed in the gabbro. These minerals preserve fresh forms for the most part, however, serpentine occurs in some olivine and the plagioclase displays sericitization. Other alteration minerals present are replacement carbonates and chlorite; hornblende and feldspars display epidote alteration.

In the gabbro, presence of sericitised (often pervasively) plagioclase feldspars, altered primary hornblende, replacement carbonates, chlorite alteration and interstitial quartz provide indication of reaction involving exchange of fluids between the intrusive rock and the country rock. This kind of alteration displays low temperature (~300°C) mineralogical assemblages in gabbro which forms chlorite, albite, quartz and magnesium hornblende (Ray et al., 2009).

Serpentinisation of olivine and secondary hornblende and epidote in pyroxenite also suggest hydration and low temperature alteration of the minerals. Pressure measurements for hornblende vary between 0-10 kbars using probe- amphibole formula calculator with classifier and barometer (Tindle and Webb., 1994). The amphibole compositions are primarily calcic hornblende and actinolite.

The sequence of formation observed in the silicate minerals is olivine- pyroxene-hornblende in the ultramafic units. The mineral sequence in gabbro is pyroxene-hornblende-feldspars and occasional quartz.

Sulphide minerals occur as inclusions in the pyroxenes (Fig 40, 41) and interstitially to the silicates (Fig 23). They occur as coarse, blebby and globular textured inclusions of chalcopyrite, pyrrhotite and pentlandite. Pyrrhotite and pentlandite occur as inclusions in the chalcopyrite. Chalcopyrite is the most abundant, followed by pyrrhotite and pentlandite as the least abundant sulphide. Lead and silver are present in trace quantities in altaite (PbTe), froodite ($PdBi_2$), and sperrylite ($PtAs_2$). PGE are present in trace quantities as Pt and Pd bismuthinides, arsenides and tellurides. Oxide minerals are also present in trace quantities;

these are magnetite, ilmenite and chrome spinel, occurring more in the gabbro than ultramafic units.

Mineral relationships indicate inclusions of sulphides in the silicates are from crystallization following sulphide saturation.

The relatively uniform medium grain size indicates moderate cooling and crystallization rate. Alteration minerals suggest re-equilibration of some silicate minerals. Sulphide minerals that form at high temperatures e.g. pentladite, are preserved at low temperatures and therefore not affected by re-equilibration in Zhongchang.

8.1.2 Mineral chemistry

The partitioning of Fe^{2+} and Mg between olivine and silicate melt can be used as a petrogenetic indicator to determine the chemical features of the melt. It can also be used as a geothermometer to calculate or interpolate the crystallization temperature of olivine (Ulmer., 1989).

Numerical calculations based on the method by Roeder and Emslie., (1970) were used to model olivine fractionation in order to determine the Mg # of the source magma. The distribution coefficient of Fe-Mg fractionation between olivine and magma; K_D presented experimentally to be = 0.3 was used in these calculations. It states that when olivine crystallizes from magma, the ratio of $(FeO/MgO)_{olivine}$ / $(FeO/MgO)_{melt}$ is a constant value of 0.3 and is independent of temperature. Kelemen et al., (2003) define, primitive magma as magmas with Mg# >60 and evolved magmas with Mg # < 50.

The formula for Mg # of olivine is 100×MgO/ (FeO+MgO) and, the formula for calculating the forsterite content is MgO/(MgO+FeO+MnO+CaO+NiO), all formulations done in molar.

Mg # calculated for the Zhongchang deposit range between 57 and 69 for the melts and between 82 and 88 for the olivine (Table 6). The high Mg # (82-88) of the olivine for the Zhongchang deposit indicates primitive magma, and suggests it rose rapidly through already established pathways encountering limited contamination and magma mixing along the way (Cole et al., 2000).

Table 6: Mg # in olivine and melt for Zhongchang deposit.

Sample	SiO2	FeO	MnO	MgO	CaO	NiO	Total	M FeO	M MnO	M MgO	M CaO	M NiO	MFeO/MMgO (in olv)	MFeO/MMgO (in melt)	Mg # melt	Mg # in olv	Fo content in olv
ZC6-1 1	40.37	12.63	0.19	46.65	0.3	0.2	100.34	0.176	0.003	1.166	0.005	0.003	0.151	0.503	**66.54**	**86.89**	0.86
ZC6-1 2	40.32	12.53	0.22	46.81	0.3	0.19	100.37	0.175	0.003	1.170	0.005	0.003	0.149	0.497	**66.80**	**87.02**	0.86
ZC6-1 3	40.29	12.49	0.16	46.89	0.32	0.2	100.35	0.174	0.002	1.172	0.006	0.003	0.148	0.495	**66.91**	**87.08**	0.86
ZC6-1 4	40.11	12.82	0.22	46.5	0.35	0.14	100.13	0.179	0.003	1.163	0.006	0.002	0.154	0.512	**66.14**	**86.69**	0.86
ZC6-1 5	39.89	13.21	0.18	46.16	0.29	0.11	99.83	0.184	0.003	1.154	0.005	0.001	0.159	0.531	**65.30**	**86.25**	0.86
ZC6-1 6	40.1	11.93	0.16	46.73	0.33	0.16	99.42	0.166	0.002	1.168	0.006	0.002	0.142	0.474	**67.84**	**87.55**	0.87
ZC6-1 7	39.73	13.36	0.21	45.71	0.33	0.16	99.5	0.186	0.003	1.143	0.006	0.002	0.163	0.543	**64.82**	**86.00**	0.85
ZC6-1 8	40.19	12.71	0.16	46.83	0.29	0.2	100.38	0.177	0.002	1.171	0.005	0.003	0.151	0.504	**66.49**	**86.87**	0.86
ZC6-1 9	40.31	12.31	0.18	46.82	0.32	0.19	100.14	0.171	0.003	1.171	0.006	0.003	0.146	0.488	**67.19**	**87.22**	0.87
ZC6-2 1	40.04	12.45	0.18	46.55	0.41	0.21	99.84	0.173	0.003	1.164	0.007	0.003	0.149	0.497	**66.82**	**87.03**	0.86
ZC6-2 2	39.85	12.63	0.12	46.36	0.31	0.2	99.47	0.176	0.002	1.159	0.006	0.003	0.152	0.506	**66.40**	**86.82**	0.86
ZC6-2 3	40.11	12.7	0.2	46.3	0.3	0.17	99.78	0.177	0.003	1.158	0.005	0.002	0.153	0.509	**66.25**	**86.74**	0.86
ZC10-6 1	40.1	12.96	0.14	45.23	0.31	0.13	98.88	0.181	0.002	1.131	0.006	0.002	0.160	0.532	**65.27**	**86.23**	0.86
ZC10-6 2	39.39	17.09	0.26	42.9	0.27	0.12	100.01	0.238	0.004	1.073	0.005	0.002	0.222	0.740	**57.48**	**81.84**	0.81
ZC10-6 3	39.52	15.12	0.27	44.32	0.29	0.11	99.64	0.211	0.004	1.108	0.005	0.001	0.190	0.634	**61.22**	**84.03**	0.83
ZC10-6 4	40.38	14.04	0.2	45.25	0.19	0.12	100.18	0.196	0.003	1.131	0.003	0.002	0.173	0.576	**63.44**	**85.26**	0.85
ZC10-5 1	40.02	14.47	0.21	44.89	0.23	0.14	99.95	0.202	0.003	1.122	0.004	0.002	0.180	0.599	**62.55**	**84.78**	0.84
ZC10-5 2	39.3	15.93	0.26	43.34	0.3	0.1	99.22	0.222	0.004	1.084	0.005	0.001	0.205	0.683	**59.43**	**83.00**	0.82
ZC10-5 3	39.44	16.23	0.21	42.99	0.25	0.11	99.23	0.226	0.003	1.075	0.004	0.001	0.210	0.701	**58.79**	**82.62**	0.82
ZC10-5 4	39.83	15.57	0.2	44.14	0.3	0.11	100.15	0.217	0.003	1.104	0.005	0.001	0.197	0.655	**60.42**	**83.58**	0.83
ZC10-5 5	40.58	14.27	0.26	43.91	0.28	0.14	99.44	0.199	0.004	1.098	0.005	0.002	0.181	0.603	**62.36**	**84.67**	0.84
ZC10-5 6	39.37	17.18	0.3	42.16	0.29	0.13	99.42	0.239	0.004	1.054	0.005	0.002	0.227	0.757	**56.92**	**81.50**	0.81
ZC10-5 7	39.56	16.34	0.27	43.34	0.3	0.12	99.93	0.228	0.004	1.084	0.005	0.002	0.210	0.700	**58.82**	**82.64**	0.82
ZC10-5 8	39.81	14.41	0.19	44.42	0.27	0.11	99.19	0.201	0.003	1.111	0.005	0.001	0.181	0.602	**62.41**	**84.69**	0.84
ZC10-5 1	39.61	14.63	0.17	44.92	0.21	0.12	99.65	0.204	0.002	1.123	0.004	0.002	0.181	0.605	**62.31**	**84.64**	0.84
ZC10-5 2	38.92	16.86	0.26	43.16	0.26	0.12	99.58	0.235	0.004	1.079	0.005	0.002	0.218	0.725	**57.96**	**82.13**	0.82
ZC2-3	40.387	14.651	0.243	44.033	0.251	0.172	99.82	0.204	0.003	1.101	0.004	0.002	0.185	0.618	**61.81**	**84.36**	0.84
ZC2-3 1	40.044	14.503	0.195	44.499	0.292	0.155	99.866	0.202	0.003	1.112	0.005	0.002	0.182	0.605	**62.30**	**84.63**	0.84
ZC2-3 2	40.838	12.935	0.195	46.06	0.311	0.167	100.633	0.180	0.003	1.152	0.006	0.002	0.156	0.522	**65.72**	**86.47**	0.86
ZC2-3 3	40.615	13	0.192	46.083	0.324	0.153	100.461	0.181	0.003	1.152	0.006	0.002	0.157	0.524	**65.62**	**86.42**	0.86
ZC2-3 4	40.485	13.872	0.227	45.46	0.238	0.135	100.536	0.193	0.003	1.137	0.004	0.002	0.170	0.567	**63.83**	**85.47**	0.85
ZC2-3 5	39.855	16.5	0.179	42.876	0.307	0.163	99.951	0.230	0.003	1.072	0.005	0.002	0.214	0.715	**58.32**	**82.35**	0.82
ZC2-3 6	40.355	12.673	0.17	46.414	0.32	0.152	100.141	0.177	0.002	1.160	0.006	0.002	0.152	0.507	**66.36**	**86.80**	0.86
ZC3-2 1	41.138	13.476	0.189	45.833	0.31	0.15	101.255	0.188	0.003	1.146	0.006	0.002	0.164	0.546	**64.68**	**85.93**	0.85
ZC3-2 2	40.57	13.017	0.191	45.478	0.299	0.137	99.751	0.181	0.003	1.137	0.005	0.002	0.159	0.532	**65.29**	**86.25**	0.86
ZC3-2 3	52.522	3.962	0.112	16.273	22.429	0.04	98.585	0.055	0.002	0.407	0.401	0.001	0.136	0.452	**68.86**	**88.06**	0.47
ZC3-2 4	40.49	12.801	0.184	45.591	0.286	0.165	99.617	0.178	0.003	1.140	0.005	0.002	0.156	0.521	**65.73**	**86.47**	0.86
ZC3-2 5	40.77	13.894	0.211	45.302	0.327	0.194	100.775	0.194	0.003	1.133	0.006	0.003	0.171	0.570	**63.71**	**85.41**	0.85
ZC3-2 6	40.02	13.528	0.204	45.444	0.329	0.172	99.777	0.188	0.003	1.136	0.006	0.002	0.166	0.553	**64.40**	**85.77**	0.85
ZC3-2 7	39.798	13.764	0.218	44.733	0.58	0.154	99.38	0.192	0.003	1.118	0.010	0.002	0.171	0.571	**63.64**	**85.37**	0.84
ZC3-2 8	40.451	13.803	0.196	45.082	0.323	0.135	100.046	0.192	0.003	1.127	0.006	0.002	0.171	0.569	**63.75**	**85.43**	0.85
ZC3-2 9	52.891	4.098	0.079	16.786	22.656	0.02	99.765	0.057	0.001	0.420	0.405	0.000	0.136	0.453	**68.81**	**88.03**	0.48

The high forsterite content of olivine (Fo $_{82-87}$) of the Zhongchang deposit indicates early crystallization. This low fayalite: forsterite ratio indicates a sulphur under-saturated magma resulting in early crystallization of olivine in normal magmatic fractionation, and late- stage sulphide segregation as a result of late sulphide saturation. The appearance of mineralization at the contact between the peridotite and pyroxenite could suggest crystallization of olivine rich peridotite triggered sulphide saturation. This would imply that Ni partitioned into olivine and only after, was there sulphur available as a result of fractionation to facilitate preferential partitioning of Ni into sulphides. Therefore, this highlights the production of a sulphur under-saturated magma that did not interact with much external sulphur and only reached sulphide saturation once crystallization was well advanced. Assimilation of the Huili carbonates wall rock as indicated the presence of carbonates in the gabbro also facilitated sulphide saturation on emplacement.

The average Ni partitioning amount into olivine in Zhongchang is up to ~0.12% /(1200 ppm). S-undersaturated primary basaltic magmas for the Emeishan province generally contain ~300 ppm Ni and 10-20 ppb Pt and Pd (Song et al., 2011). Considering a single pulse of magma, the amount that went into the olivine is quite significant for the deposits, however, multiple pulses and large volumes of magma are often required to form economic deposits. Tang et al., (2007) note that the major method of sulphide mineralization in China is deposits hosted by terminal chambers formed by multiple injections of sulphide bearing magma.

8.1.3 Whole rock geochemistry

Zhongchang peridotie shows more enriched metal values in mantle normalized plots, higher than the Zhongchang gabbro and the Yantiangou peridotite. This is a consequence of more effective sulphide saturation processes. Preservation of magmatic sulphide assemblage of pyrrhotite, chalcopyrite and pentlandite (Barnes and Lightfoot., 2005), which represents the major magmatic mineral assemblage is observed in the Zhongchang deposit. Higher sulphide content (low silicate-sulphide ratio) reduced redistribution of sulphur during alteration therefore preserving the mineral assemblage

Tenor calculations indicate average values for Zhongchang peridotite as 5%Ni, 9% Cu, 4300ppb Pt and 2000ppb Pd.

The high Cu/Pd ratio observed for Zhongchang deposit indicates that the parental magma may have reached earlier sulphide saturation and fractionation before emplacement. It suggests preferential scavenging of the PGE by the segregating sulphide before emplacement, and therefore a PGE deposit could possibly occur stratigraphically below (Maier., 2005).

8.1.4 Genetic model

Sulphide saturation occurred both as a consequence of fractional crystallization of early olivine and contamination from an external source. There appears to have been two episodes of silicate crystallization and sulphide saturation. These are indicated by early olivine crystallization reflected by high forsterite content in olivine, and early sulphide saturation that resulted in depletion of PGE as indicated in the Cu/Pd ratios. A second saturation phase occurred following intrusion into the wallrock carbonates of the Huili Formation that induced sulphide saturation together with ongoing crystallization.

Mungall., (2005) highlights that ‘magma depleted in PGE relative to their primary parental compositions is evidence to the existence of low-grade sulphide mineralization at lower levels in the system, and a similar model is indicated for Zhongchang.

The introduction of magma into the carbonate wallrocks resulted in the addition of S and CO_2 (from limestone sediments generally rich in sulphur and carbon). Heat loss due to crystallization of olivine and pyroxenes released heat to melt the wallrocks, incorporating S and CO_2 into the magma, decreasing fO_2 and triggering S saturation. The residual low density SiO_2 magma then caused convection, promoting fractional crystallization and segregation of sulphides at the interface between high density mafic minerals and lower density minerals with higher SiO_2 content (Song et al., 2003). This reaction produced the Ni-Cu sulphides which were entrained interstitially to silicates, and PGE hosted in the sulphides.

According to Arndt et al., (2005) this would be classified as type II a mineralization as it occurred after some silicates had already crystallized. The sulphides are coarse, blebby and globular textured and bounded by pyroxenite and peridotite units in what appears to have been generated in a vortex type setting.

Alkali composition of basalts and picrites are excluded by Arndt et al., (2005) for having the capacity to host major Ni-Cu-PGE deposits other than the Siberian flood basalts underlain by sedimentary beds of anhydrite. Both deposits display alkaline characteristics; Zhongchang pyroxenites reflect alkali composition displayed in sodic-potassic feldspar compositions. The intrusion was emplaced in the dolomitic sediments therefore may represent another exception to the rule. Tang et al., 2007 suggests that 'the alkalescent picrititc magma that formed these deposits must have experienced middling melting in deep- mantle and evolved to olivine and harzburgitic magma which is in turn favourable for metallogeny'.

8.2 YANTIANGOU DEPOSIT

8.2.1 Petrography and petrogenesis

The rock forming minerals in Yantiangou are olivine, pyroxene, biotite and hornblende. Alteration is apparent along reaction margins around biotite and hornblende indicating oxidation and hydration, and a drop in pressure and temperature as a result of magma pushing up. Secondary minerals formed in these reactions are chlorite, hornblende and carbonates.

The sulphide minerals in the Yantiangou deposit are hosted in biotite, suggesting crystallization occurred in a hydrous environment, and that olivine and pyroxenes formed before sulphides. The occurrence of primary amphiboles also supports involvement of water. Alteration minerals, i.e. hornblende and chlorite indicate an increase in temperature and fO_2 in the system. Some of the biotite also could be formed after pyroxene or hornblende due to late- stage alteration/ hydration of magmatic minerals. The alkali feldspar composition is indicative of an alkaline trend of the parental magma/ tephritic composition. This is somewhat consistent with the bark-arc extension and rifting model proposed in He et al., (2013).Chrome spinel is the only oxide mineral present in Yantiangou.

Sulphide minerals occur throughout the peridotite as small disseminations of only up to 200µm size. They are chalcopyrite, pyrrhotite, pyrite, pentlandite and millerite. Chalcopyrite is the most abundant with inclusions of pyrrhotite and pentlandite which were early forming. Pyrite and millerite formed at a later stage and their presence indicates hydrothermal circulation in the rock as a result of a late hydrothermal/ mesothermal event. This led to the breakdown of pyrrhotite and pentlandite in the Fe and Ni- rich mss, and the redistribution of minerals to form pyrite and millerite.

The coarse equigranular texture displayed by most of the rock indicates cooling at a slow rate. Hydrothermal/ mesothermal alteration resulted in re-equilibration of some silicate and sulphide minerals as indicated by chlorite alteration and presence of pyrite and millerite

8.2.2 Mineral chemistry

A higher forsterite to fayalite (Fo $_{(72\text{-}89)}$) ratio is observed in the Yantiangou deposit where emplacement took place through a mafic dyke. This ratio suggests olivine crystallization occured before the onset of sulphide saturation which occured as a result of fractionation. Mg numbers for Yantiangou, the Mg # for the melts range between 44 and 72 and between 72 and 89 for the olivine (Table 7). The Yantiangou magma is more evolved than the Zhongchang magma, although it retains some primitive values. This also indicates minimal differentiation and contamination.

Arndt et al., (2005) indicate that a strongly sulphide undersaturated magma crystallizes large amounts of silicate minerals before the exsolution of immiscible sulphide, and will likely form a large volume of rock containing small sulphide disserminations between silicate minerals. This is seen to be the case with the Yantiangou deposit as olivine and pyroxene crystals were formed before sulphide minerals, given by the sulphides hosted in the later forming biotite and occuring as disseminations in the rockmass.

The average amount of Ni in olivine for Yantiangou goes up to 0.17%/ (1700 ppm). Therefore, multiple pulses of magma, or a large volume of magma would have been required to supply enough metal to form an economic deposit.

8.2.3 Whole rock geochemistry

Yantiangou deposit shows less enriched metal values in mantle normalized plots, than the Zhongchang peridotite. The major mineral assemblage observed in magmatic sulphide deposits of pyrrhotite, chalcopyrite and pentlandite (Barnes and Lightfoot., 2005) is not preserved in Yantiangou. Pyrite and millerite have been added to the assemblage, replacing some of the original sulphide minerals. This is an effect of low sulphide content exposing a high surface area to volume ratio of the sulphides to alteration and sulphur redistribution (Barnes and Lightfoot., 2005).

Average tenors for Yantiangou peridotite are 3.2%Ni, 6.5% Cu, 3000ppb Pt and 1300 ppb Pd.

The Cu/Pd ratios indicate the magma is depleted in PGE relative to mantle. The depletion values in Yantiangou are however up to 10 times more than Zhongchang. These higher ratios indicate PGE depletion by early fractionation of PGE enriched sulphides from the magma (which would offset Cu vs Pd), resulting in a PGE deposit stratigraphically below similar to the model proposed by Maier (2005).

Table 7: Mg # in olivine and melt for Yantiangou deposit.

Sample	SiO2	FeO	MnO	MgO	CaO	NiO	Total	MFeO	MMnO	MMgO	MCaO	MNiO	MFeO/MMgO (in olv)	MFeO/MMgO (in melt)	Mg # melt	Mg # olv	Fo content in olv
Ytg4-1 1	39.584	15.081	0.221	43.79	0.421	0.243	99.51	0.210	0.003	1.095	0.008	0.003	0.192	0.640	**60.99**	**83.90**	0.83
Ytg4-1 1	40.08	14.76	0.27	43.57	0.41	0.28	99.38	0.206	0.004	1.089	0.007	0.004	0.189	0.629	**61.38**	**84.12**	0.83
Ytg4-1 2	40.03	14.78	0.25	43.67	0.4	0.26	99.39	0.206	0.004	1.092	0.007	0.003	0.189	0.629	**61.41**	**84.14**	0.83
Ytg4-1 3	40.17	15.47	0.26	43.7	0.37	0.25	100.21	0.215	0.004	1.093	0.007	0.003	0.197	0.657	**60.34**	**83.53**	0.83
Ytg4-2 1	39.88	15.64	0.28	43.9	0.41	0.24	100.35	0.218	0.004	1.098	0.007	0.003	0.198	0.662	**60.18**	**83.44**	0.83
Ytg4-2 2	40.17	16.61	0.36	42.65	0.37	0.23	100.38	0.231	0.005	1.066	0.007	0.003	0.217	0.723	**58.03**	**82.17**	0.81
Ytg4-2 4	40.05	14.19	0.3	44.33	0.47	0.21	99.54	0.198	0.004	1.108	0.008	0.003	0.178	0.594	**62.72**	**84.87**	0.84
Ytg4-2 5	40.37	13.78	0.28	44.51	0.4	0.28	99.62	0.192	0.004	1.113	0.007	0.004	0.172	0.575	**63.50**	**85.29**	0.84
Ytg4-3 2	39.9	15.38	0.25	43.92	0.41	0.26	100.12	0.214	0.004	1.098	0.007	0.003	0.195	0.650	**60.60**	**83.68**	0.83
Ytg4-3 3	40.46	13.71	0.24	44.91	0.41	0.26	99.98	0.191	0.003	1.123	0.007	0.003	0.170	0.567	**63.82**	**85.46**	0.85
Ytg4-4 1	38.58	24.55	0.42	36.18	0.35	0.1	100.2	0.342	0.006	0.905	0.006	0.001	0.378	1.260	**44.25**	**72.57**	0.72
Ytg4-4 2	39.31	17.26	0.32	42.13	0.41	0.21	99.63	0.240	0.005	1.053	0.007	0.003	0.228	0.761	**56.79**	**81.42**	0.81
Ytg4-4 3	37.99	24.81	0.42	36.42	0.39	0.15	100.17	0.346	0.006	0.911	0.007	0.002	0.380	1.265	**44.15**	**72.49**	0.72
Ytg4-5 1	38.36	20.24	0.29	40.47	0.43	0.2	99.99	0.282	0.004	1.012	0.008	0.003	0.279	0.929	**51.85**	**78.21**	0.77
Ytg4-5 2	39.59	16.24	0.27	43.55	0.4	0.2	100.26	0.226	0.004	1.089	0.007	0.003	0.208	0.692	**59.08**	**82.80**	0.82
YTG8-1 1	39.5	18.25	0.19	41.93	0.32	0.15	100.34	0.254	0.003	1.048	0.006	0.002	0.242	0.808	**55.30**	**80.48**	0.80
YTG8-1 2	40.8	10.22	0.13	47.68	0.37	0.33	99.52	0.142	0.002	1.192	0.007	0.004	0.119	0.398	**71.53**	**89.33**	0.88
YTG8-1 3	40.66	10.51	0.17	47.73	0.37	0.29	99.73	0.146	0.002	1.193	0.007	0.004	0.123	0.409	**70.98**	**89.07**	0.88
YTG8-1 4	40.37	12.19	0.16	46.75	0.32	0.26	100.05	0.170	0.002	1.169	0.006	0.003	0.145	0.484	**67.38**	**87.32**	0.87
YTG8-2 1	40.16	13.55	0.19	45.27	0.4	0.2	99.78	0.189	0.003	1.132	0.007	0.003	0.167	0.556	**64.27**	**85.71**	0.85
YTG8-2 2	40.34	13.87	0.19	44.55	0.37	0.22	99.53	0.193	0.003	1.114	0.007	0.003	0.173	0.578	**63.37**	**85.22**	0.84
YTG8-2 3	40.98	12.31	0.23	46.26	0.34	0.2	100.32	0.171	0.003	1.157	0.006	0.003	0.148	0.494	**66.93**	**87.09**	0.86
YTG8-2 4	40.26	12.83	0.1	46.29	0.34	0.19	100.01	0.179	0.001	1.157	0.006	0.003	0.154	0.515	**66.02**	**86.62**	0.86
YTG5-1 1	39.14	20.26	0.06	39.9	0.33	0.05	99.73	0.282	0.001	0.998	0.006	0.001	0.283	0.943	**51.47**	**77.95**	0.78
YTG3-1 2	39.32	17.29	0.03	42.91	0.45	0.27	100.26	0.241	0.000	1.073	0.008	0.004	0.224	0.748	**57.20**	**81.67**	0.81
YTG3-2 1	39.46	18.03	0	43.54	0.42	0.24	101.69	0.251	0.000	1.089	0.008	0.003	0.231	0.769	**56.53**	**81.25**	0.81
YTG3-2 2	39.51	17.78	0.04	42.9	0.5	0.29	101.01	0.248	0.001	1.073	0.009	0.004	0.231	0.770	**56.51**	**81.24**	0.80
YTG3-2 3	39.25	18.01	0.06	41.88	0.48	0.21	99.88	0.251	0.001	1.047	0.009	0.003	0.240	0.799	**55.60**	**80.67**	0.80
YTG3-2 4	39.39	15.64	0.06	43.95	0.46	0.22	99.73	0.218	0.001	1.099	0.008	0.003	0.198	0.661	**60.21**	**83.46**	0.83
YTG3-2 5	38.81	19.68	0.04	41.3	0.43	0.1	100.35	0.274	0.001	1.033	0.008	0.001	0.265	0.885	**53.05**	**79.02**	0.78
YTG3-2 5	38.68	18.37	0.05	41.26	0.42	0.28	99.06	0.256	0.001	1.032	0.008	0.004	0.248	0.827	**54.74**	**80.13**	0.79
YTG3-4 1	38.58	18.35	0.05	41.9	0.46	0.27	99.61	0.256	0.001	1.048	0.008	0.004	0.244	0.813	**55.15**	**80.39**	0.80
YTG3-4 2	38.59	17.85	0.08	41.59	0.44	0.17	98.72	0.249	0.001	1.040	0.008	0.002	0.239	0.797	**55.65**	**80.70**	0.80
YTG5-1 1	38.22	20.75	0.05	39.53	0.31	0.17	99.02	0.289	0.001	0.988	0.006	0.002	0.292	0.975	**50.64**	**77.37**	0.77
YTG5-3 1	39.09	15.45	0.07	43.87	0.25	0.3	99.04	0.215	0.001	1.097	0.004	0.004	0.196	0.654	**60.46**	**83.60**	0.83
YTG5-3 1	39.36	14.04	0.05	44.8	0.32	0.31	98.87	0.196	0.001	1.120	0.006	0.004	0.175	0.582	**63.21**	**85.14**	0.84
YTG5-3 1	39.23	19.21	0.07	40.89	0.34	0.12	99.85	0.268	0.001	1.022	0.006	0.002	0.262	0.872	**53.41**	**79.26**	0.79
YTG5-3 2	39.29	16.36	0.04	39.04	3.64	0.06	98.43	0.228	0.001	0.976	0.065	0.001	0.233	0.778	**56.24**	**81.07**	0.77
YTG5-3 3	38.94	18.24	0.06	41.92	0.29	0.14	99.59	0.254	0.001	1.048	0.005	0.002	0.242	0.808	**55.31**	**80.49**	0.80
YTG5-3 4	39.5	16.11	0.06	43.47	0.32	0.11	99.57	0.224	0.001	1.087	0.006	0.001	0.206	0.688	**59.23**	**82.89**	0.82

8.2.4 Genetic model

The genetic model for Yantiangou deposit is suggested to represent formation through a sulphide bearing mush introduced into a fault or a point of weakness in the quartz phyllite wallrocks. Sulphide segregation occurred in a staging chamber at depth and a sulphide melt was expelled through conduits such as the Yantiangou dyke (Song et al., 2005). The Yantiangou deposit could represent a conduit or a basal part of a now eroded former mafic-ultramafic intrusion. The low tenors are as a result of a less rich source compounded by a long period of sulphide undersaturation.

Relatively high proportions of Ni partitioned into olivine. These suggest that the magma stalled in a staging chamber while mafic minerals continued to crystallize, leading to much of the Ni going into olivine before sulphur became sufficient enough to scavenge chalcophiles. The staging chamber model is also supported by the earlier point on Cu accumulation, as a result of prolonged interaction between sulphur and metals before the metal enriched mush was expelled.

The Yantiangou deposit can be classified as a type II b with fine grained disseminated sulphides according to Arndt et al., 2005. If the parent magma was too sulphur undersaturated and reaches saturation well into crystallization, only small amounts of interstitial disseminated sulphides are formed (Arndt et al., 2005). However, due to overprinting of the original sulphide mineralogy, the suggested model and interpretations may not be entirely applicable.

Figure 60 modified after Song et al., 2008, attempts to illustrate the formation and deposition of the two deposits within the Permian Emeishan Large Igneous Province system.

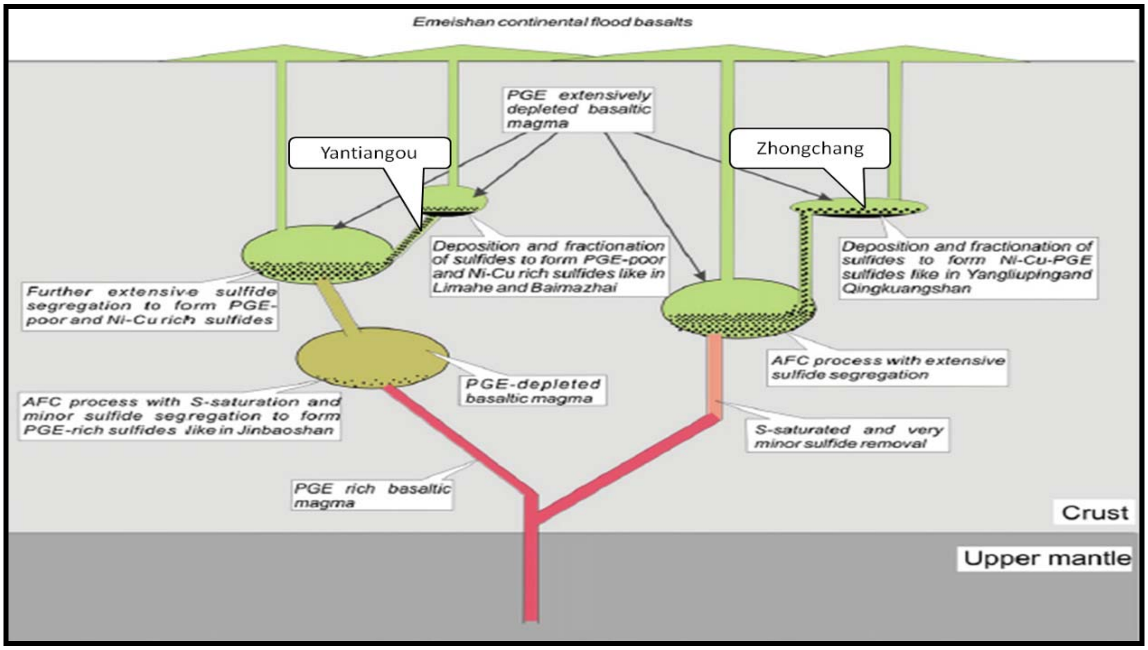

Figure 60: A petrogenetic model showing formation of three types of magmatic sulphide deposits in the ELIP. Ni-Cu-PGE deposits are related to extensive sulphide segregation from weakly PGE-depleted basaltic magmas due to prior sulphide separation. (Modified after Song et al., 2008).

The Zhongchang deposit represents a Ni-Cu-PGE deposit like Yangliupin and Qingkaunshan in the figure on the right. The Yantiangou deposit represents PGE poor Ni-Cu deposits eg Limahe and Jinbaoshan on the left in the figure. Both magmas indicate depletion of PGE relative to mantle.

The main characteristics of the Zhongchang and Yantiangou deposits are listed below.

Table 8 Zhongchang and Yantiangou characteristics

FEATURE	**ZHONGCHANG**	**YANTIANGOU**
Shape	Funnel shaped	Dyke/ conduit
Hostrock	Peridotite/ pyroxenite	Peridotite
Wallrock	Limestones/ carbonates	Quartz phyllite/ schist
Host rock petrology	Olivine, clinopyroxene, hornblende	Olivine, clinopyroxene, biotite
Alteration	Hornblende, carbonate, chlorite, epidote	Chlorite, carbonate
Mineralogy	Chalcopyrite, pyrrhotite, pentlandite	Chalcopyrite, pyrrhotite, pentlandite, millerite, pyrite
Mineral chemistry	Mildly alkaline	Highly alkaline (potassic)
Mineralization	Coarse, blebby globular sulphides	Fine grained disseminated sulphides
	PGE tellurides, bismuthinides	PGE tellurides, bismuthinides
Oxide minerals	Magnetite, ilmenite and chrome spinel	Chrome spinel
Average tenors	5%Ni, 9% Cu, 4300ppb Pt and 2000ppb Pd	3.2%Ni, 6.5% Cu, 3000ppb Pt and 1300 ppb Pd.

CHAPTER 9 EXPLORATION

Ni-Cu-PGE mineralization is hosted by mafic- ultramafic magmatic rocks. In terrains such as the Emeishan continental flood basalts, the deposits are associated with mafic- ultramafic intrusions forming sills and dykes which would have served as conduits or feeders to the larger igneous masses (Eckstrand and Hulbert, 2007).Exploration for magmatic Ni-Cu-PGE deposits is dependent on factors that suggest presence of mineralization, resulting in contrasting characteristics between mineralized and unmineralized rock.

Exploration can be performed for similar deposits in the same area for cluster occurrence (mining camp), or for resource extension in the existing deposits. Methods applicable for such purposes are presented.

9.1 REMOTE SENSING

Remote sensing is acquiring imagery and related data from space using aircrafts and satellites, processing and interpreting the data (Sabins., 1999). Electromagmetic energy that is propagated from a source will be reflected, absorbed or transmitted on interaction with different features (Gupta., 2003). Acquired data is processed to filter the different spectral responses and wavelengths. The differences in response of the features as well as the variable intensity of responses is what is used to distinguish one feature from another during data interpretation (Gupta., 2003).

Landsat Thematic Mapper (TM) is often applied in doing reconnaissance studies in mineral exploration for Ni-Cu-PGE due to its capacity to cover a large region. It is applied in planning phases to delineate features and accessibility of the area, eg rives, routes, forests that provide insight on approaching reconnaissance field work. It may also assist in delineating major geological trends such as major folds, faults and contrasts in lithologies. Spectral bands can be adjusted for higher resolution. Data from ASTER which has more enhanced spatial and spectral resolution, can be overlain on the Landsat TM data to map alteration in rocks (Gupta., 2003). This can be applied to the Zhongchang and Ynatiangou deposits as they contain some alteration minerals (hornblende and chlorite) However, the application of remote sensing in exploration of deep lying Ni-Cu-PGE deposits is currently limited due to its shallow depth of penetration.

9.2 GEOCHEMISTRY

Geochemistry can be applied in whole rock analyses as the primary environment or soil analysis which is secondary media of deposition from breakdown at source or transported material. Geochemical analyses are based on identification of elemental signatures against background values which in rocks are signatures of crustal contamination (isotopic studies) and sulphide liquid segregation (Barnes et al., 2004). In soils, the geochemical exploration will look for pathfinder elements which may indicate favourable underlying geology. For example Mg, Fe, Ti, Cr which may be indicative of ultramafic substrate. The focus will be on the whole rock geochemistry of the study deposits.

In whole rock geochemistry, Barnes et al., 2004 highlight that for magmatic sulphide deposits, magmatic signatures for the elements Mg, Fe, Si, Al, Ti and Cr can indicate if mineralization has taken place. These signatures remain somewhat undisturbed even during alteration and will retain their primary signatures. The identification of a combination of this mineral suite will point to a favourable environment for the occurrence of a mafic-ultramafic magmatic body, while enrichment of incompatible lithophile trace elements may indicate contamination and fractionation (Barnes et al., 2004).

A mantle normalized trough shaped pattern indicates depletion and that sulphide segregation has taken place and a PGE deposit may exists stratigraphically below. For plots that indicate neither depletion nor enrichment, sulphide saturation may not have occurred at that point yet, however it could have occurred stratigrapically above forming a PGE deposit (Barnes et al., 1988). To determine the proper shape of the graph, analyses for the whole magmatic metal suite (Ni Os Ir Ru Rh Pt Pd Au Cu) is required using NiS concentration method. In this case PbO analysis was used as is cheaper but does not provide the whole suite.

Depletion of the elements sought, i.e. Ni-Cu-PGE in comagmatic rocks (Song et al., 2011) can be an indication of mineralization at depth and some element ratios can also be used to identify proximal mineralization. PGE depletion normalised to mantle values against less depletion of Ni and Cu is an indicator that sulphide segregation has taken place as will be reflected in Cu/Pd and Ni/Ir ratios less than mantle values (Barnes and Lightfoot 2005).

Both Cu and Pd show strong affinity for sulphides, however, the strongly chalcophile Pd is preferentially depleted during sulphide segregation by up to 10 times more than Cu, resulting in an increase in Cu/Pd and subsequently, the sulphide melt concentrates mostly Pd (and other PGE), leading to its depletion at a rate much higher than Cu (Maier et al., 2004; Li et al., 2001). Therefore, PGE-enriched zones will show Cu/Pd ratios lower than the mantle range (Li et al., 2001). Zhongchang and Yantiangou deposits have Cu/Pd ratios that show depletion relative to the mantle, and the ranges (1000-10000), suggest genesis from magmas fertile in chalcophile elements.

The whole rock Cu/Zr ratio is a useful tool for Ni-Cu exploration. Both Cu and Zr are highly incompatible, but Cu is chalcophile. If sulphide melt separates from the magma, Cu concentrates in the sulphide melt. Undepleted mantle values for Cu/Zr ratios are close to 1, and mantle depletion owing to sulphide segregation results in Cu/Zr ratios of less than 1 (Keays and Lightfoot, 2010).

Geochemical signatures for contamination e.g. identification compatible and incompatible lithophile elements REEs for magma composition and evolution (Arndt et al., 2005) can be a useful tool in exploration as it shows if crustal contamination has taken place.

A higher degree of depletion of Ni in olivine relative to the depletion caused by crystallization of silicate minerals can signify sulphide segregation (Li et al., 2001; Song et al., 2011). Ni partitioning into olivine without the influence of a sulphide typically shows a linear correlation with MgO attributed to olivine accumulation and fractionation (Arndt et al., 2005). For Zhongchang and Yantiangou deposits, nickel is observed in Figs 5354 to have partitioned into olivine under sulphide undersaturated conditions. The occurrence of sulphide saturation however resulted in higher accumulation of Ni in sulphides as seen in tenor calculations and mantle normalized plots.

9.3 GEOPHYSICS

Application of geophysics is largely dependent on the physical contrasts between mineralized and unmineralized rock. Geophysical responses of subsurface geology are measured through input of natural energy fields or artificially generated energy, and are interpreted to determine the cause of the variation. Different geophysical methods used in exploration for magmatic Ni-Cu PGE sulphide deposits include gravity and magnetic methods which use natural energy of the earth and objects to generate a response, and electrical and electromagnetic methods which can use the earth's natural electrical and electromagnetic energy or can be operated by artificially generated energy.

9.3.1 Gravity Surveying

Subsurface geology is investigated using variations in the earth's gravitational potential field and these variations are as a result of differences in the rock densities. An anomalous buried body will register a localized response/ pertubation different from its surrounding or host rock (Kearey et al., 2002). This gravitational response constrain buried or concealed mafic-ultramafic bodies (Lightfoot., 2007), and also reveal the depth and the shape of the anomaly. Therefore, dense ultramafic bodies are often discovered through the use of gravity and if mineralized, sulphides can serve to increase the response. Airborne gravity surveys are the recommended method as they can cover a large surface area in little time and are therefore useful in regional and local scale applications (Lightfoot., 2007).This technique can be applied deposits in the same area as Zhongchang and Yantiangou due to lithological differences between ultramafic intrusions and the country rocks.

9.3.2 Electrical Surveying

Electrical surveying has variable methods some which use the earth's potential fields and others artificially generated direct or low frequency alternating currents introduced into the ground

Induced polarisation utilises capacitive action of the subsurface to locate zones of disseminated mineralization within the host rocks. Electric current is introduced into the ground which then acts as a capacitor by storing electrical charge, apparent resistivity is measured and can be used to identify the presence of low grade disseminated sulphide deposits which have strong IP effect but are non-conducting (Kearey et al., 2002). Disseminated sulphides typically are unconnected, so they can be targeted using induced polarization methods (Lighfoot., 2007). Induced polarization is the most effective method for search of disseminated sulphide bodies and is therefore applicable to the Zhongchang, Yantiangou and similar deposits whose sulphides are unconnected.

CHAPTER 10 CONCLUSIONS

Based on the observations and the data presented, the following conclusions have been made:

Ca-Mg clinopyroxene is dominant in both deposits, and feldspars for both deposits show alkaline tendencies indicating a tephritic source. This is more obvious in Yantiangou due to prevalent biotite.

Zhongchang and Yantiangou deposits show Cu/Pd depletion relative to mantle indicating sulphide saturation has taken place before emplacement. Mantle normalised plots for the deposits indicate enrichment in metals relative to the mantle due to sulphide accumulation. Zhongchang mineralization is more enriched than Yantiangou.

Early olivine crystallization is evident in both deposits, this is seen in high Fo values, and indicates nickel partitioning into olivine before sulphide saturation.

Fractional crystallization is the main mechanism that induced sulphide saturation following removal of early olivine from the melt. This is apparent in most sulphide minerals being hosted by biotite in Yantiangou. In Zhongchang, both fractional crystallization and contamination played a part in sulphide saturation as observed in sulphides hosted mainly by clinopyroxene and along margins with olivine.

The low tenors for Yantiangou indicate that magma was too sulphur undersaturated, reaching saturation well into crystallization, hence forming small amounts of interstitial disseminated sulphides. Olivine retained a relatively large amount of Ni (~0. 26%) as a result of sulphur undersaturation.

The interaction of the Zhongchang magma with Huili carbonates triggered a second sulphide saturation phase, forming a Ni-Cu-PGE deposit. Alteration minerals came about as a result of temperature changes and fluid exchange with the wallrocks.

PGE underwent partitioning into sulphides and into other forms (bismurthinides, arsenides and tellurides,), during variable stages of sulphur content in the magma. PGE minerals precipitated to form michenerite (PdBiTe) and sperrylite ($PtAs_2$), and also occur as inclusions within sulphides.

Zhongchang retained magmatic sulphide assemblage of chalcopyrite, pyrrhotite and pentlandite even during alteration, while Yantiangou sulphide assemblage has been altered due to a high silicate- sulphide ratio in the rock.

The average tenor values for Zhongchang are 5% Ni, 9% Cu, 4300ppb Pt and 2000ppb Pd, while the average tenors for Yantiangou are 3.2% Ni, 6.5% Cu, 3000ppb Pt and 1300 ppb Pd.

Geophysical exploration methods that utitise gravity contrasts and electrical coductivity and/ or resistivity can be used to search for similar types deposits. Ultramafic rocks register gravity highs, and unconnected sulphides register induced polarization anomalies.

Where alteration is expected to be present, remote sensing can be applied for such a prospect as well as being useful for low resolution geological and structural mapping. Magmatic signatures for the mafic mineral elements Mg, Fe, Si, Al, Ti and Cr, commonly associated with magmatic deposits, can indicate if mineralization has taken place.

Geochemical values of Cu/Pd and Cu/Zr ratios that show metal depletion relative to the mantle values can signal sulphide saturation and fractionation occured at depth, and are good tools to use. Mantle normalized values showing metal enrichment for a prospect also signal presence of metal that could be of economic interest.

REFERENCES

Ali, J.R., Thompson, G.M., Zhou, M.F., and Song, X., 2005. Emeishan Large Igneous Province, SW China. Lithos (79), pp 475– 489.

Arndt, N.T., Lesher, C.M., Czamanske, G.K., 2005. Mantle-derived magmas and magmatic Ni-Cu-(PGE) deposits. 100th Anniversary Volume, Society of Economic Geologists, pp 5–23.

Barnes, S.J., and Francis, D., 1995. The Distribution of platinum-group elements, nickel, copper, and gold in the Muskox Layered Intrusion, Northwest territories, Canada. Economic Geology, (90), pp. 135–154.

Barnes, S. J., and Lightfoot, P.C., 2005. Formation of magmatic nickel-sulphide ore deposits and processses affecting their copper and platinum-group element contents. In; Hedenquist, J.W., Thompson, J.F.H., Goldfarb, R.J. and Richards, J.P. (eds.) Economic Geology 100th Anniversary Volume, pp. 179–213.

Barnes, S. J., and Maier, W.D., 1999. The fractionation of Ni, Cu and the noble metals in silicate and sulphide liquids. In; Keays, R.R., Lesher, C.M. Lightfoot, P.C. and Farrow (eds): Dynamic processes in magmatic ore deposits and their application in mineral exploration. Geological Association of Canada, Short course (13), pp. 69–106.

Barnes, S.J., Naldrett, A.J., and Gorton, M.P., 1985. The origin of the fractionation of platinum group elements in terrestrial magmas. Chemical Geology (53), pp. 303–320.

Barnes, S.J., Boyd, R., Korneliussen, A., Nilsson L.P., Often M., Pedersen R.B., and Robins B., 1988.The use of mantle normalization and metal ratios in discriminating between the effects of partial melting, crystal fractionation and sulphide segregation on platinum-group elements, gold, nickel and copper: Examples from Norway. In; Pritchard H.M and Potts P.J (eds). Geo- Platinum (87), pp. 113–143. Elsiever Science Publishers.

Barnes, S.J., Makovicky, E., Makovicky, M., Rose- Hansen, J., and Karup-Moller, S., 1997. Partition coefficients for Ni, Cu, Pd, Pt, Rh, and Ir between monosulphide solid solution and sulphide liquid and the formation of compositionally zoned Ni- Cu sulphide bodies by fractional crystallization of sulphide liquid. Canadian Journal of Earth Sciences, (34), pp. 366–374, 10.1139/e17-032.

Barnes, S.J., Hill, R.E.T., Perring, C.S., and Dowling, S.E., 2004. Lithogeochemical exploration for komatiite-associated Ni-sulphide deposits: strategies and limitations. Mineralogy and Petrology, (82), pp. 259–293.

Begg, G.C., Hronsky, J.A.M., Arndt, N.T., Griffin, W.L., O'Reilly, S.Y., and Hayward, N., 2010.Lithospheric, cratonic, and geodynamic setting of Ni-Cu-PGE sulphide deposits. Economic geology, (105), pp. 1057–107.

Campbell, I.H., and Naldrett, A.J., 1979. The influence of silicate: sulphide ratios on the geochemistry of magmatic sulphides: Economic Geology (74), pp. 1503–1505.

Chung S.L., and Jahn .B.M., 1995. Plume-lithosphere interaction in generation of the Emeishan flood basalts at the Permian-Triassic boundary. The Geological Society of America (23), pp. 889-892; doi: 10.1130/0091-7613(1995)023<0889:PLIIGO>2.3.CO;2.

Chung, S.L., Lee, T.Y., Lo, C.H., Wang P.L., Chen C.Y., Yem N.T., Hoa, T.T., and Genyao, W., 1997. Intraplate extension prior to continental extrusion along the Ailao Shan-Red River shear zone. The Geological Society of America (25), pp. 311-314; doi: 10.1130/0091-7613(1997)025<0311:IEPTCE>2.3.CO;2.

Cole, J.W., Thordarson, T., and Burt, R.M., 2000. Magma origin and evolution of White Island (Whakaari) Volcano, Bay of Plenty, New Zealand. Journal of Petrology (41), pp. 867–895. doi: 10.1093/petrology/41.6.867.

Eckstrand, O.R., and Hulbert, L.J., 2007. Magmatic nickel-copper-platinum group element deposits, In; Goodfellow, W.D., (ed)., Mineral Deposits of Canada: A Synthesis of major deposit types, district metallogeny, the evolution of geological provinces, and exploration methods: Geological Association of Canada, Mineral Deposits Division, Special Publication No. 5, pp. 205–222.

Fan, W., Zhang, C., Guo, W.F., and Peng, T., 2008.Geochronology and geochemistry of Permian basalts in western Guangxi Province, Southwest China: Evidence for plume-lithosphere interaction. Lithos (102), pp. 218–236.

Ganino, C., Arndt, N.T., Zhou, M.F., Gaillard, F., and Chauvel, C., 2008.Interaction of magma with sedimentary wall rock and magnetite ore genesis in the Panzhihua mafic intrusion, SW China. Mineralum Deposita (43), pp. 677–694. DOI: 10, 1007/s00126-008-0191-5.

Gupta, R.P., 2003. Remote sensing geology. Springer-Verlag. Heidelberg, Germany, pp. 3-4.

He, B., Xu, Y.G., Chung, S.L., Xiao, L., and Wang, Y., 2003.Sedimentary evidence for a rapid, kilometer-scale crustal doming prior to the eruption of the Emeishan flood basalts. Earth and Planetary Science Letters 213, pp. 391–405.

He, B., Xu, Y.G., Wang, Y.M., and Luo, Z.Y., 2006. Sedimentation and lithofacies palaeogeography in Southwestern China before and after the Emeishan flood volcanism: New insights into surface response to mantle plume activity. The Journal of Geology, (114), pp. 117–132.

He, B., Xu, Y. G., Guan, J.P., and Zhong, Y.T., 2010.Paleokarst on the top of the Maokou Formation: further evidence for domal crustal uplift prior to the Emeishan flood volcanism. Lithos (119), pp. 1–9.

Howarth, G.H., Prevec, S.A., and Zhou, M.F., 2013. Timing of Ti-magnetite crystallisation and silicate disequilibrium in the Panzhihua mafic layered intrusion: Implications for ore-forming processes. Lithos (170–171), pp. 73–89.

Kamenetsky, V.S., Chung, S., Kamenetsky, M. B., and Kuzmin, D. V., 2012. Picrites from the Emeishan Large Igneous Province, SW China: A compositional continuum in primitive magmas and their respective mantle sources, Journal of Petrology, (53), pp. 2095–2113, doi:10.1093/petrology/egs045.

Kearey, P., Brooks, M., and Hill, I., 2002.An introduction to geophysical exploration, 3rd Ed Blackwell Science Ltd. Oxford, pp. 125–230.

Keays, R. R., and Lightfoot, P.C., 2010.Crustal sulphur is required to form magmatic Ni–Cu sulphide deposits: evidence from chalcophile element signatures of Siberian and Deccan Trap basalts. Miner Deposita (45), pp. 241–257, doi:10.1007/s00126-009-0271.

Kerr, A.C., and Arndt, N.T., 2001. A note on the IUGS Reclassification of the high-Mg and picritic volcanic rocks. Journal of Petrology (42), pp. 2169–2171.

Lambert, D.D., Foster, J.G., Frick, L.R., Ripley, E.M., and Zientek, M.L., 1998. Geodynamics of magmatic Cu-Ni-PGE sulphide deposits; new insights from the Re-Os isotope system. Economic Geology, (93), pp. 121–136.

Li, C., Barnes, S.J., Makovicky, E., Rose-Hansen, J., and Makovicky, M., 1996. Partitioning of nickel, copper, iridium, rhenium, platinum, and palladium between monosulphide solid solution and sulphide liquid; effects of composition and temperature. Geochimica et Cosmochimica Acta, (60), pp. 1231–1238.

Li, C., Maier, W.D., and De Waal, S.A., 2001.Magmatic Ni-Cu versus PGE deposits: contrasting genetic controls and exploration implications. South African Journal of Geology (104), pp. 309–318.

Lightfoot, P. C., 2007. Advances in Ni-Cu-PGE sulphide deposit models and implications for exploration technologies, In; Milkereit B (ed), Proceedings of exploration, : Fifth Decennial International Conference on Mineral Exploration, pp. 629–646.

Lo, C.H., Chung, S.L., Lee, T.Y., and Wu, G., 2002.Age of the Emeishan flood magmatism and relations to Permian-Triassic boundary events. Earth and Planetary Science Letters (198), pp. 449–458.

Maier, W.D., 2005. Platinum-group element (PGE) deposits and occurrences: Mineralization styles, genetic concepts, and exploration criteria. Journal of African Earth Sciences (41), pp. 165–191.

Maier, W.D., Barnes, S.J., and De Waal, S.A., 2004. Exploration for magmatic Ni-Cu-PGE sulphide deposits; a review of recent advances in the use of geochemical tools, and their application to some South African ores. South African Journal of geology, (101), pp. 237–253.

Morimoto, N., Fabries, J., Ferguson, A.K., Ginzburg, I.V., Ross, M., Seifert, F.A., Zussman, J., Aoki, K., and Gottardi, G., 1988. Nomenclature of pyroxenes. American Mineralogist (73), pp. 1123–1133.

Mungall, J.E., 2005. Magmatic geochemistry of the platinum group elements. Mineralogical Association of Canada Short Course 35, Oulu, Finland, pp. 1–34

Mungall, J.E., Andrew, D.R.A., Cabri, L.J., Sylvester, P.J., and Tubrett, M., 2005. Partitioning of Cu, Ni, Au, and platinum-group elements between monosulphide solid solution and sulphide melt under controlled oxygen and sulphur fugacities. Geochimica et Cosmochimica Acta, (69), pp. 4349–4360.

Munteanu, M., Yao, Y., Cioaca, M., Chunnett, G., and Luo, Y., 2011. A reconnaissance study on selected intrusive bodies south of Panzhihua, Sichuan Province, South-West China: petrogenetic and metallogenetic implications Romanian Journal of Earth Sciences, (85), pp. 19–34.

Munteanu, M., Yao, Y., Wilson, A. H., Chunnett, G., Luo, Y., He, H., Cioaca, M., Wen, M., 2013. Panxi region (South-West China): Tectonics, magmatism and metallogenesis. A review, Tectonophysics .doi: 10.1016/j.tecto.2013.09.008.

Naldrett, A.J., 2004. Magmatic sulphide deposit; Geology, geochemistry and exploration. Springer, Germany.

Pang, K.N., 2008. Origin of the Permian Panzhihua layered gabbroic intrusion and the hosted Fe-Ti-V Oxide Deposit, Sichuan Province, SW China. A thesis submitted in partial fulfilment of the requirements for the Degree of Doctor of Philosophy at The University of Hong Kong.

Pang, K.N., Zhou, M.F., and Ma, Y., 2010. Fe-Ti-V oxide mineralization in the Permian Panzhihua gabbro, Emeishan Large Igneous P rovince, SW China, pp. 453–456.

Pasava, J., Barnes, S.J., and Vymazalova, A., 2003.The use of mantle normalization and metal ratios in the identification of the sources of platinum-group elements in various metal-rich black shales. Mineralium Deposita (38), pp. 775–783. DOI 10.1007/s00126-003-0366-z.

Peate, I. U., and Bryan, S.E., 2008. Re-evaluating plume-induced uplift in the Emeishan Large Igneous Province, SW China. Nature Geoscience, (1), pp. 625–629.

Piña, R., Gervilla, F., Ortega, L., and Lunar, R., 2011.The role of crustal contamination in the genesis of Ni-Cu sulphide ores from the Cortegana Igneous Complex (SW Spain) In;

Proceeds of 11th SGA Biennial Meeting. Society for Geology Applied to Mineral Deposits, pp. 612–614.

Pirajno, F., 2013. The geology and tectonic settings of China's mineral deposits. Springer e-book, pp. 576–623.

Ray, D., Mevel, C., and Banerjee, R., 2009. Hydrothermal alteration studies of gabbros from Northern Central Indian ridge and their geodynamic implications. Journal of Earth Systems and Sciences (118), pp. 659–676.

Richard, L.R., 1995. Minpet: Mineralogical and petrological data processing. Minpet Geological Software, Ver 2.02. Quebec.

Roeder, P.L., and Emslie, R.F., 1970. Olivine-liquid equilibrium. Contributions to Mineralogy and Petrology (29), pp. 275–289.

Sabins, F.F., 1999. Remote sensing for mineral exploration. Ore Geology reviews (14), pp. 157–183.

Schulz, K.J., Chandler, V.W., Nicholson, S.W., Piatak, N., Seal II, R.R., Woodruff, L.G., and Zientek, M.L., 2010. Magmatic sulphide-rich nickel-copper deposits related to picrite and (or) tholeiitic basalt dike-sill complexes- A preliminary deposit model: U.S. Geological Survey Open-File Report 2010–1179, 25 p. (available at http://pubs.usgs.gov/of/2010/1179/).Accessed 10/10/2013

Shellnutt, J.G., and Jahn, B.M., 2011. Origin of late Permian Emeishan basaltic rocks from the Panxi region (SW China): Implications for the Ti-classification and spatial–compositional distribution of the Emeishan flood basalts. Journal of Volcanology and Geothermal Research (199), pp. 85–95.

Shellnutt, J.G., and Iizuka, Y., 2012. Oxidation zonation within the Emeishan large igneous province: Evidence from mantle-derived syenitic plutons. Journal of Asian Earth Sciences (54–55), pp. 31–40.

Shellnutt, J.G., and Zhou, M.F., 2007. Permian peralkaline, peraluminous and metaluminous A-type granites in the Panxi district, SW China: Their relationship to the Emeishan mantle plume. Chemical Geology (243), pp. 286–316.

Shellnutt, J.G., Zhou, M.F., and Zellmer, G.F., 2009. The role of Fe–Ti oxide crystallization in the formation of A-type granitoids with implications for the Daly gap: An example from the Permian Baima igneous complex, SW China. Chemical Geology (259), pp. 204–217.

Shellnutt, J.G., Jahn, B.M., and Zhou, M.F., 2011. Crustally derived granites in the Panzhihua region, SW China: Implications for felsic magmatism in the Emeishan large igneous province. Lithos (123), pp. 145–157.

Shellnutt, J.G., Wang, K.L., Zellmer, G.F., Iizuka, Y., Jahn, B.M., Pang, K.N., Qi, L., and Zhou, M.F., 2011. Three Fe-Ti Oxide ore-bearing gabbro-granitoid complexes in the Panxi region of the Permian Emeishan Large Igneous Province, SW China. American Journal of Science, (311), pp. 773–812, DOI 10.2475/09.2011.02.

Sichuan Geological Bureau., 2013. Exploration data- geological and mineral resources.

Smith, J.V., 1974. Nomenclature and general properties of feldspars. Springer-Verlag Berlin Heidelberg. pp. 415–460.

Song, X.Y., Zhou, M.F., Cao, Z.M., Sun, M., and Wang, Y.L., 2003. Ni–Cu–(PGE) magmatic sulphide deposits in the Yangliuping area, Permian Emeishan igneous province, SW China. Mineralium Deposita (38), pp. 831–843. DOI 10.1007/s00126-003-0362-3.

Song, X.Y., Zhong, H., Tao, Y., and Zhou, M. F., 2005. Magmatic sulphide deposits in the Permian Emeishan large igneous province, SW China. Mineral deposit research; meeting the global challenge, pp. 465–467.

Song, X. Y., Zhou, M.F., Tao, Y., and Xiao, J.F., 2008. Controls on the metal compositions of magmatic sulphide deposits in the Emeishan large igneous province, SW China. Chemical Geology (253) pp. 38–49.

Song, X.Y., Keays, R.R., Xiao, L., Qi, H.W., and Ihlenfeld, C., 2009. Platinum-group element geochemistry of the continental flood basalts in the central Emeisihan Large Igneous Province, SW China. Chemical Geology (262), pp. 246–261.

Song, X.Y., Wang, Y., and Chen, L., 2011. Magmatic Ni-Cu-(PGE) deposits in magma plumbing systems: Features, formation and exploration. Geoscience Frontiers (2), pp. 375–384.

Sproule., R.A., Lesher, C.M., Ayer, J.A., and Thurston, P.C., 2003. Geochemistry and metallogenesis of komatiitic rocks in the Abitibi greenstone belt, Ontario; Ontario Geological Survey, Open File Report 6073, 119p.

Tang, Z., Yan, H., Jiao, J., and Pan, Z., 2007. Regional Metallogenic Controls of Small-intrusion-hosted Ni-Cu (PGE) Ore Deposits in China. Earth Science Frontiers (14), pp. 92–103.

Tao, Y., Li, C., Hu, R., Qi, L., Qu, W., and Du, A., 2010. Re–Os isotopic constraints on the genesis of the Limahe Ni–Cu deposit in the Emeishan large igneous province, SW China. Lithos (119), pp. 137–146.

Thakurta, J., Ripley, E.M., Li, C., and Stifner, E., 2012.Geochemical constraints on the concentrations of platinum group elements in the Ural-Alaskan Type Complexes. GSA Annual Meeting in Charlotte, Paper No. 213-9, Abstract. Web page https://gsa.confex.com/gsa/2012AM/finalprogram/abstract_207300.htm accessed on 29 Oct. 2013.

Tindle, A.G., and Webb, P.C., 1994. PROBE-AMPH a spreadsheet program to classify microprobe-derived amphibole analyses. Computers and Geosciences, (20), pp. 1201–1228.

Ulmer, P., 1989. The dependence of the Fe 2^+ and Mg cation-partitioning between olivine and basaltic liquid on pressure, temperature and composition. An experimental study at 30 k-bars. Contributions to Mineralogy and Petrology, (101), pp. 261–273.

Wang, C.Y., and Zhou, M. F., 2006. Genesis of the Permian Baimazhai magmatic Ni–Cu–(PGE) sulphide deposit, Yunnan, SW China. Miner Deposita, (41), pp. 771–783. DOI 10.1007/s00126-006-0094-2.

Xiao, L., Xu, Y.G., Chung, S.L., He, B., and Mei, H., 2003. Chemostratigraphic correlation of upper Permian lavas from Yunnan Province, China: Extent of the Emeishan Large Igneous Province, International Geology Review, (45), pp. 753–766.

Xiao, L., Xu, Y.G., Mei, H.J., Zheng, Y.F., He, B., and Pirajno, F., 2004. Distinct mantle sources of low-Ti and high-Ti basalts from the western Emeishan Large Lgneous Province, SW China: Implications for plume-lithosphere interaction. Earth and Planetary Science Letters (228), pp. 525– 546.

Xing, C.M., Wang, C.Y., and Zhang, M.J., 2012. Volatile and C-H-O isotopic compositions of giant Fe-Ti-V oxide deposits in the Panxi region and their implications for the sources of volatiles and the origin of Fe-Ti oxide ores. Science China Earth Science (55) pp. 1782–1795, doi: 10.1007/s11430-012-4468-2.

Xu, Y., Chung, S.L., Jahn, B., and Wu, G., 2001. Petrologic and geochemical constraints on the petrogenesis of Permian- Triassic Emeishan flood basalts in South-Western China. Lithos (58), pp. 145–168.

Xu, Y.G., He, B., and Chung, S.L., 2004. The Emeishan large igneous province: Integrated geologic, geophysical and geochemical evidence for a fossil mantle plume. Published on Large Igneous Provinces Commission, (http://www.largeigneousprovinces.org) Accessed 23/10.2013.

Xu, Y.G., He, B., Chung, S.L., Menzies, M.A., and Frey, F.A., 2004. Geologic, geochemical, and geophysical consequences of plume involvement in the Emeishan flood-basalt province. Geological Society of America (32), pp. 917–920.

Xu, Y.G., Bin, H., Xiaolong, H., Zhenyu, L., Dan, Z., Jinlong, M., and Hui, S., 2007. Late Permian Emeishan flood basalts in Southwestern China. Earth Science Frontiers, (14), pp. 1–9.

Xu, Y. G., He, B., Huang, X., Luo, Z., Chung, S.L., Xiao, L., Zhu, D., Shao, H., Fan, W.M., Xu, J., and Wang, Y.J., 2007.Identification of mantle plumes in the Emeishan Large Igneous Province Episodes, (30), pp. 32–42.

Xu, Y.G., Chung, S.L., Shao, H., and He, B., 2010. Silicic magmas from the Emeishan Large Igneous Province, Southwest China: Petrogenesis and their link with the end-Guadalupian biological crisis. Lithos (119), pp. 47–60.

Zhang, Z., Mao, J., Mahoney, J.J., Wang, F., and Qu, W., 2005.Platinum group elements in the Emeishan Large Igneous Province, SW China: Implications for mantle sources. Geochemical Journal, (39), pp. 371– 382.

Zhang, Z., Mahoney, J.J., Mao, J., and Wang, F., 2006. Geochemistry of picritic and associated basalt flows of the Western Emeishan flood basalt province, China. Journal of Petrology, (47), pp. 1997–2019, doi:10.1093/petrology/eg l034.

Zhang, Z., Zhi, X., Chen, L., Saunders, A.D., and Reichow, M.K., 2008. Re–Os isotopic compositions of picrites from the Emeishan flood basalt province, China. Earth and Planetary Science Letters (276), pp. 30–39.

Zhang, Z., Mao, J., Saunders, A.D., Ai, Y., Li, Y., and Zhao, L., 2009. Petrogenetic modeling of three mafic–ultramafic layered intrusions in the Emeishan Large Igneous Province, SW China, based on isotopic and bulk chemical constraints. Lithos (113), pp. 369–392.

Zhong, H., Hu, R.Z., Wilson, A.H., and Zhu, W.G., 2005.Review of the link between the Hongge layered intrusion and Emeishan flood basalts, Southwest China. International Geology Review,(47), pp. 971–985.

Zhou, M.F., Arndt, N., Malpas, J., Wang, C.Y., and Kennedy, A.K., 2008. Two magma series and associated ore deposit types in the Permian Emeishan large igneous province, SW China. Lithos (103), pp. 352–368.

Zhou, M.F., Chen, W.T., Wang, C.Y., Prevec, S.A., Liu, P.P., and Howarth, G.H., 2013. Two stages of immiscible liquid separation in the formation of Panzhihua-type Fe-Ti-V oxide deposits, SW China. Geoscience Frontiers (4) pp. 481–502.

Zientek, M.L., 2012. Magmatic ore deposits in layered intrusions; Descriptive model for reef-type PGE and contact-type Cu-Ni-PGE deposits: U.S. Geological Survey Open-File Report 2012–1010, 48 pages. (pp. 6– 10).

APPENDICES

APPENDIX 1: SILICATES COMPOSITION

Zhongchang Olivine composition

SAMPLE	ZC2-3	ZC2-3 1	ZC2-3 2	ZC2-3 3	ZC2-3 4	ZC2-3 5	ZC2-3 6	ZC3-2 1	ZC3-2 2	ZC3-2 3	ZC3-2 4	ZC3-2 5
SIO2	40.39	40.04	40.84	40.62	40.49	39.86	40.36	41.14	40.57	52.52	40.49	40.77
FEO	14.65	14.50	12.94	13.00	13.87	16.50	12.67	13.48	13.02	3.96	12.80	13.89
MNO	0.24	0.20	0.20	0.19	0.23	0.18	0.17	0.19	0.19	0.11	0.18	0.21
MGO	44.03	44.50	46.06	46.08	45.46	42.88	46.41	45.83	45.48	16.27	45.59	45.30
CAO	0.25	0.29	0.31	0.32	0.24	0.31	0.32	0.31	0.30	22.43	0.29	0.33
NIO	0.17	0.16	0.17	0.15	0.14	0.16	0.15	0.15	0.14	0.04	0.17	0.19
TOTAL	**99.74**	**99.69**	**100.51**	**100.37**	**100.42**	**99.88**	**100.08**	**101.10**	**99.69**	**95.34**	**99.52**	**100.70**
SI	1.01	1.01	1.01	1.01	1.01	1.01	1.00	1.01	1.01	1.34	1.01	1.01
FE2	0.31	0.31	0.27	0.27	0.29	0.35	0.26	0.28	0.27	0.09	0.27	0.29
MN	0.01	0.00	0.00	0.00	0.01	0.00	0.00	0.00	0.00	0.00	0.00	0.00
MG	1.65	1.67	1.70	1.70	1.69	1.62	1.72	1.68	1.69	0.62	1.70	1.67
CA	0.01	0.01	0.01	0.01	0.01	0.01	0.01	0.01	0.01	0.61	0.01	0.01
NI	0.00	0.00	0.00	0.00	0.00	0.00	0.00	0.00	0.00	0.00	0.00	0.00
CATIONS	**2.99**	**2.99**	**2.99**	**2.99**	**2.99**	**2.99**	**3.00**	**2.99**	**2.99**	**2.66**	**2.99**	**2.99**
FE_FEMG	0.16	0.15	0.14	0.14	0.15	0.18	0.13	0.14	0.14	0.12	0.14	0.15
MG_FEMG	0.84	0.85	0.86	0.86	0.85	0.82	0.87	0.86	0.86	0.88	0.86	0.85

SAMPLE	ZC3-2 6	ZC3-2 7	ZC3-2 8	ZC3-2 9	ZC6-1 1	ZC6-1 2	ZC6-1 3	ZC6-1 4	ZC6-1 5	ZC6-1 6	ZC6-1 7	ZC6-1 8
SIO2	40.02	39.80	40.45	52.89	40.37	40.32	40.29	40.11	39.89	40.10	39.73	40.19
FEO	13.53	13.76	13.80	4.10	12.63	12.53	12.49	12.82	13.21	11.93	13.36	12.71
MNO	0.20	0.22	0.20	0.08	0.19	0.22	0.16	0.22	0.18	0.16	0.21	0.16
MGO	45.44	44.73	45.08	16.79	46.65	46.81	46.89	46.50	46.16	46.73	45.71	46.83
CAO	0.33	0.58	0.32	22.66	0.30	0.30	0.32	0.35	0.29	0.33	0.33	0.29
NIO	0.17	0.15	0.14	0.02	0.20	0.19	0.20	0.14	0.11	0.16	0.16	0.20
TOTAL	**99.70**	**99.25**	**99.99**	**96.53**	**100.34**	**100.37**	**100.35**	**100.14**	**99.84**	**99.41**	**99.50**	**100.38**
SI	1.00	1.00	1.01	1.33	1.00	1.00	1.00	1.00	1.00	1.00	1.00	1.00
FE2	0.28	0.29	0.29	0.09	0.26	0.26	0.26	0.27	0.28	0.25	0.28	0.26
MN	0.00	0.01	0.00	0.00	0.00	0.01	0.00	0.01	0.00	0.00	0.00	0.00
MG	1.70	1.68	1.68	0.63	1.72	1.73	1.73	1.72	1.72	1.74	1.71	1.73
CA	0.01	0.02	0.01	0.61	0.01	0.01	0.01	0.01	0.01	0.01	0.01	0.01
NI	0.00	0.00	0.00	0.00	0.00	0.00	0.00	0.00	0.00	0.00	0.00	0.00
CATIONS	**3.00**	**3.00**	**2.99**	**2.67**	**3.00**	**3.00**	**3.00**	**3.00**	**3.00**	**3.00**	**3.00**	**3.00**
FE_FEMG	0.14	0.15	0.15	0.12	0.13	0.13	0.13	0.13	0.14	0.13	0.14	0.13
MG_FEMG	0.86	0.85	0.85	0.88	0.87	0.87	0.87	0.87	0.86	0.87	0.86	0.87

SAMPLE	ZC6-1 9	ZC6-2 1	ZC6-2 2	ZC6-2 3	ZC10-6 1	ZC10-6 2	ZC10-6 3	ZC10-6 4	ZC10-5	ZC10-5
SIO2	40.31	40.04	39.85	40.11	40.10	39.39	39.52	40.38	39.81	38.92
FEO	12.31	12.45	12.63	12.70	12.96	17.09	15.12	14.04	14.41	16.86
MNO	0.18	0.18	0.12	0.20	0.14	0.26	0.27	0.20	0.19	0.26
MGO	46.82	46.55	46.36	46.30	45.23	42.90	44.32	45.25	44.42	43.16
CAO	0.32	0.41	0.31	0.30	0.31	0.27	0.29	0.19	0.27	0.26
NIO	0.19	0.21	0.20	0.17	0.13	0.12	0.11	0.12	0.11	0.12
TOTAL	**100.13**	**99.84**	**99.47**	**99.78**	**98.87**	**100.03**	**99.63**	**100.18**	**99.21**	**99.58**
SI	1.00	1.00	1.00	1.00	1.01	1.00	1.00	1.01	1.01	0.99
FE2	0.26	0.26	0.26	0.27	0.27	0.36	0.32	0.29	0.30	0.36
MN	0.00	0.00	0.00	0.00	0.00	0.01	0.01	0.00	0.00	0.01
MG	1.73	1.73	1.73	1.72	1.70	1.62	1.67	1.68	1.67	1.64
CA	0.01	0.01	0.01	0.01	0.01	0.01	0.01	0.01	0.01	0.01
NI	0.00	0.00	0.00	0.00	0.00	0.00	0.00	0.00	0.00	0.00
CATIONS	**3.00**	**3.00**	**3.00**	**3.00**	**2.99**	**3.00**	**3.00**	**2.99**	**2.99**	**3.01**
FE_FEMG	0.13	0.13	0.13	0.13	0.14	0.18	0.16	0.15	0.15	0.18
MG_FEMG	0.87	0.87	0.87	0.87	0.86	0.82	0.84	0.85	0.85	0.82

Yantiangou Olivine composition

SAMPLE	**Ytg4-1 1**	**Ytg4-1 2**	**Ytg4-1 3**	**Ytg4-2**	**Ytg4-3**	**Ytg4-4**	**Ytg4-5**	**YTG8-1 1**	**YTG8-1 2**	**YTG8-1 3**	**YTG8-1 4**	**YTG8-2 1**
SIO2	40.08	40.03	40.17	40.37	40.46	37.99	39.59	39.50	40.80	40.66	40.37	40.16
FEO	14.76	14.78	15.47	13.78	13.71	24.81	16.24	18.25	10.22	10.51	12.19	13.55
MNO	0.27	0.25	0.26	0.28	0.24	0.42	0.27	0.19	0.13	0.17	0.16	0.19
MGO	43.57	43.67	43.70	44.51	44.91	36.42	43.55	41.93	47.68	47.73	46.75	45.27
CAO	0.41	0.40	0.37	0.40	0.41	0.39	0.40	0.32	0.37	0.37	0.32	0.40
NIO	0.28	0.26	0.25	0.28	0.26	0.15	0.20	0.15	0.33	0.29	0.26	0.20
TOTAL	**99.37**	**99.39**	**100.22**	**99.62**	**99.99**	**100.18**	**100.25**	**100.34**	**99.53**	**99.73**	**100.05**	**99.77**
SI	1.01	1.01	1.01	1.01	1.01	1.00	1.00	1.00	1.01	1.00	1.00	1.01
FE2	0.31	0.31	0.33	0.29	0.29	0.55	0.34	0.39	0.21	0.22	0.25	0.28
MN	0.01	0.01	0.01	0.01	0.01	0.01	0.01	0.00	0.00	0.00	0.00	0.00
MG	1.64	1.64	1.64	1.66	1.67	1.43	1.64	1.59	1.76	1.76	1.73	1.69
CA	0.01	0.01	0.01	0.01	0.01	0.01	0.01	0.01	0.01	0.01	0.01	0.01
NA	0.00	0.00	0.00	0.00	0.00	0.00	0.00	0.00	0.00	0.00	0.00	0.00
K	0.00	0.00	0.00	0.00	0.00	0.00	0.00	0.00	0.00	0.00	0.00	0.00
NI	0.01	0.01	0.01	0.01	0.01	0.00	0.00	0.00	0.01	0.01	0.01	0.00
CATIONS	**2.99**	**2.99**	**2.99**	**2.99**	**2.99**	**3.00**	**3.00**	**3.00**	**2.99**	**3.00**	**3.00**	**3.00**
FE_FEMG	0.16	0.16	0.17	0.15	0.15	0.28	0.17	0.20	0.11	0.11	0.13	0.14
MG_FEMG	0.84	0.84	0.83	0.85	0.85	0.72	0.83	0.80	0.89	0.89	0.87	0.86

SAMPLE	**YTG8-2 2**	**YTG8-2 3**	**YTG8-2 4**	**YTG5-1 1**	**YTG3-1**	**YTG3-2**	**YTG3-4**	**TG5-3 1 b**	**YTG5-3 2**	**YTG5-3 3**	**YTG5-3 4**
SIO2	40.34	40.98	40.26	38.22	39.32	38.68	38.59	39.23	39.29	38.94	39.50
FEO	13.87	12.31	12.83	20.75	17.29	18.37	17.85	19.21	16.36	18.24	16.11
MNO	0.19	0.23	0.10	0.05	0.03	0.05	0.08	0.07	0.04	0.06	0.06
MGO	44.55	46.26	46.29	39.53	42.91	41.26	41.59	40.89	39.04	41.92	43.47
CAO	0.37	0.34	0.34	0.31	0.45	0.42	0.44	0.34	3.64	0.29	0.32
NIO	0.22	0.20	0.19	0.17	0.27	0.28	0.17	0.12	0.06	0.14	0.11
TOTAL	**99.54**	**100.32**	**100.01**	**99.03**	**100.27**	**99.06**	**98.72**	**99.86**	**98.43**	**99.59**	**99.57**
SI	1.01	1.01	1.00	1.00	1.00	1.00	1.00	1.01	1.02	1.00	1.00
FE2	0.29	0.25	0.27	0.45	0.37	0.40	0.39	0.41	0.35	0.39	0.34
MN	0.00	0.01	0.00	0.00	0.00	0.00	0.00	0.00	0.00	0.00	0.00
MG	1.67	1.70	1.72	1.54	1.62	1.59	1.60	1.56	1.51	1.60	1.64
CA	0.01	0.01	0.01	0.01	0.01	0.01	0.01	0.01	0.10	0.01	0.01
NA	0.00	0.00	0.00	0.00	0.00	0.00	0.00	0.00	0.00	0.00	0.00
K	0.00	0.00	0.00	0.00	0.00	0.00	0.00	0.00	0.00	0.00	0.00
NI	0.00	0.00	0.00	0.00	0.01	0.01	0.00	0.00	0.00	0.00	0.00
CATIONS	**2.99**	**2.99**	**3.00**	**3.00**	**3.01**	**3.00**	**3.00**	**2.99**	**2.98**	**3.00**	**3.00**
FE_FEMG	0.15	0.13	0.13	0.23	0.18	0.20	0.19	0.21	0.19	0.20	0.17
MG_FEMG	0.85	0.87	0.87	0.77	0.82	0.80	0.81	0.79	0.81	0.80	0.83

Zhongchang Pyroxenes

SAMPLE	**ZC3-2**	**ZC3-2**	**ZC1-1**	**ZC1-3**	**ZC1-3**	**ZC6-2**	**ZC4-1**	**ZC4-1**	**ZC1-1**
SIO2	52.52	52.89	51.28	50.27	50.97	50.68	48.64	48.65	52.71
TIO2	0.71	0.70	1.10	1.26	1.20	1.31	2.16	2.19	0.86
AL2O3	1.90	1.87	3.51	3.69	3.16	4.15	5.64	5.67	2.96
FEO	3.96	4.10	4.60	4.96	4.55	5.57	7.56	8.50	4.41
CR2O3	0.65	0.66	0.00	0.77	0.84	0.00	0.00	0.00	0.00
MNO	0.11	0.08	0.11	0.10	0.11	0.06	0.17	0.22	0.07
MGO	16.27	16.79	15.71	15.51	16.02	15.56	13.30	13.20	16.12
CAO	22.43	22.66	22.17	22.35	22.66	22.04	21.17	21.07	22.04
NA2O	0.00	0.00	0.35	0.00	0.00	0.43	0.47	0.41	0.37
TOTAL	**98.55**	**99.75**	**98.83**	**98.91**	**99.51**	**99.80**	**99.11**	**99.91**	**99.54**
SI	1.95	1.94	1.90	1.87	1.88	1.87	1.82	1.82	1.93
TI	0.02	0.02	0.03	0.04	0.03	0.04	0.06	0.06	0.02
AL	0.08	0.08	0.15	0.16	0.14	0.18	0.25	0.25	0.13
FE2	0.12	0.13	0.14	0.15	0.14	0.17	0.24	0.27	0.14
CR	0.02	0.02	0.00	0.02	0.02	0.00	0.00	0.00	0.00
MN	0.00	0.00	0.00	0.00	0.00	0.00	0.01	0.01	0.00
MG	0.90	0.92	0.87	0.86	0.88	0.86	0.74	0.74	0.88
CA	0.89	0.89	0.88	0.89	0.90	0.87	0.85	0.84	0.87
NA	0.00	0.00	0.03	0.00	0.00	0.03	0.03	0.03	0.03
SUM_CAT	**3.98**	**3.99**	**4.00**	**4.00**	**4.00**	**4.02**	**4.01**	**4.01**	**3.99**
WO	46.49	45.98	46.47	46.68	46.64	45.84	46.31	45.56	45.95
EN	46.92	47.40	45.82	45.07	45.88	45.02	40.48	39.72	46.76
FS	6.59	6.62	7.71	8.25	7.49	9.14	13.20	14.72	7.29

SAMPLE	**ZC1-1**	**ZC1-5**	**ZC3-2**	**ZC3-2**	**ZC3-2**	**ZC3-2**	**ZC2-3**	**ZC6-1**
SIO2	53.37	51.13	52.21	53.43	52.26	53.50	52.42	50.37
TIO2	0.91	1.26	0.97	0.72	0.92	0.72	0.90	1.64
AL2O3	2.49	3.79	2.94	1.97	2.83	1.73	2.68	5.01
FEO	4.41	5.36	4.57	4.19	4.65	4.64	4.51	6.32
CR2O3	0.00	0.00	0.00	0.00	0.00	0.00	0.00	0.00
MNO	0.11	0.09	0.08	0.11	0.09	0.10	0.06	0.00
MGO	16.31	15.40	16.42	16.91	16.21	17.22	16.16	15.08
CAO	22.88	22.04	22.18	22.41	22.09	21.83	22.01	21.57
NA2O	0.32	0.35	0.31	0.28	0.34	0.27	0.32	0.37
TOTAL	**100.80**	**99.42**	**99.68**	**100.02**	**99.39**	**100.01**	**99.06**	**100.36**
SI	1.94	1.89	1.92	1.95	1.92	1.95	1.93	1.85
TI	0.02	0.04	0.03	0.02	0.03	0.02	0.02	0.05
AL	0.11	0.17	0.13	0.08	0.12	0.07	0.12	0.22
FE2	0.13	0.17	0.14	0.13	0.14	0.14	0.14	0.19
CR	0.00	0.00	0.00	0.00	0.00	0.00	0.00	0.00
MN	0.00	0.00	0.00	0.00	0.00	0.00	0.00	0.00
MG	0.88	0.85	0.90	0.92	0.89	0.94	0.89	0.83
CA	0.89	0.87	0.87	0.88	0.87	0.85	0.87	0.85
NA	0.02	0.03	0.02	0.02	0.02	0.02	0.02	0.03
SUM_CAT	**4.00**	**4.01**	**4.00**	**4.00**	**4.00**	**4.00**	**4.00**	**4.01**
WO	46.60	46.18	45.58	45.46	45.69	44.11	45.79	45.43
EN	46.22	44.90	46.95	47.73	46.65	48.41	46.78	44.19
FS	7.19	8.92	7.46	6.81	7.66	7.48	7.42	10.39

Yantiagou Pyroxene

SAMPLE	**Ytg4-1 4**	**Ytg4-1 5**	**Ytg4-1 6**	**Ytg4-2**	**Ytg4-3**	**Ytg4-1**	**Ytg4-1**	**Ytg4-2**	**Ytg4-3**
SIO2	51.36	53.19	51.57	51.46	51.83	51.70	49.20	50.61	51.74
TIO2	1.98	0.94	1.37	1.86	1.45	1.62	3.00	2.21	1.51
AL2O3	2.56	1.18	1.63	1.94	2.08	1.92	3.38	2.44	1.79
FEO	6.50	5.04	7.02	6.66	5.69	7.62	7.23	7.21	5.36
MNO	0.12	0.07	0.14	0.13	0.12	0.16	0.14	0.14	0.13
MGO	14.22	15.82	14.85	14.30	14.74	13.76	13.75	13.98	15.48
CAO	22.23	22.23	21.37	22.26	21.93	22.09	21.29	21.46	22.13
NA2O	0.62	0.40	0.49	0.55	0.86	0.61	0.89	0.77	0.79
K2O	0.02	0.02	0.03	0.02	0.03	0.03	0.05	0.04	0.03
TOTAL	**99.61**	**98.87**	**98.46**	**99.18**	**98.74**	**99.50**	**98.95**	**98.85**	**98.95**
SI	1.91	1.97	1.94	1.92	1.94	1.93	1.85	1.90	1.93
TI	0.06	0.03	0.04	0.05	0.04	0.05	0.09	0.06	0.04
AL	0.11	0.05	0.07	0.09	0.09	0.08	0.15	0.11	0.08
FE2	0.20	0.16	0.22	0.21	0.18	0.24	0.23	0.23	0.17
MN	0.00	0.00	0.00	0.00	0.00	0.01	0.00	0.00	0.00
MG	0.79	0.87	0.83	0.80	0.82	0.77	0.77	0.78	0.86
CA	0.89	0.88	0.86	0.89	0.88	0.88	0.86	0.86	0.88
NA	0.04	0.03	0.04	0.04	0.06	0.04	0.07	0.06	0.06
K	0.00	0.00	0.00	0.00	0.00	0.00	0.00	0.00	0.00
SUM_CAT	**4.00**	**3.99**	**4.00**	**4.00**	**4.01**	**4.00**	**4.02**	**4.01**	**4.02**
WO	47.11	46.09	44.86	46.91	46.68	46.70	46.10	46.00	46.15
EN	41.93	45.64	43.39	41.93	43.67	40.46	41.43	41.70	44.93
FS	10.95	8.27	11.75	11.16	9.66	12.84	12.47	12.30	8.93

SAMPLE	**Ytg4-4**	**YTG8-1 1**	**YTG8-1 2**	**YTG8-1 3**	**YTG8-1 4**	**YTG8-1 5**	**YTG8-1 6**	**YTG8-2**
SIO2	52.31	52.95	53.22	53.05	52.80	53.12	53.90	53.89
TIO2	1.44	1.11	1.08	1.24	1.19	1.10	1.06	1.56
AL2O3	2.25	0.84	0.82	0.88	0.91	0.67	0.82	2.89
FEO	6.42	4.77	3.84	4.82	5.23	5.32	4.04	9.06
MNO	0.12	0.06	0.06	0.08	0.09	0.00	0.08	0.14
MGO	15.22	16.55	16.78	16.27	15.84	16.36	16.79	18.67
CAO	21.85	22.53	22.79	22.26	22.32	22.59	22.59	6.93
NA2O	0.70	0.38	0.35	0.41	0.38	0.33	0.38	5.72
K2O	0.03	0.03	0.03	0.02	0.03	0.02	0.02	0.67
TOTAL	**100.34**	**99.22**	**98.98**	**99.04**	**98.79**	**99.51**	**99.68**	**99.53**
SI	1.93	1.96	1.96	1.96	1.96	1.96	1.97	1.97
TI	0.04	0.03	0.03	0.03	0.03	0.03	0.03	0.04
AL	0.10	0.04	0.04	0.04	0.04	0.03	0.04	0.12
FE2	0.20	0.15	0.12	0.15	0.16	0.16	0.12	0.28
MN	0.00	0.00	0.00	0.00	0.00	0.00	0.00	0.00
MG	0.84	0.91	0.92	0.90	0.88	0.90	0.92	1.02
CA	0.86	0.89	0.90	0.88	0.89	0.89	0.89	0.27
NA	0.05	0.03	0.03	0.03	0.03	0.02	0.03	0.41
K	0.00	0.00	0.00	0.00	0.00	0.00	0.00	0.03
SUM_CAT	**4.01**	**4.01**	**4.00**	**4.00**	**4.00**	**4.01**	**3.99**	**4.14**
WO	45.40	45.67	46.34	45.68	46.01	45.64	45.94	17.29
EN	44.00	46.69	47.47	46.47	45.43	45.98	47.52	64.80
FS	10.61	7.64	6.19	7.85	8.56	8.38	6.54	17.92

Zhongchang Feldspars

SAMPLE	**ZC9 1**	**ZC9 2**	**ZC6-2 1**	**ZC6-2 2**	**ZC6-2 3**	**ZC8-1 1**	**ZC8-1 2**	**ZC8-1 3**	**ZC8-1 4**	**ZC8-2 2**	**ZC8-2 3**
SIO2	55.28	63.35	60.33	59.96	61.95	68.68	69.91	67.91	68.31	69.12	69.22
AL2O3	29.28	24.37	25.52	25.30	24.67	20.70	20.89	20.53	21.38	21.28	21.55
FEO	0.20	0.18	0.22	0.21	0.24	0.09	0.00	0.14	0.07	0.00	0.10
MNO	0.00	0.03	0.00	0.04	0.01	0.00	0.00	0.00	0.00	0.00	0.00
MGO	0.06	0.00	0.03	0.05	0.49	0.01	0.00	0.00	0.00	0.00	0.00
CAO	10.41	4.46	6.06	5.79	4.78	0.25	0.23	0.07	0.91	0.31	0.77
NA2O	5.71	7.50	7.48	6.97	6.31	10.54	8.86	1.29	9.66	9.78	8.41
K2O	0.32	0.93	0.87	0.88	0.86	0.06	0.07	9.54	0.09	0.09	0.71
TOTAL	**101.27**	**100.82**	**100.51**	**99.20**	**99.31**	**100.33**	**99.96**	**99.48**	**100.42**	**100.58**	**100.76**
SI	9.86	11.10	10.71	10.75	11.00	11.91	12.05	12.10	11.82	11.91	11.91
AL	6.15	5.03	5.33	5.34	5.16	4.23	4.24	4.31	4.36	4.32	4.37
FE2	0.03	0.03	0.03	0.03	0.04	0.01	0.00	0.02	0.01	0.00	0.01
MN	0.00	0.01	0.00	0.01	0.00	0.00	0.00	0.00	0.00	0.00	0.00
MG	0.02	0.00	0.01	0.01	0.13	0.00	0.00	0.00	0.00	0.00	0.00
CA	1.99	0.84	1.15	1.11	0.91	0.05	0.04	0.01	0.17	0.06	0.14
NA	1.97	2.55	2.57	2.42	2.17	3.54	2.96	0.45	3.24	3.27	2.81
K	0.07	0.21	0.20	0.20	0.20	0.01	0.02	2.17	0.02	0.02	0.16
CATIONS	**20.09**	**19.76**	**20.00**	**19.88**	**19.60**	**19.75**	**19.31**	**19.05**	**19.62**	**19.57**	**19.39**
AB	48.90	70.90	65.60	64.90	66.30	98.40	98.10	17.00	94.50	97.70	90.40
AN	49.30	23.30	29.40	29.80	27.70	1.30	1.40	0.50	4.90	1.70	4.60
OR	1.80	5.80	5.00	5.40	6.00	0.40	0.50	82.50	0.60	0.60	5.00

SAMPLE	**ZC4-2 1**	**ZC4-2 2**	**ZC4-2 3**	**ZC4-2 5**	**ZC11-1 1**	**ZC11-1 2**	**ZC11-1 3**	**ZC11-1 5**	**ZC11-1 8**	**ZC11-1 8**	**ZC11-1**
SIO2	60.01	54.29	55.60	57.09	63.16	67.44	55.61	56.72	54.62	68.32	66.52
AL2O3	26.10	29.54	28.72	27.98	23.72	20.29	28.21	27.17	28.53	22.19	19.23
FEO	0.40	0.59	0.68	0.71	0.29	0.19	0.33	0.18	0.30	0.08	0.21
MNO	0.01	0.06	0.00	0.03	0.02	0.00	0.03	0.00	0.02	0.01	0.00
MGO	0.02	0.06	0.04	0.02	0.02	0.00	0.02	0.03	0.01	0.00	0.00
CAO	7.25	11.25	10.42	9.22	4.21	0.61	9.73	8.72	10.39	1.84	0.07
NA2O	6.56	5.36	5.72	6.39	7.48	2.20	6.09	6.29	5.63	7.06	0.31
K2O	0.82	0.33	0.42	0.53	1.11	10.13	0.38	0.42	0.36	0.34	12.90
TOTAL	**101.16**	**101.47**	**101.60**	**101.96**	**100.01**	**100.86**	**100.40**	**99.53**	**99.86**	**99.84**	**99.24**
SI	10.59	9.71	9.90	10.10	11.16	11.98	9.99	10.23	9.89	11.82	12.11
AL	5.43	6.22	6.02	5.83	4.94	4.24	5.97	5.77	6.08	4.52	4.12
FE2	0.06	0.09	0.10	0.11	0.04	0.03	0.05	0.03	0.05	0.01	0.03
MN	0.00	0.01	0.00	0.01	0.00	0.00	0.01	0.00	0.00	0.00	0.00
MG	0.00	0.02	0.01	0.01	0.01	0.00	0.01	0.01	0.00	0.00	0.00
CA	1.37	2.16	1.99	1.75	0.80	0.12	1.87	1.69	2.02	0.34	0.01
NA	2.24	1.86	1.98	2.19	2.56	0.76	2.12	2.20	1.98	2.37	0.11
K	0.18	0.08	0.10	0.12	0.25	2.30	0.09	0.10	0.08	0.08	3.00
CATIONS	**19.89**	**20.13**	**20.11**	**20.12**	**19.76**	**19.42**	**20.11**	**20.02**	**20.09**	**19.14**	**19.38**
AB	59.10	45.50	48.70	54.00	71.00	23.90	52.00	55.20	48.50	85.10	3.50
AN	36.10	52.70	49.00	43.10	22.10	3.70	45.90	42.30	49.50	12.20	0.40
OR	4.80	1.80	2.40	2.90	6.90	72.40	2.10	2.40	2.00	2.70	96.10

Yantiangou Feldspars

SAMPLE	**Ytg4-1**	**Ytg4-2**	**Ytg4-4**
SIO2	65.17	65.29	62.17
AL2O3	20.01	19.42	27.47
FEO	2.20	0.46	0.14
MNO	0.03	0.02	0.00
MGO	0.40	0.00	0.02
CAO	0.09	0.07	0.03
NA2O	2.27	3.45	10.27
K2O	9.56	11.12	0.23
TOTAL	**99.73**	**99.82**	**100.33**
SI	11.74	11.87	10.86
AL	4.25	4.16	5.65
FE2	0.33	0.07	0.02
MN	0.01	0.00	0.00
MG	0.11	0.00	0.01
CA	0.02	0.01	0.01
NA	0.79	1.22	3.48
K	2.20	2.58	0.05
CATIONS	**19.53**	**19.93**	**20.07**
AB	26.40	31.90	98.40
AN	0.60	0.30	0.20
OR	73.10	67.80	1.40

Zhongchang and Yantiangou Biotite

SAMPLE	**ZC6-1**	**ZC2-3**	**SAMPLE**	**YTG8-1 1**	**YTG8-2**	**YTG8-2 2**	**YTG8-4 2**	**YTG8-4 3**
SIO2	37.57	38.49	SIO2	39.89	38.96	41.71	38.17	38.87
TIO2	3.08	2.96	TIO2	6.15	6.37	1.63	6.79	6.76
AL2O3	15.79	16.20	AL2O3	12.32	12.35	11.31	13.08	13.34
FEO	15.04	10.54	FEO	11.25	11.09	8.87	10.76	10.97
MNO	0.08	0.05	MNO	0.06	0.00	0.08	0.06	0.07
MGO	16.33	18.09	MGO	18.09	17.14	21.83	17.33	17.19
CAO	0.13	0.09	CAO	0.03	0.11	0.05	0.05	0.02
NA2O	0.70	0.87	NA2O	1.09	1.17	1.09	0.81	0.84
K2O	7.60	6.42	K2O	9.11	8.57	8.84	9.90	8.59
TOTAL	**96.32**	**93.70**	**TOTAL**	**97.98**	**95.76**	**95.40**	**96.95**	**96.64**
Si	5.748	5.866	SI	5.952	5.939	6.285	5.786	5.856
Ti	0.354	0.339	TI	0.690	0.730	0.184	0.774	0.766
Al	2.847	2.909	AL	2.167	2.218	2.009	2.337	2.368
Fe	1.924	1.343	FE2	1.403	1.414	1.118	1.365	1.383
Mn	0.010	0.007	MN	0.007	0.000	0.010	0.007	0.009
Mg	3.724	4.109	MG	4.025	3.896	4.903	3.917	3.860
Ca	0.021	0.015	CA	0.004	0.017	0.009	0.008	0.004
Na	0.208	0.256	NA	0.314	0.346	0.318	0.239	0.246
K	1.483	1.249	K	1.734	1.666	1.699	1.914	1.650
CATIONS	**16**	**16**	**CATIONS**	**16.298**	**16.227**	**16.535**	**16.348**	**16.142**
FE_FEMG	0	0	FE_FEMG	0	0	0	0	0
MG_FEMG	1	1	MG_FEMG	1	1	1	1	1

APPENDIX 2: SULPHIDES COMPOSITION

Zhongchang Sulphides

Sample	As	S	Fe	Cu	Ni	Co	Total
ZC6-1 sulfide 1	0.00	39.76	58.42	0.00	0.89	0.09	99.15
ZC6-1 sulfide 2	0.02	39.96	58.34	0.00	1.32	0.16	99.79
ZC6-1 sulf incl in px 1	0.00	40.14	58.49	0.00	1.25	0.12	100.00
ZC6-1 sulf incl in px 2	0.00	40.64	57.55	0.00	1.52	0.11	99.83
ZC6-1 sulf incl in px 3	0.03	40.16	58.97	0.00	1.19	0.12	100.47
ZC6-1 sulf incl in px 4	0.00	39.99	58.24	0.00	1.18	0.10	99.51
ZC6-1 sulf incl in px 5	0.02	40.30	58.49	0.00	1.28	0.07	100.16
2ZC5-2 sulf 1	0.00	53.04	46.41	0.02	0.00	0.08	99.56
2ZC5-2 sulf 2	0.00	52.77	46.56	0.00	0.00	0.07	99.40
2ZC5-1 sulf 3	0.01	53.59	47.08	0.03	0.00	0.06	100.76
2ZC10-6 sulf in oliv	0.03	39.25	58.39	0.00	1.19	0.07	98.93
2ZC10-6 sulf2 in oliv	0.01	34.73	30.35	34.41	0.00	0.01	99.50
2ZC10-6 sulf3 in oliv	0.00	39.93	58.75	0.19	1.31	0.13	100.30
2ZC10-6 sulf4 in oliv	0.00	40.34	58.76	0.00	1.13	0.15	100.38
2ZC10-6 sulf5 in oliv	0.03	39.73	58.81	0.00	1.41	0.09	100.08
2ZC10-6 sulf 6 in hb	0.00	39.85	58.74	0.00	1.43	0.08	100.10
2ZC10-6 sulf 7in hb	0.05	35.62	29.82	34.40	0.02	0.03	99.93
2ZC10-6 sulf 8in hb	0.00	39.63	59.57	0.00	1.39	0.10	100.69
2ZC10-6 sulf 9 in hb	0.00	40.13	58.46	0.00	1.43	0.11	100.12
ZC10-1 sulf in intercum px	0.03	39.34	58.88	0.03	1.30	0.05	99.62
ZC10-1 sulf in oliv	0.00	38.26	59.50	0.02	1.26	0.11	99.14
ZC10-1 sulf in interc px 2	0.01	39.29	58.02	0.00	1.29	0.08	98.68
ZC10-1 sulf in interc px 3	0.00	39.42	59.35	0.07	1.12	0.07	100.03
ZC10-1 irreg sulf 1	0.00	39.23	58.58	0.05	1.45	0.09	99.41
ZC10-4 sulf 1 zone 2	0.00	34.28	30.77	34.83	0.00	0.02	99.91
ZC10-4 sulf 1 zone 3	0.03	34.45	30.59	33.72	0.03	0.05	98.87
ZC10-4 sulf 1 zone 4	0.01	33.33	26.48	0.00	35.54	3.14	98.49
ZC10-4 sulf in px	0.00	40.14	58.17	0.12	1.21	0.06	99.69
ZC10-4 sulf 2 in px	0.00	40.63	58.37	0.14	1.48	0.08	100.70
ZC11-1 sulfide 1	0.005	52.83	46.42	0.163	0.23	0.075	99.73
ZC11-1 sulfide 2	0.043	53.14	46.14	0.000	0.34	0.040	99.70
ZC11-1 sulfide 3	0.000	54.16	45.58	0.085	0.00	0.61	100.43
ZC11-1 sulfide 4	0.012	52.90	46.72	0.002	0.11	0.007	99.75
ZC11-1 sulfide 5	0.000	52.06	47.65	0.243	0.19	0.038	100.18
ZC11-1 sulfide 6	0.000	53.15	46.28	0.000	0.47	0.056	99.95
ZC11-1 sulfide 7	0.005	53.89	45.58	0.045	0.04	0.35	99.91
ZC2-1 sulphide 5	0.000	35.80	30.91	33.53	0.012	0.06	100.30
ZC2-1 sulphide 6	0.025	39.52	59.55	0.00	0.404	0.04	99.54
ZC2-2 sulphide 1	0.000	35.46	30.31	34.42	0.000	0.03	100.23
ZC2-2 sulphide 2	0.000	35.82	30.01	34.54	0.013	0.01	100.39
ZC2-2 sulphide 3	0.000	35.50	29.75	34.44	0.006	0.02	99.72
ZC2-3 sulphide 1	0.000	35.64	29.89	34.26	0.003	0.06	99.84
ZC3-1sulphide 1	0.018	34.62	29.17	0.00	35.91	0.34	100.06
ZC3-1sulphide 2	0.000	35.14	29.78	34.55	0.027	0.03	99.52
ZC3-1sulphide w incl pge 1-5	0.017	40.70	57.30	0.00	2.28	0.06	100.36
ZC3-1sulphide w incl pge 1-5 pt 2	0.000	40.33	57.16	0.00	2.37	0.09	99.96
ZC3-1sulphide 2	0.025	34.27	28.98	0.00	36.49	0.34	100.11
ZC3-1sulphide 3	0.000	40.65	57.49	0.18	2.00	0.08	100.40
ZC3-1sulphide 4	0.000	34.66	27.71	0.00	37.40	0.33	100.10
ZC3-1sulphide 5	0.044	35.64	30.00	33.82	0.011	0.03	99.55
ZC3-1sulphide 6	0.000	40.39	57.16	0.00	2.45	0.10	100.10
ZC3-1sulphide 7	0.035	35.44	29.86	34.80	0.00	0.01	100.15
ZC3-1cpy w incl pge 10	0.025	35.69	30.36	34.67	0.00	0.02	100.76
ZC3-2 sulf w pge 1	0.039	40.37	57.46	0.00	2.19	0.07	100.13
ZC3-2 sulf 2	0.000	35.05	29.80	35.48	0.00	0.05	100.38
ZC3-2 sulf 3 with pge 3	0.023	40.29	58.19	0.00	1.87	0.06	100.44
ZC2-1 sulphide 1	0.05	39.34	60.07	0.00	0.33	0.09	99.87
ZC2-1 sulphide 2	0.01	35.62	30.45	34.24	0.02	0.04	100.37
ZC2-1 sulphide 3	0.00	32.99	31.84	0.00	34.72	0.35	99.89
ZC2-1 sulphide 1	0.053	38.242	61.104	0	0.317	0.084	99.8
ZC2-1 sulphide 2	0.01	34.95	31.36	33.59	0.02	0.04	99.96
ZC2-1 sulphide 3	0.00	32.35	32.78	0.00	34.04	0.34	99.51

Yantiangou Sulphides

Sample	Fe	Ni	Cu	Co	S	Total
YTG1-4	57.39	1.95	0.02	0.14	40.04	99.53
YTG1-5	31.46	0.09	32.72	0.10	34.77	99.15
YTG1-6	14.53	26.80	0.33	13.53	43.91	99.09
YTG1-8	29.90	0.00	33.40	0.05	36.67	100.02
YTG1-9	58.63	1.29	0.02	0.13	41.12	101.19
YTG1-10	59.81	0.71	0.00	0.13	40.75	101.40
YTG1-11	57.36	1.15	0.11	0.08	41.54	100.24
YTG1-12	31.17	0.05	33.16	0.08	35.49	99.95
YTG1-13	57.64	1.81	0.03	0.10	40.99	100.58
YTG1-14	28.78	34.47	1.05	1.51	34.83	100.64
YTG1-15	31.31	0.00	32.81	0.02	35.96	100.10
YTG1-16	58.60	1.18	0.02	0.10	40.63	100.53
YTG1-17	30.53	0.01	32.75	0.17	36.25	99.71
YTG1-18	30.26	0.09	32.75	0.01	36.46	99.56
YTG1-19	57.93	1.72	0.00	0.07	40.55	100.27
YTG1-20	30.22	0.04	32.11	0.04	36.50	98.91
YTG1-23	30.33	0.02	33.13	0.05	36.32	99.85
YTG1-24	41.69	3.51	0.07	0.06	55.06	100.38
YTG1-25	31.57	0.15	33.15	0.01	35.50	100.38
YTG1-26	0.91	61.84	0.24	0.92	35.95	99.86
YTG1-27	30.70	0.06	33.18	0.03	36.40	100.38
YTG1-28	28.60	0.00	33.98	0.02	37.40	100.01
YTG1-30	1.37	60.78	0.41	0.42	37.07	100.06
YTG1-31	28.26	0.05	33.94	0.02	37.41	99.69
YTG1-32	30.42	0.04	33.01	0.03	36.33	99.83
YTG1-33	1.68	61.67	0.86	0.51	36.71	101.42
YTG1-34	45.88	0.62	0.12	0.29	52.84	99.75
YTG1-35	42.29	2.59	0.00	0.20	54.48	99.55
YTG1-36	31.06	0.00	33.12	0.02	36.70	100.90
YTG1-37	31.70	0.24	33.05	0.01	35.78	100.78
YTG1-38	42.53	2.46	0.03	0.20	54.71	99.93
YTG1-39	31.37	0.00	33.26	0.00	35.98	100.61
YTG1-40	44.79	1.77	0.00	0.09	54.27	100.92
YTG1-41	31.68	0.00	32.53	0.05	34.95	99.21
YTG1-42	26.23	39.10	0.04	0.76	33.84	99.97
YTG1-43	27.53	38.86	0.00	0.93	33.87	101.19
YTG1-44	31.73	0.00	32.67	0.03	36.08	100.50
YTG1-46	45.29	2.13	0.00	0.11	53.86	101.40
YTG1-47	31.14	0.00	33.32	0.00	36.03	100.49
YTG1-48	31.83	0.00	33.01	0.03	36.09	100.96
YTG1-49	42.68	2.16	0.03	0.12	54.66	99.66
YTG1-50	26.09	41.04	0.05	0.27	33.99	101.44
YTG1-51	25.28	41.31	0.02	0.29	34.04	100.93
YTG1-52	30.63	0.00	33.01	0.04	35.65	99.33
YTG1-53	57.08	1.62	0.09	0.10	42.29	101.18
YTG1-54	39.15	18.98	0.17	0.16	42.04	100.50
YTG1-55	45.65	0.70	1.67	0.06	53.30	101.39
YTG1-56	31.45	0.25	32.91	0.01	35.91	100.53
YTG1-57	46.04	0.58	0.03	0.06	53.49	100.20
YTG1-58	25.64	41.56	0.08	0.12	32.14	99.55

APPENDIX 3: OXIDES COMPOSITION

Zhongchang Oxides

Sample	SiO2	TiO2	Al2O3	Cr2O3	FeO	MnO	MgO	CaO	ZnO	NiO	V2O3	Total
ZC2-3 spin 1	0.067	2.764	12.021	43.216	29.847	0.341	10.521	0	0	0.083	0	98.86
ZC2-3 spin 2	0.004	2.763	11.278	43.508	31.782	0.358	9.323	0	0.015	0.1	0	99.131
ZC2-3 spin 3	0.028	2.867	11.426	42.976	32.083	0.315	9.526	0	0.011	0.088	0	99.32
ZC2-3 spin 4	0.007	6.948	5.642	9.327	70.165	0.451	1.164	0	0.116	0.294	0	94.114
ZC2-3 spin 5	0.014	1.499	9.875	38.942	42.707	0.424	4.363	0	0.119	0.14	0	98.083
ZC3-2 spin 1	0.006	2.924	10.622	44.209	31.648	0.256	9.911	0	0.28	0.075	0	99.931
ZC3-2 spin 2	0.027	2.652	10.849	44.839	30.411	0.27	10.546	0	0.168	0.099	0	99.861
ZC3-2 spin 3	0	2.811	11.038	43.282	32.825	0.306	9.054	0	0	0.043	0	99.359
ZC3-2 spin 4	0.018	1.976	10.321	37.165	43.16	0.455	4.828	0	0.054	0.144	0	98.121
ZC3-2 spin 5	41.282	4.207	13.871	0.066	10.362	0.138	14.313	11.652	0.034	0.1	0	96.025
ZC3-2 spin 6	0.031	4.456	11.037	37.281	37.476	0.355	7.807	0	0	0.109	0	98.552
ZC9 ox eq 1	0.01	48.29	0.22	0.09	48.44	2.89	0.06	0.00	0.05	0.00	0.00	100.05
ZC9 ox eq 2	0.01	49.32	0.02	0.05	47.25	2.93	0.06	0.00	0.00	0.02	0.00	99.66
ZC9 ox long 3	0.00	49.00	3.18	0.08	43.86	3.41	0.04	0.00	0.00	0.01	0.00	99.59
ZC9 ox long 4	0.01	48.12	0.01	0.10	47.72	3.59	0.03	0.03	0.00	0.05	0.00	99.65
ZC8-1 ox lamell	0.002	47.468	0	0.008	45.111	4.974	0.073	0.005	0.143	0	0	97.784
ZC8-1 ox lamell	0.027	47.711	0.639	0.018	44.116	5.011	0.047	0.012	0	0.005	0	97.586
ZC8-1 ox lamell	0.009	46.059	0.59	0.035	44.989	5.577	0.039	0.017	0.083	0.026	0	97.424
ZC11-1 ox 1	0.026	47.398	0.699	0.081	45.638	3.217	0.031	0	0.49	0	0	97.58
ZC11-1 ox 2 skel	0	47.577	0.346	0.103	47.709	3.146	0.042	0	0.147	0.028	0	99.098
ZC11-1 ox 3 skel	0.015	47.661	1.224	0.065	45.404	3.203	0.04	0	0.299	0.001	0	97.912
ZC11-1 ox 3 skel	0.002	47.617	0.044	0.076	47.207	3.148	0.046	0	0	0.009	0	98.149
ZC1-1 ox 1	0.02	3.719	11.083	40.817	35.701	0.385	8.164	0	0	0.117	0	100.006
ZC1-1 ox 2	0.022	3.524	10.52	39.68	37.916	0.347	7.264	0	0.086	0.11	0	99.469
ZC1-1 ox 3	0.014	3.152	12.131	30.016	46.737	0.441	5.131	0	0.244	0.176	0	98.042
ZC1-3 ox 4	0.027	4.038	10.756	38.869	35.387	0.308	8.661	0	0.066	0.073	0	98.185
ZC1-3 ox 5	0.018	3.437	10.807	39.44	37.463	0.347	7.297	0	0	0.125	0	98.934

Yantiangou Oxides

Sample	SiO2	TiO2	Al2O3	Cr2O3	FeO	MnO	MgO	NiO	ZnO	Total
YTG8-2 ox 1	0.012	51.062	0.042	0.304	40.107	1.521	5.113	0.001	0.189	98.351
YTG8-2 ox 2 in bi 1	0.003	49.589	0.071	0.918	41.628	0.53	5.479	0.029	0	98.247
YTG8-2 ox 3	0.041	6.325	0.46	16.425	68.103	0.416	2.028	0.106	0.043	93.947
YTG8-3 ox 1	0.019	5.552	0.834	32.782	50.876	0.571	5.488	0.216	0.208	96.546
YTG8-3 ox 2	0	50.537	0.029	0.628	40.784	0.515	5.762	0.054	0	98.309
YTG8-3 ox 3	0.013	50.363	0.066	0.452	41.074	0.471	5.984	0.058	0.184	98.665
YTG8-4 ox 1 bright	0	50.022	0.068	0.378	42.017	0.507	4.792	0.029	0.065	97.878
YTG8-4 ox 3 dark	0.033	3.927	4.144	51.69	29.557	0.336	8.686	0.085	0.118	98.576
YTG3-2 ox in margin of	0.047	10.685	4.34	14.499	61.559	1.557	0.473	0.099	0	93.259
YTG3-2 ox 2	0.018	10.338	4.977	20.748	57.058	4.066	0.033	0.083	0	97.321
YTG3-2 ox 3	0.105	12.405	4.58	17.692	55.642	4.073	0.035	0.012	0	94.544
YTG5-1ox 1	0.014	48.552	0.029	1.064	39.911	1.678	5.617	0.029	0	96.894
YTG5-3ox 1	0.057	3.255	2.266	45.041	39.335	1.841	4.292	0.039	0	96.126
YTG4-1 ox 1	0.49	22.149	2.167	9.332	65.165	1.094	0.027	0.031	0	100.455
YTG4-1 ox 2	2.88	21.158	0.46	11.153	61.428	0.514	0.059	0.013	0	97.665
YTG4-1 ox 3	0	22.756	2.185	4.397	66.496	0.514	0.004	0.062	0	96.414

APPENDIX 4: MINERAL PLOTS

Altaite, froodite and museumite plots from Zhongchang

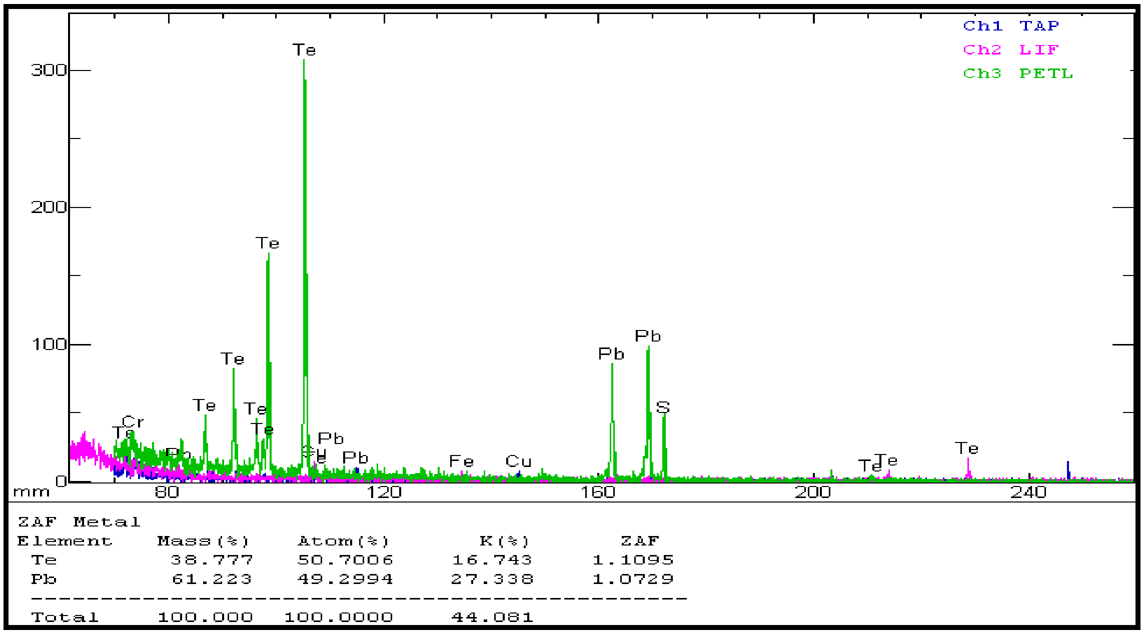

```
ZAF  Metal
Element          Mass(%)     Atom(%)       K(%)       ZAF
 Te               38.777     50.7006      16.743    1.1095
 Pb               61.223     49.2994      27.338    1.0729
 ----------------------------------------------------------
 Total           100.000    100.0000      44.081
```

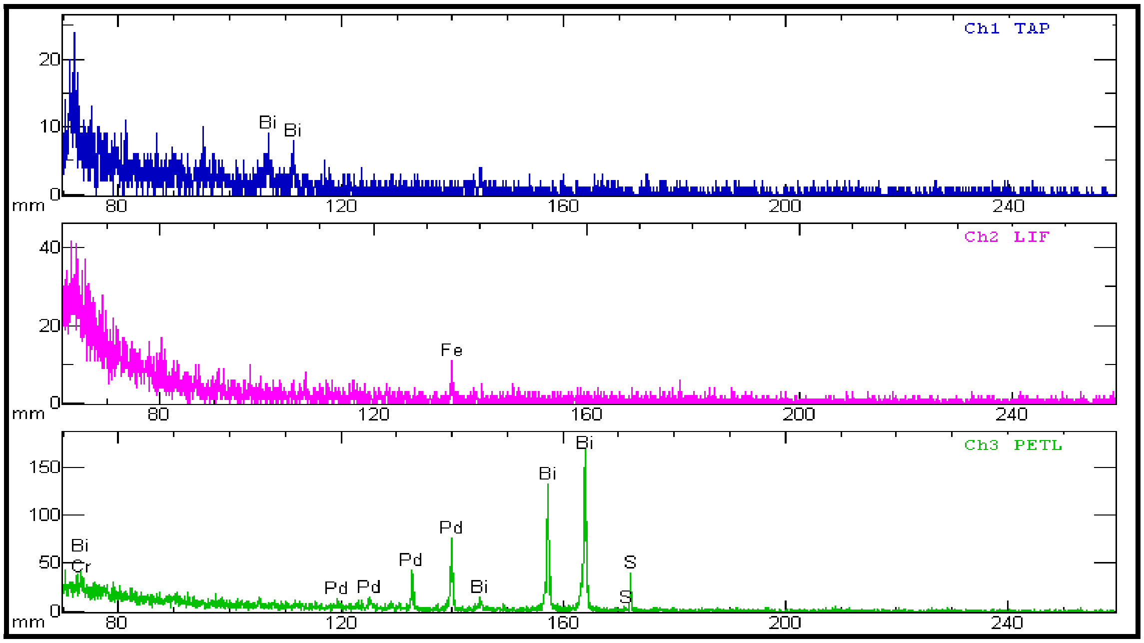

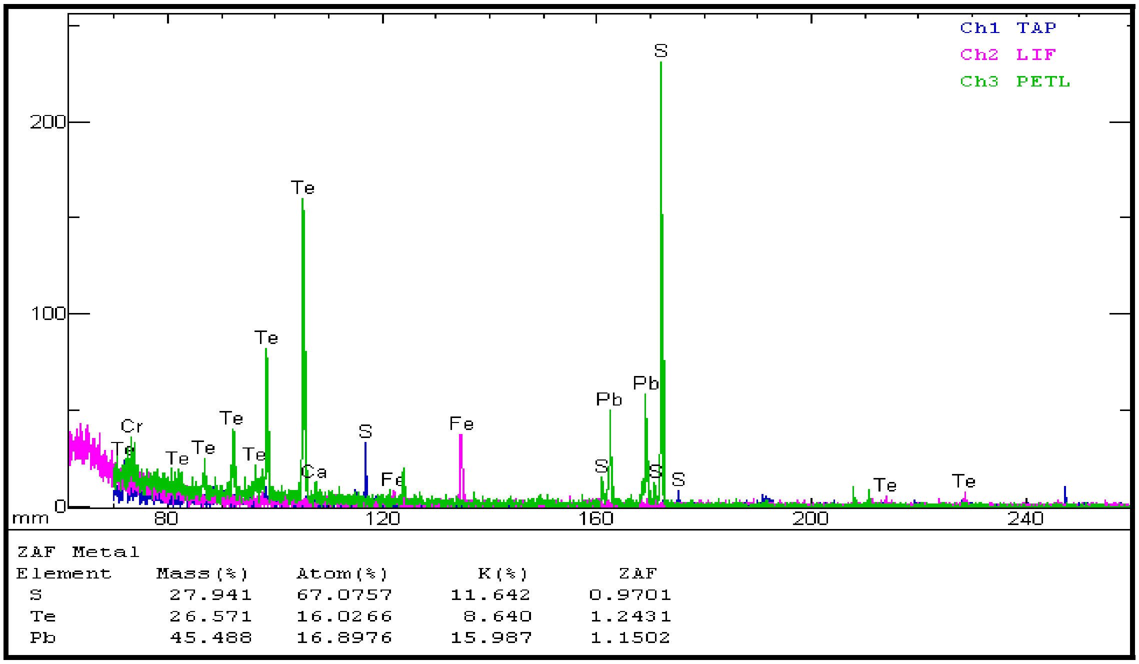

```
ZAF Metal
Element      Mass(%)     Atom(%)       K(%)       ZAF
 S            27.941     67.0757     11.642     0.9701
 Te           26.571     16.0266      8.640     1.2431
 Pb           45.488     16.8976     15.987     1.1502
```

APPENDIX 5: METAL TERNOR CALCULATIONS FORMULA (Modified after Barnes and Francis, 1995)

Composition of the Sulphide fraction;

The concentration of an element in the sulphide fraction (C_s) equals the element concentration in the sulphide rich rock (C_r) divided by the weight fraction of sulphides present (W).

$C_s = C_r/W$ (eq... 1)

To allow for the proportion of each of the elements present in the silicate and oxide components of the rocks, the concentration of the element in sulphide poor rocks (C_p) was subtracted from C_r. Therefore;

$C_s = (C_r - C_p)/W$ (eq...2)

The weight fraction sulphide present equals the sum of the sulphur (S), copper (Cu), nickel (Ni) and iron (Fe) in sulphides divided by 100.

$W = ((S_r - S_p) + (Cu_r - Cu_p) + (Ni_r - Ni_p) + Fe)/ 100$ (eq...3)

The amount of Fe in sulphide (Fes) was calculated by assuming that the sulphides consist of pentlandite (pn), chalcopyrite (cpy), pyrrhotite (po) and have compositions similar to the probed compositions.

$Fe_s = Fe_{pn} + Fe_{cpy} + Fe_{po}$ (eq...4)

The amount of pentlandite formed is controlled by the amount of Ni present; assuming that the formula of pentlandite is

$Fe_{4.5}Ni_{4.5}S_8$

Moles Fe_{pn} = moles Ni = wt percent Ni/ molecular wt Ni

Wt percent $Fe_{pn} = (Ni_r - Ni_p)/ 58.7 \times$ molecular wt Fe

Wt percent $Fe_{pn} = (Ni_r - Ni_p)/ 58.7 \times 55.847$ **(eq... 5)**

The amount of chalcopyrite formed is controlled by the amount of Cu present; assuming that the formula of chalcopyrite is $CuFeS_2$

Moles Fe_{cpy} = 2 × moles Cu = wt percent Cu/ molecular wt Cu

Wt percent $Fe_{cpy} = 2\ (Cu_r - Cu_p)/\ 63.54 \times 55.847$ **(eq...6)**

The amount of pyrrhotite formed is controlled by the amount of S remaining (S_T) after allowing for the pentlandite and cubanite. Assuming the formula for pyrrhotite is Fe_7S_8 then:

Moles Fe_{po} = 7/8 (moles S_T- moles S_{pn} - moles S_{cb}),

Moles Fe_{po} = 7/8 (wt % S/ molecular wt S – 8/4.5 (wt % Ni/ 58.7) – 3 (wt % Cu/ 63.54))

Moles $Fe_{po} = 7/8\ ((S_r\text{-}S_p)/32\text{-}\ 8/4.5\ (Ni_r\text{-}Ni_p)/\ 58.7 - 3\ (Cu_r\text{-}Cu_p)/\ 63.54)$

Wt percent $Fe_{po} = 55.847 \times 7/8\ ((S_r\text{-}S_p)/32\text{-}\ 8/4.5\ (Ni_r\text{-}Ni_p) - 3\ (Cu_r\text{-}Cu_p)/\ 63.54))$ **(eq...7)**

Substituting equations 5 to 7 in equation (4) gives:

$Fe_s - 1.527\ (S_r\text{-}S_p) - 0.5285\ (Ni_r\text{-}\ Ni_p) - 0.5493\ (Cu_r\text{-}Cu_p)$ **(eq...8)**

Substituting equation 8 into equation 3 gives:

$W = (2.527\ (S_r\text{-}S_p) + 0.4715\ (Ni_r\text{-}Ni_p) + 0.4507\ (Cu_r\text{-}Cu_p))/\ 100$ **(eq...9)**

Substituting equation 9 in equation 2 gives:

$C_s = ((C_r\text{-}C_p) \times 100)/\ (2.527(S_r\text{-}S_p) + 0.4515\ (Ni_r\text{-}Ni_p) + 0.\ 4507\ (Cu_r\text{-}Cu_p))$ **(eq...10)**